



Virginia Commonwealth University
VCU Scholars Compass

Theses and Dissertations

Graduate School

2018

DEVELOPMENT OF SMALL MOLECULE NEUROPROTECTANTS

Ashley Boice

Follow this and additional works at: <https://scholarscompass.vcu.edu/etd>

 Part of the [Medicinal and Pharmaceutical Chemistry Commons](#)

© Ashley G. Boice

Downloaded from

<https://scholarscompass.vcu.edu/etd/5372>

This Dissertation is brought to you for free and open access by the Graduate School at VCU Scholars Compass. It has been accepted for inclusion in Theses and Dissertations by an authorized administrator of VCU Scholars Compass. For more information, please contact libcompass@vcu.edu.

DEVELOPMENT OF SMALL MOLECULE NEUROPROTECTANTS

A dissertation submitted in partial fulfillment of the requirements for the degree of Doctor of
Philosophy at Virginia Commonwealth University.

by

Ashley G. Boice

Bachelor of Science, Virginia Commonwealth University, May 2014

Director: Shijun Zhang

Associate Professor, Department of Medicinal Chemistry

©Ashley G. Boice 2018

All Rights Reserved

Acknowledgements

First, I would like to thank VCU and the Department of Medicinal Chemistry for the opportunity to earn my PhD. I would like to thank my advisor, Dr. Shijun Zhang, for the opportunity to work on an intriguing and meaningful research project. I would also like to thank my committee members: Dr. Matthew Halquist, Dr. Martin Safo, Dr. Xiang-Yang Wang, and Dr. Aaron May for the advice and assistance. In particular, I would like to thank Dr. Matthew Halquist and Mr. Justin Poklis for guidance in LC-MS studies, as well as Dr. Darrell Peterson for the opportunity to learn how to engineer the NLRP3 protein. I would also like to acknowledge my lab group members: Dr. Yuqi Jiang, Dr. Liu He, and Dr. Jacob Fulp. I would especially like to express my sincere gratitude for Dr. Liu He who provided advice, mentoring, and encouragement which proved invaluable for the completion of my research. Finally, I would like to thank the mice that sacrificed their lives for science.

Table of Contents

| | Page |
|--|------|
| Acknowledgements..... | ii |
| Table of Contents..... | iii |
| List of Tables..... | viii |
| List of Figures..... | ix |
| Abbreviations..... | xiii |
| Abstract..... | xix |
| Chapter | |
| 1. Introduction..... | 1 |
| 1.1 Alzheimer's Disease..... | 2 |
| 1.1.1 AD History and Disease Presentation..... | 2 |
| 1.1.2 AD Histopathology..... | 3 |
| 1.1.3 A β Hypothesis..... | 4 |
| 1.1.4. Tau Hypothesis..... | 6 |
| 1.2 Multiple Sclerosis..... | 7 |
| 1.2.1 MS History and Disease Presentation..... | 7 |
| 1.2.2 MS Histopathology..... | 8 |

| | |
|--|----|
| 1.3 The Immune System and Neurodegenerative Disorders..... | 9 |
| 1.3.1 The Immune System..... | 9 |
| 1.3.2 The Immune System in the Central Nervous System..... | 10 |
| 1.3.3 Microglia Cells..... | 11 |
| 1.3.4 Astrocytes..... | 12 |
| 1.3.5 Inflammation Signaling Pathway..... | 13 |
| 1.3.6 Cytokines and Chemokines..... | 14 |
| 1.3.7 Innate Immunity and Inflammasomes..... | 14 |
| 1.3.8 The NLRP3 Inflammasome..... | 15 |
| 1.3.9 Activation of the NLRP3 Inflammasome..... | 16 |
| 1.3.10 Downstream Effects of Activation the NLRP3 Inflammasome..... | 18 |
| 1.3.11 Dysregulation of the NLRP3 Inflammasome in Neurodegenerative Disorders..... | 19 |
| 1.3.12 NLRP3 Inflammasome as Novel Target for the Treatment of Neurodegenerative Disorders..... | 20 |
| 2. Preliminary Data..... | 22 |
| 2.1 Design of Sulfonamide-based Small Molecule Inhibitors of the NLRP3 Inflammasome..... | 22 |

| | |
|--|----|
| 2.2. JC-21 Analog, JC-171, Inhibits the NLRP3 Inflammasome..... | 26 |
| 3. Mechanistic Studies of Sulfonamide-based Small Molecule NLRP3 Inflammasome Inhibitors..... | 29 |
| 3.1 MST Assay..... | 29 |
| 3.1.1 Introduction to MST..... | 29 |
| 3.1.2 MST Results and Discussion..... | 31 |
| 3.1.2.1 Binding Interaction with the Recombinant Full-length NLRP3 Protein..... | 31 |
| 3.1.2.2 Binding Interaction with the Mutant NLRP3 (K232A) Protein..... | 33 |
| 3.1.2.3 Binding Interaction with the LRR component of the NLRP3 protein..... | 35 |
| 3.1.2.4 Binding Interaction with the ASC Protein..... | 38 |
| 3.2 Direct Binding to the NLRP3 Protein..... | 39 |
| 3.3 ATPase Activity of the NLRP3 Protein..... | 40 |
| 3.3.1 Introduction to the NLRP3 ATPase..... | 40 |
| 3.3.2 Results and Discussion..... | 40 |
| 3.4 Molecular Modeling Studies..... | 42 |
| 3.4.1 Introduction to Molecular Modeling of the NLRP3 Protein.... | 42 |

| | |
|---|----|
| 3.4.2 Results and Discussion..... | 43 |
| 3.4.2.1 Sequence Alignment..... | 43 |
| 3.4.2.2 Structure and Validation..... | 45 |
| 3.4.2.3 Docking Studies of JC-171 and other analogs..... | 47 |
| 3.5 Production of the NLRP3 Protein..... | 49 |
| 3.5.1 Plasmid Preparation..... | 49 |
| 3.5.2 Transfection..... | 56 |
| 3.6 Liquid Chromatography-Mass Spectrometry (LC-MS)..... | 56 |
| 3.6.1 Method Development..... | 56 |
| 3.6.2 Validation..... | 59 |
| 3.6.3 Application and Discussion..... | 66 |
| 4. Methods and Materials..... | 68 |
| 4.1 MST..... | 68 |
| 4.1.1 NLRP3 (full length), NLRP3 (K232A), and NLRP3 (LRR).... | 68 |
| 4.1.2 ASC..... | 68 |
| 4.2 ADP-Glo..... | 70 |
| 4.3 Molecular Modeling..... | 70 |
| 4.4 NLRP3 Production..... | 71 |

| | |
|-------------------------------------|----|
| 4.4.1 Plasmid and Materials..... | 71 |
| 4.4.2 PCR..... | 72 |
| 4.4.3 Transformation..... | 72 |
| 4.4.4 Transfection..... | 73 |
| 4.4.5 SDS-PAGE..... | 74 |
| 4.4.6 Immunoblot..... | 75 |
| 4.5 LC-MS..... | 75 |
| 4.5.1 Materials..... | 75 |
| 4.5.2 Brain extraction..... | 76 |
| 4.5.3 LC-MS Calibration and QC..... | 76 |
| 4.5.4 LC-MS Parameters..... | 77 |
| 4.5.5 LC-MS Analysis..... | 78 |
| Conclusion..... | 79 |
| References..... | 80 |

List of Tables

| | Page |
|---|------|
| Table 1: Run 1 calibration curve and low, medium, and high QC samples..... | 62 |
| Table 2: Run 2 calibration curve and low, medium, and high QC samples..... | 63 |
| Table 3: Run 3 calibration curve and low, medium, and high QC samples..... | 64 |
| Table 4: In-between precision and bias for low medium and high MCC950 samples... | 65 |
| Table 5: In-between precision and bias for low medium and high GA4 samples..... | 65 |
| Table 6: Concentration of drug detected from the brain tissue of mice given the concentration of drug indicated by intraperitoneal injection..... | 67 |

List of Figures

| | Page |
|--|------|
| Figure 1: Histopathology of AD in the brain compared with healthy brain..... | 3 |
| Figure 2: The processing of APP..... | 4 |
| Figure 3: The structure of the NLRP3 inflammasome..... | 16 |
| Figure 4: Canonical and non-canonical pathways of activation of the NLRP3 inflammasome..... | 17 |
| Figure 5: Chemical structure of MCC950..... | 20 |
| Figure 6: Structures of Glyburide and Glipizide..... | 22 |
| Figure 7: Inhibition of the production of cytokines by Glyburide and Glipized..... | 22 |
| Figure 8: Inhibition of the production of caspase-1 cleavage product p20..... | 23 |
| Figure 9: Structure of JC-21..... | 24 |
| Figure 10: Inhibition of caspase-1 activity and cell death by JC-21..... | 24 |
| Figure 11: Inhibition of caspase-1 activity and cell death by JC-21 given activators of inflammasome AIM2 and NLRC4..... | 25 |
| Figure 12: Structure of JC-171..... | 26 |
| Figure 13: Inhibition of production of cytokines by JC-171..... | 26 |
| Figure 14: Inhibition of ASC association to NLRP3 by JC-171..... | 27 |

| | |
|--|----|
| Figure 15: Clinical scores of EAE mice dosed with either 10 mg/kg of JC-171 (green line) or 10 mg/kg of MCC950 (red line)..... | 27 |
| Figure 16: Determination of demyelination of spinal cord and frequency of MOG specific Th17 cells in the spinal cord and spleen..... | 28 |
| Figure 17: MST assay for affinity of JC-171 for fluorescently tagged (NT-647) full length NLRP3..... | 32 |
| Figure 18: MST assay for affinity of MCC950 for fluorescently tagged (NT-647) full length NLRP3..... | 33 |
| Figure 19: MST assay for affinity of JC-171 for fluorescently tagged (NT-647) full length NLRP3 mutant (K232A)..... | 34 |
| Figure 20: MST assay for affinity of GA3 and MCC950 for fluorescently tagged (NT-647) NLRP3 LRR segment..... | 36 |
| Figure 21: MST assay for affinity of JC-171 analogs for fluorescently tagged (NT-647) NLRP3 LRR segment..... | 37 |
| Figure 22: MST assay for affinity of GA3 and MCC950 for fluorescently tagged (NT-647) ASC protein..... | 38 |
| Figure 23: Immunoblot of J774A.1 lysate incubated with biotin probes of CY-09 or JC-171 analog (HL-79) using antibody specific for NLRP3..... | 39 |
| Figure 24: Representative standard curve tested alongside samples from one assay of the triplicate performed..... | 41 |

| | |
|--|----|
| Figure 25: ADP-Glo assay to determine inhibition of the ATPase activity of the NLRP3 protein by JC-171 and other analogs..... | 42 |
| Figure 26: Sequence alignment of mouse NLRC4 NACHT domain and human NLRP3 NACHT domain with emboss needle pairwise sequence alignment..... | 44 |
| Figure 27: Ramachandran plots of NACHT domain..... | 45 |
| Figure 28: ADP docked in the ATP binding pocket of homology model 70..... | 46 |
| Figure 29: Interactions of ADP docked into the ATP binding pocket | 47 |
| Figure 30: JC-171 docked in pocket next to ATP binding pocket | 48 |
| Figure 31: JC-171 binding interactions within pocket of NACHT domain | 49 |
| Figure 32: pEGFP-C2 vector with full length human NLRP3 protein insert..... | 50 |
| Figure 33: The insert sequence with found restriction sites highlighted and labeled ... | 51 |
| Figure 34: PCR products run on agarose gel..... | 52 |
| Figure 35: pcDNA 3.1/Hygro mammalian expression vector with necessary restriction sites indicated in red circles..... | 53 |
| Figure 36: Cloned pcDNA 3.1/Hygro+inserts digested with appropriate enzymes..... | 53 |
| Figure 37: Cloned pcDNA 3.1/Hygro+inserts sequenced..... | 54 |
| Figure 38: Colonies 1-4 of clones pcDNA 3.1/Hygro+ NheI/BamHI and BamHI/XhoI inserts cut with either NheI and XhoI restriction enzymes or BamHI and XhoI restriction enzymes..... | 55 |

| | |
|--|----|
| Figure 39: Purified colony of pcDNA 3.1/Hygro+ full NLRP3 insert | 55 |
| Figure 40: Immunoblot of HEK 293 cell lysates transfected with pcDNA 3.1/Hygro+ full NLRP3 insert..... | 56 |
| Figure 41: Retention times and total ion count for transition ions of JC-171(GA4), MCC950, and Glipizide..... | 57 |
| Figure 42: Multiple reaction monitoring for GA4, MCC950, and Glipizide in double blank sample..... | 58 |
| Figure 43: Calibration curve of GA4 from brain tissue at concentrations: 2.5, 25, 125, 250, 500, 1,250 ng/g..... | 59 |
| Figure 44: Calibration curve of MCC950 from brain tissue at concentrations: 2.5, 25, 125, 250, 500, 1,250 ng/g..... | 60 |
| Figure 45: Purified fractions from fluorescently tagged (NT-647) labeled ASC protein. | 69 |

List of Abbreviations

| | | |
|---------------|---|---|
| A β -42 | - | Amyloid-beta peptide 42 |
| ACH | - | Amyloid Cascade Hypothesis |
| CAN | - | Acetonitrile |
| AD | - | Alzheimer's Disease |
| AIM2 | - | Absent in melanoma 2 inflammasome |
| ALR | - | AIM2-like receptors |
| ALS | - | Amyotrophic Lateral Sclerosis |
| AP-1 | - | Activator protein 1 |
| APP | - | Amyloid precursor protein |
| ASC | - | Apoptosis-associated speck-like card containing protein |
| ATP | - | Adenosine triphosphate |
| BACE-1 | - | Beta-site APP cleaving enzyme 1 |
| BBB | - | Blood-brain barrier |
| BMDM | - | Bone marrow-derived macrophage |
| C/EBP | - | CCAAT- enhancer binding protein |
| CAD | - | Collision-activated dissociation |
| CAPS | - | Cryopyrin associated periodic syndrome |

| | | |
|-------|---|---|
| CARD | - | Caspase recruitment domain |
| CCAAT | - | Cytosine-cytosine-adenosine-adenosine-thymidine |
| CCR | - | Chemokine receptor |
| Cdk5 | - | Cyclin-dependent-like kinase 5 |
| CE | - | Collision energy |
| CNS | - | Central nervous system |
| COX-2 | - | Cyclooxygenase-2 |
| CV | - | Coefficient of variation |
| CXP | - | Collision cell exit potential |
| DAMP | - | Damage associated molecular pattern |
| DNA | - | Deoxyribonucleic acid |
| DP | - | Declustering potential |
| EAE | - | Experimental autoimmune encephalomyelitis |
| ELISA | - | Enzyme-linked immunosorbent assay |
| EOAD | - | Early onset Alzheimer's disease |
| EP | - | Entrance potential |
| FA | - | Formic acid |
| FADD | - | Fas-associated protein with death domain |

| | | |
|-------|---|---|
| FCAS | - | Familial cold autoinflammatory syndrome |
| GSK-3 | - | Glycogen synthase kinase-3 |
| HEK | - | Human embryonic kidney cells |
| HRP | - | Horseradish peroxidase |
| IFI16 | - | Interferon gamma inducible protein 16 |
| IFNAR | - | Interferon-alpha/beta receptor |
| IKK | - | I κ B kinase |
| IL | - | Interleukin |
| iNOS | - | Inducible nitric oxide synthase |
| IRF | - | Interferon-regulatory factor |
| JAK | - | Janus Kinase |
| JNK | - | C-jun n-terminal kinase |
| LC-MS | - | Liquid chromatography-mass spectrometry |
| LOAD | - | late-onset Alzheimer's disease |
| LPS | - | Lipopolysaccharide |
| LRR | - | Leucine-rich repeat |
| MAC | - | Membrane attack complex |
| MCP | - | Methyl-accepting chemotaxis protein |

| | | |
|----------------|---|--|
| MHC | - | Major histocompatibility complex |
| MIP | - | Macrophage inflammatory protein |
| MMP | - | Matrix metalloproteinase |
| MRM | - | Multiple reaction monitoring |
| MS | - | Multiple Sclerosis |
| MST | - | Microscale Thermophoresis |
| MWS | - | Muckel-Wells syndrome |
| MyD88 | - | Myeloid differentiation primary response 88 |
| NACHT | - | NAIP (neuronal apoptosis inhibitor protein), C2TA (MHC class 2 transcription activator), HET-E (incompatibility locus protein from <i>Podospora anserina</i>) and TP1 (telomerase-associated protein) |
| NALP | - | NACHT, LRR and PYD domains-containing protein 3 |
| NBD | - | Nucleotide binding domain |
| NBM | - | Nucleus basalis of Meynert |
| ND | - | Not detected |
| NF- κ B | - | Nuclear factor kappa-light-chain-enhancer of activated B cells |
| NFT | - | Neurofibrillary tangles |
| NLR | - | NOD-like receptor |
| NLRP3 | - | NOD-like receptor pyrin containing 3 |

| | | |
|--------------|---|--|
| NOD | - | nucleotide-binding oligomerization domain |
| P38MAPK | - | P38 mitogen-activated protein kinase |
| PAMP | - | Pathogen-associated molecular pattern |
| PCR | - | Polymerase chain reaction |
| PD | - | Parkinson's Disease |
| PHF | - | Paired helical filament |
| Poly (dA:dT) | - | Poly(deoxyadenylic-deoxythymidylic) acid |
| PRR | - | Pattern recognition receptor |
| PYD | - | Pyrin domain |
| QC | - | Quality control |
| RAGE | - | Receptor for advanced glycation endproducts |
| RIPA | - | Radioimmunoprecipitation assay buffer |
| RLR | - | RIG-I-like receptors |
| ROS | - | Reactive oxygen species |
| RPM | - | Revolutions per minute |
| SD | - | Standard deviation |
| SDS-PAGE | - | Sodium dodecyl sulfate- poly-acryl gel electrophoresis |
| STAT | - | Signal transducers and activators of transcription |

| | | |
|-----|---|----------------------------|
| TBI | - | Traumatic brain injury |
| TGF | - | Transforming growth factor |
| Th | - | T helper cells |
| TLR | - | Toll-like receptor |
| TNF | - | Tumor necrosis factor |
| UV | - | Ultraviolet |
| WT | - | Wild type |

Abstract

Development of Small Molecule Neuroprotectants

By Ashley G. Boice, Ph.D.

A dissertation submitted in partial fulfillment of the requirements for the degree of Doctor of Philosophy at Virginia Commonwealth University.

Virginia Commonwealth University, 2018.

Major Director: Shijun Zhang Associate Professor, Department of Medicinal Chemistry

Neurodegenerative diseases are a class of conditions that lead to progressive atrophy of different parts of the central nervous system (CNS). These diseases lead to devastating clinical outcomes to patients and give rise to an enormous socio-economical burden on society.¹ One commonality among some of the most well-known neurodegenerative disorders, e.g. Alzheimer's disease (AD), Parkinson's disease (PD), and multiple sclerosis (MS), is neuroinflammation.²⁻⁴ Neuroinflammation stems from interactions of the innate immune system with toxins and insults to the central nervous system. In the case of irremovable or chronic insults and toxins, this leads to chronic damaging inflammation that hastens neuronal degeneration and exacerbates disease pathology.^{5,6} Recently, inflammasomes of the innate immune system have been indicated in playing essential roles in the observed inflammatory responses. The most studied inflammasome is the nod-like receptor pyrin containing 3 (NLRP3) inflammasome.⁷⁻⁹ Recently our research group has successfully developed sulfonamide-based small molecule inhibitors of the NLRP3 inflammasome, such as JC-21 and JC-171, as potential

therapeutics for AD and MS. Our studies established that JC-21 is a selective inhibitor of the NLRP3 inflammasome.^{10,11} Structural modifications led to the development of JC-171 with improved pharmacokinetic properties. More importantly, our studies demonstrated the *in vivo* activity of JC-171 to effectively ameliorate the experimental autoimmune encephalomyelitis (EAE), a mouse model of MS.¹² Our data also strongly suggested that inhibitors based on this chemical scaffold may directly target the NLRP3 inflammasome.¹⁰⁻¹² In this dissertation, we conducted biophysical, biochemical, and modeling studies to further elucidate the mechanistic information of these compounds as inhibitors of the NLRP3 inflammasome. In order to conduct further mechanistic studies, the NLRP3 protein was produced via transfection of HEK 293 cells with a modified plasmid of full-length human NLRP3 protein.¹³ Furthermore, LC-MS studies were conducted to confirm the blood-brain barrier penetration (BBB) of JC-171. Our studies established that JC-171 directly binds to the NLRP3 protein. The results also suggested that JC-171 may bind to the NACHT domain of NLRP3 while in a site that is distinct from the ATP binding site. This notion is supported by the fact that our compounds do not interfere with the ATPase activity of NLRP3. Docking studies of JC-171 to the homology model of the NACHT domain of NLRP3 also supported this assertion by showing the interaction of JC-171 with residues that are not overlapping with the ATP binding pocket. BBB penetration studies in combination with LC-MS analysis confirmed that JC-171 shows better BBB penetration when compared to MCC950. Collectively, our results strongly support that our compounds function as NLRP3 inflammasome inhibitors by directly binding to the NLRP3 protein, a novel and distinct mechanism of action when compared to the known inhibitors that target the NLRP3 inflammasome pathway. These

results strongly encourage further development of such inhibitors as potential therapeutics for neurodegenerative diseases.

Chapter 1: Introduction

Neurodegenerative diseases are a class of conditions that lead to progressive atrophy of different parts of the nervous system. These diseases can lead to a broad range of symptoms presented, from motor dysfunction in Parkinson's disease (PD) to the significant cognitive decline seen in Alzheimer's disease (AD). Various genetic mutations, toxins, insults, and autoimmune responses have been known to cause these ailments and the incidence of such diseases often increases with age. In addition to the detrimental effects to the health and well-being of the affected individuals, neurodegenerative diseases have become a growing concern as the healthcare costs are increasing as the senior population increases in numbers.^{14,15} The most well-known neurodegenerative diseases are AD, PD, amyotrophic lateral sclerosis (ALS), and multiple sclerosis (MS).¹⁶ AD, the most common type of dementia, is estimated to affect more than 5 million Americans of all ages in 2017 and up to 36 million individuals worldwide currently. It is predicted that more than 88 million Americans will have AD by 2050.¹⁷ AD will cost Americans an estimated 277 billion dollars for the year 2018.¹⁸ The estimated occurrence of PD, the second most common neurodegenerative disease, in 2010 was approximately 630,000 in the United states and is projected to double by 2040. Additionally, PD cost Americans more than 14.4 billion dollars in 2010.¹⁹ Finally, MS affects an estimated 400,000 Americans and the least common but well known, ALS, affects an estimated 30,000.^{20,21} Each neurodegenerative disease has its own distinct and comparably devastating clinical manifestations but based on the data presented the disease with the greatest socioeconomical burden is AD.

1.1 Alzheimer's Disease

1.1.1 AD History and Disease Presentation

AD was discovered by Dr. Alois Alzheimer who examined a patient of Frankfurt Asylum who died of an undocumented mental illness characterized by memory loss, paranoia, and personality changes. In his examination, Dr. Alzheimer identified atrophy of the cerebral cortex and the abnormal histopathology including the deposits of neuritic plaques and neurofibrillary tangles.²² Since then, the scientific community has made further progress in characterizing AD. AD is the most common form of dementia and accounts for 60 to 80% of all dementia cases.¹⁷ In early stages of the disease, the cognitive symptoms are milder and consist of episodic memory loss, taking longer to finish tasks, and increased anxiety. In moderate AD, the symptoms become more impactful and can include retrograde memory loss, paranoia, personality changes, difficulty with simple tasks, and getting lost. In severe AD, patients can lose the ability to communicate, have difficulty swallowing, and loss of bladder and bowel control.^{17,23}

There are two types of AD, early-onset AD (EOAD) and late-onset AD (LOAD). Of all AD diagnoses, 10% are diagnosed with EOAD. Patients with EOAD begin to present with symptoms from as young as age 30 to 65. The main difference in the disease presentation of EOAD and LOAD is the increased frequency of symptoms aside from memory impairment in EOAD, such as visual dysfunction, language impairment, and difficulty executing purposeful movements.²⁴ The cause of these symptoms in EOAD is mutations to genes for either amyloid precursor protein (APP), presenilin-1 (PSEN1), or presenilin-2 (PSEN-2). A variant of apolipoprotein E, apolipoprotein ε4, is also known to

increase susceptibility to the disease for LOAD or EOAD.

However, the cause of LOAD is largely unknown but might be a combination of genetic risks and environmental factors.^{1,25} Some of these potential risk factors that have been investigated include air pollution,²⁶ insecticide DDT,²⁷ head injury,²⁸ chronic inflammation,²⁹ and type 2 diabetes mellitus.³⁰ Despite its prevalence and unclear cause, LOAD is not considered to be a part of the normal aging process. This being apparent from the similarities in both pathology and clinical presentation to EOAD.³¹ The devastating emotional, physical, and socioeconomical impact of AD has sparked an enormous effort of the scientific community to find an effective therapeutic treatment or cure for this disease. Without one certain cause in this multifactorial disease, multiple targets have been investigated based on the known histopathology.

1.1.2 AD Histopathology

The known histopathological changes in AD include toxic amyloid- β (1-42) ($A\beta_{42}$) oligomers and the fibrillar form of amyloid- β , which deposits of lead to the formation of neritic plaques. Additionally, the disease is characterized by anomalously phosphorylated tau that forms filaments and lead to the buildup of neurofibrillary tangles.

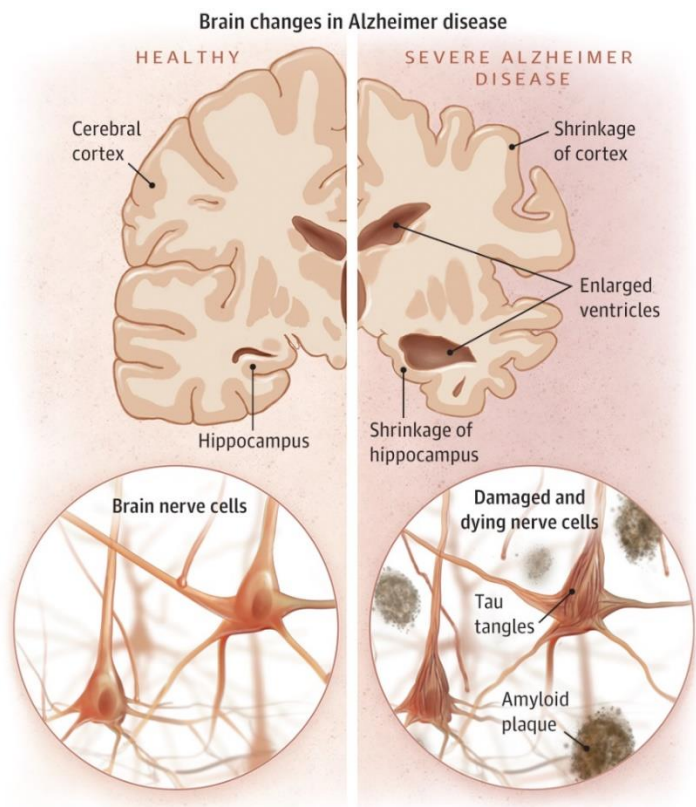


Figure 1. The histopathology of AD in the brain compared with healthy brain. Adapted from Jin.³⁴

With chronic sources of inflammation, glial scar formation from failed attempts correct these insults, and synaptic loss,³² in time, neurons fail to function properly or interact and eventually can lead to neuronal death. Neuronal death in AD frequently occurs with cholinergic neurons in the hippocampus and neocortex of the brain.³³ With the increasing loss of dendrites, axons, and neurons, the brain shrinks.^{34,35} This atrophy of the brain becomes apparent as the cortex and hippocampus visibly shrink and the ventricles fill with fluid (Figure 1).³⁴ To better understand these toxic insults that trigger the degeneration in the AD brain, further details on the two hallmarks, amyloid- β and tau, need to be discussed.

1.1.3 A β hypothesis

The first hypothesis to explain the pathology in AD, the amyloid cascade hypothesis (ACH), argues that amyloid- β peptide deposition in the brain is the triggering event leading to the pathology of AD. The major supporting evidence of this hypothesis is EOAD. Mutations to amyloid precursor protein (APP) and part of its gamma-secretase

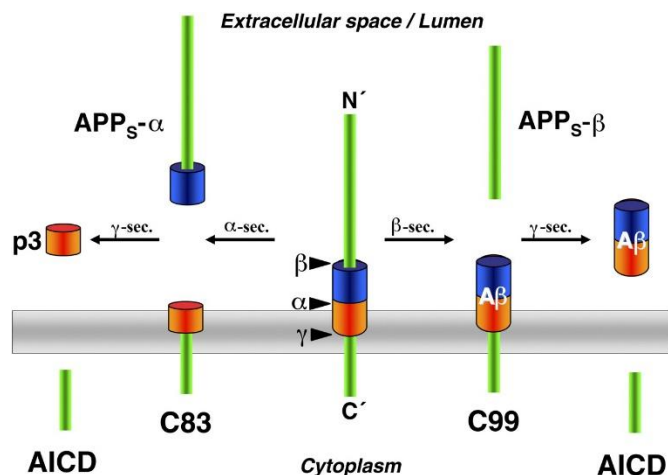


Figure 2. The processing of APP. Adapted from Kaether and Haass.³⁷

complex, presenilin, lead to AD pathology, directly connecting amyloid- β to AD.³⁶ A key player in the hypothesis is APP, APP is a transmembrane protein with the larger N-terminal on the extracellular side of the membrane and the smaller C-terminal on the intracellular side. From knock-out and mutation studies, the function of the

protein appears to be the maintenance of synapses and regulation of signaling the growth of dendrites and axons. APP can be cleaved by alpha-secretase to produce sAPP-alpha and C83. When cleaved by beta-site APP-cleaving enzyme 1 (BACE-1) it can produce sAPP- β and C99. C83 and C99 can then be further cleaved by gamma-secretase to produce P3 or amyloid- β , respectively, (Figure 2).³⁷ The amyloidogenic pathway, following cleavage of C99 can produce amyloid- β at varying sizes but more frequently amyloid- β -40.^{38,39}

A β 42 is one of the most dangerous fragments because of its ability to form fibrils and oligomerize.⁴⁰ The levels of soluble A β 42 is associated with how severe AD is. A β 42 normally spreads throughout the neuronal tissue until it hits high enough levels that it then aggregates and forms fibrils and eventually plaques.³⁸ It has been demonstrated that A β 42 trimeric and tetrameric oligomers are the most dangerous. These can attach to synapses and lead to their dysfunction, and eventually lead to neuronal death.⁴⁰ In order to investigate the effects A β 42, in one study, researchers created an artificial plaque by the injection of pre-aggregated A β 42 into the nucleus basalis of Meynert (NBM) in the brains of rats. They concluded that the injection led to the formation of amyloid- β plaques, as well as astrocyte and microglial infiltration and activation. The injection also led to iNOS and COX-2 expression, interleukin-1- β (IL-1- β) production, cholinergic neuron death, and p38MAPK pathway activation. The artificial plaque produced demonstrated many characteristics of the plaques found in AD brains.⁴¹ amyloid- β fibrils and mutant APP are also linked to the formation of neurofibrillary tangles (NFT) in transgenic mouse models *in vivo*.⁴²⁻⁴⁴ Despite the clear connection of deposition of amyloid- β to AD pathology, the ACh is not without its weaknesses. Some studies have indicated that both amyloid- β and

NFT may be a reaction instead of a cause. Similar AD pathology in regards to amyloid- β has been found in brains of survivors of traumatic brain injury (TBI)^{45,46} or with damage inflicted to the nucleus basalis of rats.⁴⁷ Altogether, ACH is supported by ample data and a well-established hypothesis for the development of AD pathology.³⁶

1.1.4. Tau hypothesis

The second hallmark of AD is NFT triggered by atypically phosphorylated tau. The tau hypothesis states that abnormally or hyper-phosphorylated tau is the causative event from which AD pathology originates. The major supporting evidence of this hypothesis is the strong correlation of the spread of tau pathology and the development of cognitive decline seen in AD.⁴⁸ Specifically, the cognitive symptoms presented in AD patients correspond functionally to regions of the brain burdened by NFTs.⁴⁹ Additionally, some studies have reported the presence of tau pathology before the deposition of the amyloid- β peptide.^{50,51} The center of this hypothesis, tau, is a microtubule-associated cytoskeletal protein expressed throughout the CNS. Tau functions to regulate neurite outgrowth and stabilize microtubules. When tau is phosphorylated by kinases such as glycogen synthase kinase-3, its ability to stabilize microtubules is decreased.⁵² When tau is hyperphosphorylated, it detaches from the microtubule of the cytoskeleton; this creates paired helical filaments (PHFs) which triggers the formation of neurofibrillary tangles that impede neuronal transport in AD and other tauopathies.⁵³ The exact trigger which leads to tau hyperphosphorylation is not well established. However, studies have found multiple contributing factors. One study demonstrated that administration of cytokine IL-6 to hippocampal neurons could elicit an increase in the hyperphosphorylation of tau with dependence on cdk5/p35, which is a complex of cyclin-dependent kinase 5 and activator

p35. ^{54,55} Despite the distinct hypotheses, there have been unifying theories for the role in amyloid- β and NFTs in the pathology of AD that propose possible explanations for discrepancies in either theories. ^{48,56}

The involvement of both of these AD hallmarks and the failure of the immune system to correct these insults is the major contributing factor of the neuronal atrophy seen in AD. Additionally, they provoke a chronic and damaging cycle of inflammatory response from the innate immune system.^{2,57}

1.2 Multiple Sclerosis

1.2.1 MS History and Disease Presentation

Between the late 1700s and early 1800s Multiple Sclerosis (MS) was first described in separate accounts by its clinical presentation and a depiction of its characteristic plaques by Robert Carswell and Jean Cruveilhier.⁵⁸ It wasn't classified as a distinct disease until 1868 when pathologist Jean-Martin Charcot connected the histopathological changes from autopsies of MS patients with their clinical symptoms.^{59,60} Multiple sclerosis is an autoimmune disease characterized by sclerotic lesions in the brain and spinal cord. The clinical signs of the disease are limb weakness and numbness, bladder dysfunction, fatigue, depression, mood swings, and blurred vision. The disease is also often characterized by an exacerbation of symptoms with higher temperatures, known as Uhthoff's phenomenon.^{20,61} There are multiple different types of MS which are distinguished by the progression of symptoms and the presence of relapses and remissions. The most common type of MS diagnosed in patients initially, 80%, is relapsing-remitting MS. This is characterized by symptoms lasting days to months

followed by remission in which a patient is symptom-free until the next relapse.⁶² The second type of MS, secondary-progressive, is defined by a slow progression in severity of symptoms and can include relapses. The third type of MS, primary-progressive, does not have relapses and remissions but instead a continuous progression of symptoms. Finally, 5% of patients initially diagnosed with MS are diagnosed with progressive-relapsing MS. Progressive-relapsing MS, the rarest form of MS, is characterized by symptom flare-ups and a continuous decline and may or may not include remissions.⁶³ Risk factors for the development of MS include genetic mutations to the human leukocyte antigen (HLA) gene which encodes a cell surface antigen presenting protein (major histocompatibility complex)⁶⁴ and genes important for cytokine pathways such as interleukin-7 receptor.⁶⁵ Another risk factor for MS is previous infection with the Epstein Barr virus.⁶⁶

1.2.2 MS Histopathology

MS is characterized by sclerotic plaques primarily in the white matter of the CNS. These lesions often occur in the corpus callosum, lateral ventricles, brain stem, optic nerves, and spinal cord.⁶¹ The plaques stem from the autoimmune demyelination of neurons. The myelin is a highly lipid-based multilayer sheath that protects the axons of neurons. The myelin sheath is produced and maintained by the oligodendrocyte glial cell. Gaps in the myelin are left to form the nodes of Ranvier which the electrical signal uses to travel down the axon by saltatory conduction.⁶⁷ With demyelination, axonal injury or altered nodal components along axon lead to disrupted signal transduction. This then can lead to the symptoms seen during relapses in MS; symptoms continue until remyelination can occur.^{68,69} Other characteristics of lesions in MS are glial scarring around plaques to

block off inflamed tissue and infiltrated autoreactive leukocytes.⁶⁸ Autoreactive leukocytes are recruited to the CNS by chemokines expressed during neuroinflammation.⁴

1.3 The Immune System and Neurodegenerative Disorders

The commonality among these neurodegenerative disorders is neuroinflammation. Neuroinflammation is inflammation of the nervous system brought upon by the immune system in order to remove the agent causing damage and promote healing.² When exposed to disease-specific trigger, immune cells are activated and release pro-inflammatory factors. When chronically exposed to pro-inflammatory factors further neuronal dysfunction and damage occurs and leads to the release of damage-associated molecular patterns (DAMPs). DAMPs can then activate pattern recognition receptors (PRR) of the innate immune system and continue the cycle of damaging neuroinflammation.^{3,70}

1.3.1 The Immune System

The immune system is divided into 2 categories, the innate and the adaptive immune system. When confronted with foreign pathogens or damage, the innate immune system responds immediately with its defensive repertoire. This response is quick and is often not as specific as the adaptive immune system; damage and pathogens are recognized by their molecular patterns.^{71,72} There are multiple key components of innate immunity; one such category of innate immune cells are granulocytes which can release cytotoxic and pro-inflammatory substances.⁷³ Another component is complement that functions to enhance phagocytosis of pathogens and damaged cells or form the membrane attack complex (MAC) which can rupture cell membranes.^{74,75} Additionally,

the natural killer cells support the innate immune system by the release of cytotoxic substances or by inducing apoptosis.⁷² Another important cell for the innate immune system is the macrophage, these large cells phagocytose cellular debris or pathogens as well as secrete pro-inflammatory factors.⁷⁶ Finally, dendritic cells, which primarily function as antigen presenting cells, can stimulate a response from the adaptive immune system.⁷⁷

The adaptive immune system serves to remember pathogens not already well recognized by the innate immune system. After antigen presenting cells reach the lymph nodes or spleen, this triggers the induction of clonal selection and expansion of B or T cells which recognize the antigen. Mature B cells main function is to produce antibodies to target pathogens for destruction or neutralization. T cells include CD4⁺ helper T cells (Th) which regulate other immune cells and CD8⁺ cytotoxic T cells which can release cytotoxins to lyse pathogens or infected cells and induce apoptosis with Fas-Fas ligand interactions.^{78–80} These leukocytes recognize antigen presented on major histocompatibility complexes (MHC). CD4⁺ T cells recognize antigen presented by MHC type II by other leukocytes and CD8⁺ T cells can recognize antigen presented by MHC type I by any nucleated cells.^{81,82} Other adaptive leukocytes include: natural killer T cells, $\gamma\delta$ T cells,⁷² regulatory B and T cells,⁸³ and memory B and T cells.^{84,85} The innate and adaptive immune work together to protect the body from infection and disease. However, the immune system has limited access to some parts of the body.

1.3.2 The Immune System in the Central Nervous System

The central nervous system (CNS) was first depicted as being immune privileged, meaning that the immune system has restricted access to the CNS. In the late 19th

century, Paul Ehrlich injected dyes intravenously and found that they stained all organs with the exception of the spinal cord and brain. The reason for this was in fact the blood brain barrier.⁸⁶ In 1898, Ledwadowsky coined the term "blood-brain barrier," after he found that neurotoxic agents had an effect on the brain only when injected directly into it, instead of intravenously.⁸⁷ Multiple studies have demonstrated that the blood brain barrier (BBB) functions to limit the trafficking of ions, molecules, and cells.⁹⁴⁻⁹⁰ However, the CNS is not completely immune privileged as it might appear; the CNS has resident innate immune cells made up of glial cells and a lymphatics system that has been described.⁸¹ Back in 1869 the lymphatic system in the brain was first described as an apparent connection between the brain and the cervical lymphatic system in rabbits and dogs.⁹¹ Despite numerous other experiments in the 40s and 60s describing lymphatics in the brain,^{92,93} the idea that the brain was immune privileged persisted until more recent studies by Louveau and colleagues on mouse brain lymphatics and of human brain lymphatics by Reich were published.^{94,95} In addition to a lymphatic system, the brain has its own immune cells, glial cells.^{81,96} Glial cells are one of the main type of cells that make up the CNS and consist of microglia, oligodendrocytes, and astrocytes. They play important roles in the maintenance of neurons, production of myelin sheath, and protection of the CNS.^{96,97}

1.3.3 Microglial Cells

In 1919, the "father of microglia" Pio del Rio-Ortega demonstrated the distribution of microglia throughout the brain using silver carbonate and their ability to alter morphology when confronted with a disease state.⁹⁸ Microglia cells have since then been described as the central nervous system's first line of defense. They are important in

maintaining the homeostasis of tissues in the brain. They keep tabs on their environment seeking signs of disturbed functional or structural integrity. To maintain and protect the CNS, they can phagocytose worn-out cells, pathogens, or improperly formed synapses. However, they are also involved in the pathogenesis of neurodegenerative diseases like AD and MS.¹⁰⁴⁻¹⁰⁰ In the AD brain, microglia are recruited from surrounding blood vessels. They migrate and gather into dense perivascular plaques.¹⁰¹ Despite recruitment to the plaques, the number of microglial cells around the lesion does not correlate with amyloid- β degradation and instead it actually contributes to the volume of plaques. Instead of effectively executing their function, the removal of the insults, some studies report that they actually promote the converting amyloid- β oligomers in the plaques into fibrils (fibrillogenesis).^{32,102} Additionally, the microglia is involved in the pathogenesis of MS by demyelination of neurons and phagocytosis of myelin. Following the phagocytosis of myelin, the microglia further perpetuates MS pathology by antigen presentation to autoreactive T cells.¹⁰³

1.3.4 Astrocytes

Astrocytes have many physiological functions in the innate immune system as well as structural. It is believed that they support the structure of the blood brain barrier, as their lengthy cytoplasmic extensions enclose capillaries in the brain. They also maintain homeostasis and regulate plasticity with the release of neurotransmitters and trophic factors. To combat pathologies, astrocytes undergo astrogliosis, altering both structure and function. When activated, astrocytes cease homeostasis maintenance duties and may evoke nerve cell damage.¹⁰⁴⁻¹⁰⁶ Multiple studies have shown that amyloid plaques and aggregated amyloid- β can activate astrocytes. The astrocytes then work to clear the

amyloid- β in the brain and take in A β 42 into granules in their cytoplasm. They do this likely by either phagocytosis or endocytosis mediated by a receptor.^{105,107} Astrocytes also work to remove non-fibrillar amyloid with metalloproteases such as insulysin and neprilisin.^{57,108} The encasement and penetration of amyloid plaques by astrocytes with their cytoplasmic extensions can lead to scarring. The distribution of astrocytes within the cortex of AD brains appears to correlate with the breadth of the AD pathology.¹⁰⁵ In MS, the astrocyte contributes to disease pathology by inhibition of remyelination by the formation of glial scar.¹⁰³ Furthermore, activated astrocytes provide a source of cytotoxic factors.¹⁰⁹

1.3.5 Inflammation Signaling Pathway

When the brain is confronted with damage or infection of any sort, the innate immune system uses inflammation as a defense. The purpose of inflammation is to remove harmful irritants and to halt their destructive effects. In the brain, what signals inflammation to occur is usually the accumulation of abnormal proteins or injured neurons.^{110,111} Glial cells, and neurons have a myriad of PRRs that recognize these DAMPs. These PRRs include receptor for advanced glycation end-products (RAGE), rig-like receptors (RLR), toll-like receptors (TLR), AIM2-like receptors (ALR), C-type lectin receptors, and NOD-like receptors.¹¹² The signal transduction pathways triggered by these PRRs elicit inflammation.¹¹³ One example of these PRRs, TLRs, are receptors that can signal and activate protein kinases like p38-MAPK, IKKs, and JNK. These kinases spark inflammatory responses by transcription factors, such as IRF3/7, AP-1, and NF- κ B.^{114,115} These inflammatory responses include the secretion of chemokines, prostaglandins, oxygen radicals, and cytokines. Even though the purpose of inflammation

is to remove toxins and insults, this inflammatory response can be harmful to the brain in the case of chronic or irremovable insults.¹¹⁶⁻¹²²

1.3.6 Cytokines and Chemokines

Cytokines are important for inflammatory and anti-inflammatory processes. In general, anti-inflammatory cytokines antagonize the effects of pro-inflammatory cytokines, such as decreasing the synthesis of pro-inflammatory cytokines, inhibiting apoptosis, or inhibiting the secretion of harmful proteases like matrix metalloproteinases (MMP). Anti-inflammatory cytokines include: IL-10, IL-4, and TGF- β -1.¹¹⁷ An imbalance of higher pro-inflammatory than anti-inflammatory cytokines can lead to the amplification of cytotoxic processes. If glial cells are activated for too long they can kill the neurons surrounding them by releasing toxic products, such as nitric oxide, excitotoxins, proteolytic enzymes like MMP, or reactive oxygen species (ROS).¹¹⁸ Pro-inflammatory cytokines secreted by glial cells can trigger this cycle and can activate complement cascades, cyclooxygenase enzyme, and inducible nitric oxide synthase (iNOS). Additionally, activated microglia has been shown to produce chemokines, e.g., macrophage inflammatory protein-1alpha (MIP-1alpha), monocyte chemoattractant protein-1 (MCP-1), and IL-8.¹¹¹ Chemokines are responsible for the recruitment of immune cells to the site of inflammation. Therefore, they are responsible for the extent or spread of the local inflammation.^{124,71}

1.3.7 Innate immunity and Inflammasomes

One of the innate immune systems major contributors of proinflammatory cytokines is the inflammasome. The inflammasome is a highly regulated multi-component

PRR that responds to DAMPs or PAMPs for the purpose of protection against viral, bacterial, fungal, parasitic infections, or any disruption in homeostasis.¹¹⁹ However overactivation of the inflammasome is implicated multiple inflammatory diseases, such as familial cold autoinflammatory syndrome, type II diabetes mellitus, Crohn's disease, and vitiligo-associated multiple autoimmune disease.¹²⁰ Inflammasomes are characterized by the domains which they contain. PYHIN family of inflammasomes consist of DNA-binding HIN domain and an N-terminal pyrin (PYD) domain. This family includes the AIM2 and IFI16 inflammasomes.¹²¹ The NLR family, for example, contains a nucleotide oligomerization domain (NOD aka NACHT), a C-terminal leucine rich repeat (LRR) domain, and a variable N-terminal domain. The N-terminal domain can vary from a PYD domain in NLRPs to a caspase recruitment domain (CARD) in NLRC4. The NLR family inflammasomes include: NLRC4, NLRP1, NLRP2, NLRP3, NLRP6, NLRP7, and NLRP12.¹¹⁹ Inflammasomes without attached CARD use adapter protein apoptosis-associated speck-like protein containing a caspase-recruitment domain (ASC) which contains both a PYD domain for associating with inflammasome and a CARD domain for caspase recruitment. With recruitment and activation of the caspase the inflammasome can cleave precursor cytokines into mature pro-inflammatory cytokines. The process is highly regulated, the inflammasome protein can be modified by phosphorylation and ubiquitination and requires a priming step to upregulate inflammasome components and precursor cytokines.²⁵ Of the inflammasomes, the best characterized and most implicated in the progression of AD and MS is NLRP3.¹²²⁻¹²³

1.3.8 The NLRP3 Inflammasome

Nod-like receptor pyrin containing 3 inflammasome (NLRP3) belongs to the family of nucleotide oligomerization domain (NOD)-like receptors (NLR). NLRP3 consists of a LRR, NACHT, and PYD domain (Figure 3).⁹ NLRP3 inflammasome also includes the adaptor protein ASC and caspase-1. LRR functions as a sensor for DAMPs and PAMPs. In its autoinhibition conformation LRR interacts with the NACHT domain to prevent association with ASC.⁸ The NACHT domain is thought to play a role in oligomerization and has ATPase activity. ATP binds at a conserved site among NLRPs, the Walker A motif GxxxxGK(S/T). The NACHT domain also contains a Walker B motif necessary for ATP hydrolysis.¹²⁴ The PYD domain mediates interaction with ASC and ASC recruits caspase-1 with CARD domain. NLRP3 inflammasome activation can occur in 2 ways canonical or non-canonical (Figure 4).¹²⁵

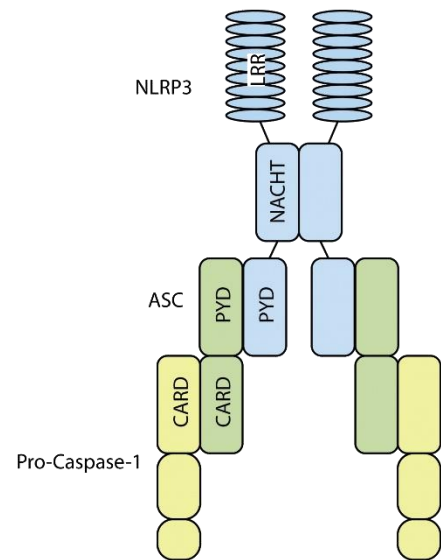


Figure 3. The structure of NLRP3 inflammasome. Adapted from Lawlor et al.⁹

1.3.9 Activation of the NLRP3 Inflammasome

In the canonical activation of NLRP3, the first step is the priming step for the upregulation of NLRP3 inflammasome components, pro-IL-1- β , and pro-IL-18 by the activation of NF- κ B. Priming can occur via toll-like receptors (TLRs), such as MyD88 or TNFR with TLR agonists, agonists for NOD-like receptors, or CLR. Additionally, cytokines TNF-alpha and IL-1- β can also serve as priming promoters.^{126,127} The second step involves the activation of NLRP3. The LRR senses DAMPs or PAMPs. These signals include: extracellular ATP, potassium efflux, ROS, mitochondrial damage, pore-forming

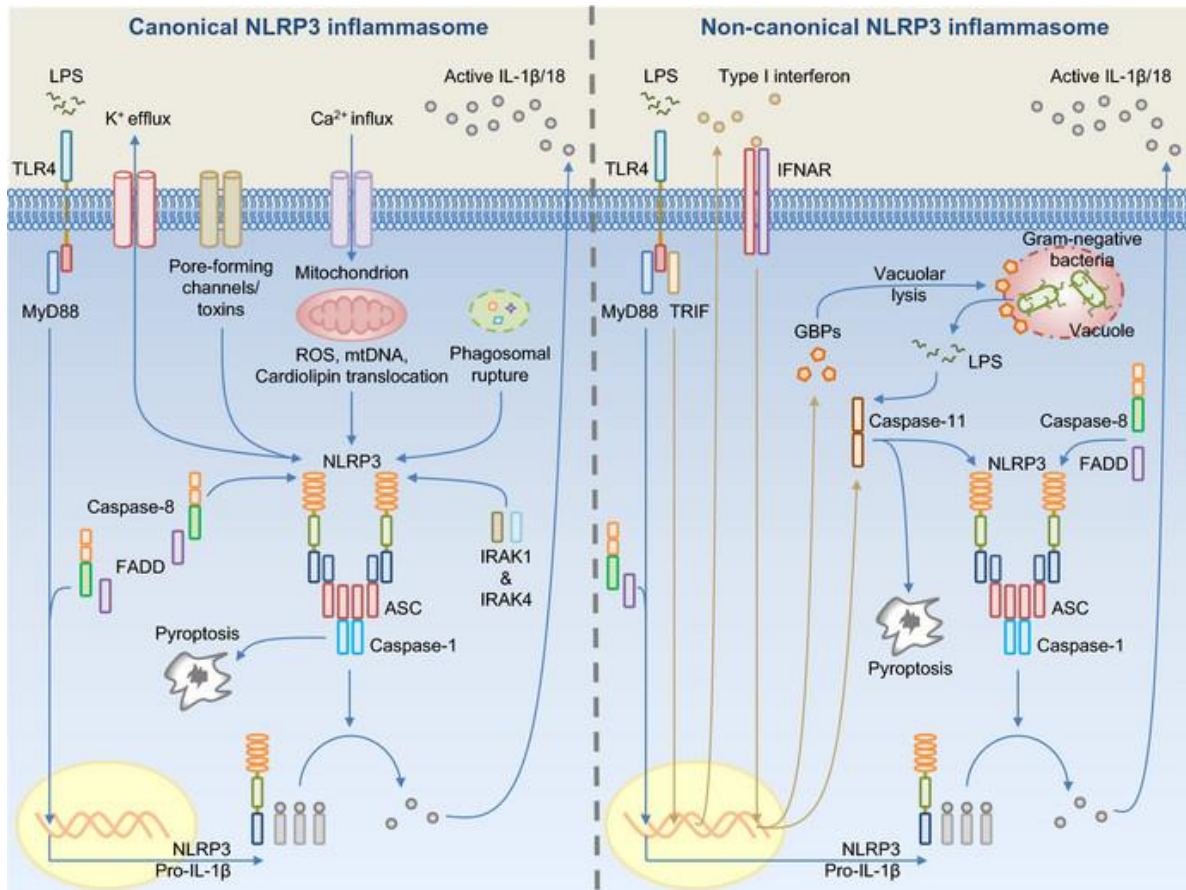


Figure 4. Canonical and non-canonical pathways of activation of the NLRP3 inflammasome. Adapted from Man and Kanneganti.¹²⁸

toxins, and nigericin. Another possible trigger for NLRP3 activation is the rupture of the lysosome. Rupture of the lysosome can occur after the phagocytosis of amyloid- β , aluminum salts, and silica crystals and is dependent on lysosome protease cathepsin.^{127,128} After activation, the LRRs interaction with the NACHT domain opens up and allows interaction with the PYD of ASC and ATP-dependent oligomerization. The PYD domain on NLRP3 recruits ASC and continues to do so as initiation of speck formation occurs. ASC nucleates caspase-1 filaments which then recruits local enzymes for trans-autocleavage of caspase-1 into subunits p10/p20 tetramer. Activated caspase-

1 can then process pro-IL-1- β and pro-IL-18 into proinflammatory cytokines IL-1- β and IL-18.^{8,129}

Non-canonical activation occurs when gram-negative bacteria activate TLRs which in turn activate NF- κ B. In addition to transcription of the NLRP3 inflammasome components and cytokine precursors, interferon regulatory factors IRF-7 and IRF-3 genes are also transcribed. IRF-7 and IRF-3 then form a complex and trigger IFN-alpha/beta secretion. IFN-alpha/beta then activates the IFNAR1/IFNAR2 receptor which activates the JAK/STAT pathway, increasing the expression of pro-caspase-11. Activation of caspase-11 is not well established but it is believed that either procaspase-11 can be auto-activated on its own or the gram-negative bacteria activates a receptor which downstream can activate caspase-11. Activation of caspase-11 can then induce inflammatory cell death (pyroptosis) and activate the NLRP3 inflammasome caspase-1 pathway.^{126,130} Another non-canonical pathway that may activate NLRP3 is via caspase-8. In some macrophages, after activation with fungal cell wall component, β -glucan, caspase-8 with Fas-associated death domain (FADD) can both prime and activate NLRP3.¹²⁵

1.3.10 Downstream Effects of Activation of the NLRP3 Inflammasome

Pro-inflammatory cytokine IL-1- β is of the major class of IL-1 cytokines. IL-1beta has been demonstrated to elicit inflammatory cascades through multiple pathways. IL-1- β can simulate inducible nitric oxide synthase (iNOS) via transcription factor NF- κ B and CCAAT-enhancer binding protein (C/EBP) activation.^{131,132} It can also induce the production of granulocyte-macrophage colony-stimulating factor (GM-CSF).^{133,134} Additionally, IL-1- β can trigger production of IL-6 which can then activate microglia, and

promote astrogliosis.¹³⁵ The second cytokine produced by activation of NLRP3 inflammasome, IL-18, is also a key player in neuroinflammation. This cytokine appears to exacerbate AD pathology by regulating the tau kinases GSK3- β and Cdk5. Additionally, levels of beta secretase enzyme BACE-1, subunit of gamma secretase n-terminal fragment of presenilin-1, APP, and adaptor protein Fe56 were found to be increased by IL-18.¹³⁶ Furthermore, IL-18 can trigger production of interferon-gamma (IFN-gamma) from helper T-cells Th1.¹³⁷ IFN-gamma, a pro-inflammatory cytokine can in turn induce production of nitric oxide.¹³⁸

1.3.11 Dysregulation of the NLRP3 Inflammasome in Neurodegenerative Disorders

Recently numerous studies have suggested the essential role of the NLRP3 inflammasome in many human diseases including myocardial infarction, traumatic brain injury, diabetes type II, gout, AD, and MS. In an effort to better demonstrate the direct impact of NLRP3 inflammasome activation in these disease processes two well documented examples, AD and MS, will be briefly further discussed.

In AD, amyloid- β has been implicated to be a trigger for activation of NLRP3. In particular, soluble amyloid- β is phagocytosed by microglia leading to destabilization of the lysosome, releasing cathepsin B into the cytosol and triggering NLRP3 activation. Additionally, NLRP3 activation can occur when the amyloid- β oligomers elicit a potassium efflux from neurons.¹¹⁶ Aside from activation of NLRP3 by AD hallmarks, NLRP3 inflammasome activation is implicated in the impediment of phagocytosis of amyloid- β by microglia. When microglia from APP/PS1/NLRP3 $-/-$ were compared with microglia from APP/PS1 mice it was found that the microglia from the APP/PS1/NLRP3 $-/-$ mice were significantly more efficient at phagocytosis of amyloid- β . Additionally, the level of amyloid-

- β aggregates in APP/PS1/NLRP3 $-/-$ were diminished without a change in total APP.^{139,140}

Multiple Sclerosis is another neurodegenerative disease closely associated with the NLRP3 inflammasome.¹⁴¹ Caspase-1 and IL-1- β was found elevated in plaques in MS patients and elevated alongside cytokine IL-18 in peripheral blood mononuclear cells.^{145-146,7} In experimental autoimmune encephalomyelitis (EAE), a mouse model of MS, the NLRP3 inflammasome demonstrated a role in the recruitment of T-helper cells to the CNS. NLRP3 $-/-$ mice displayed protection from development of EAE as well as decreased infiltration of T cells into the CNS. Th17 cells in these mice exhibited decreased expression of chemokine receptors CCR2 and CXCR6, important for infiltration of the CNS.¹⁴⁷

1.3.12 NLRP3 inflammasome as Novel Target for the Treatment of Neurodegenerative Disorders

Given the demonstrated role of NLRP3 inflammasome dysregulation in the development of multiple human diseases, small molecules targeting the NLRP3 inflammasome pathway represents an innovative strategy to develop more effective

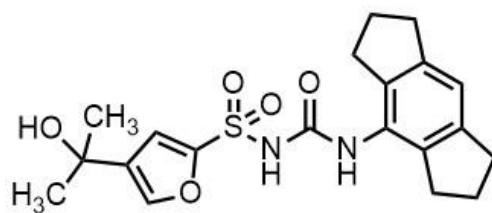


Figure 5. Chemical structure of MCC950.¹⁴⁷

treatments. Recently, several small molecule compounds have been reported to inhibit the NLRP3 inflammasome pathway. Acrylate derivative NLRP3 inhibitor demonstrated *in vivo* therapeutic potential for inflammatory bowel disease,¹⁴⁴ ketone metabolite beta-hydroxybutyrate a specific NLRP3 inhibitor which was shown to block ASC oligomerization,¹⁴⁵ and selective NLRP3 inhibitor CY-09 which prevented death in a

mouse model of CAPs.¹⁴⁶ The most potent however, MCC950, a diarylsulfonylurea compound, was discovered to inhibit the processing of IL-1-beta (IC_{50} 7.5 nM) (Figure 5).¹⁴⁷ Additionally, MCC950 demonstrated selectivity to NLRP3 among other inflammasomes by failing to inhibit IL-1- β secretion by AIM2 and NLRC4 after administration of selective activators dsDNA and bacteria *Salmonella typhimurium* to BMDMs respectively. Furthermore, MCC950 has shown effectiveness *in vivo* in a mouse model of Muckle-Wells Syndrome which is cryopyrin associated periodic syndrome (CAPS) that involves a mutation to NLRP3 and results in increased levels of IL-1- β and IL-18.¹⁵¹ In general, the exact mechanism of action of these NLRP3 inhibitors is not well established

Chapter 2: Preliminary Data

2.1 Design of Sulfonamide-based Small Molecule Inhibitors of the NLRP3 inflammasome

Given the success of selective NLRP3 inflammasome inhibitors in *in vivo* models, the NLRP3 inflammasome appears to be a promising therapeutic target for the treatment of neuroinflammation. Recently, Glyburide, the commonly used anti-diabetic, has been shown to inhibit the NLRP3 inflammasome.¹⁴⁸ Glyburide **1**, is a commonly used drug to treat type 2 diabetes, belonging to the class of sulfonylurea

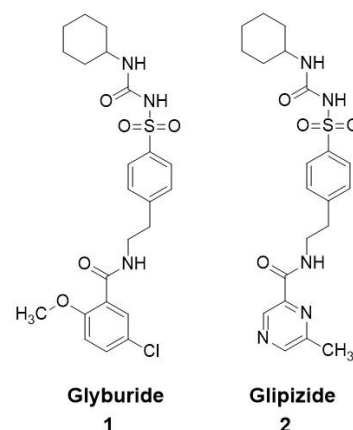


Figure 6. Structures of Glyburide and Glipizide.¹⁴⁸

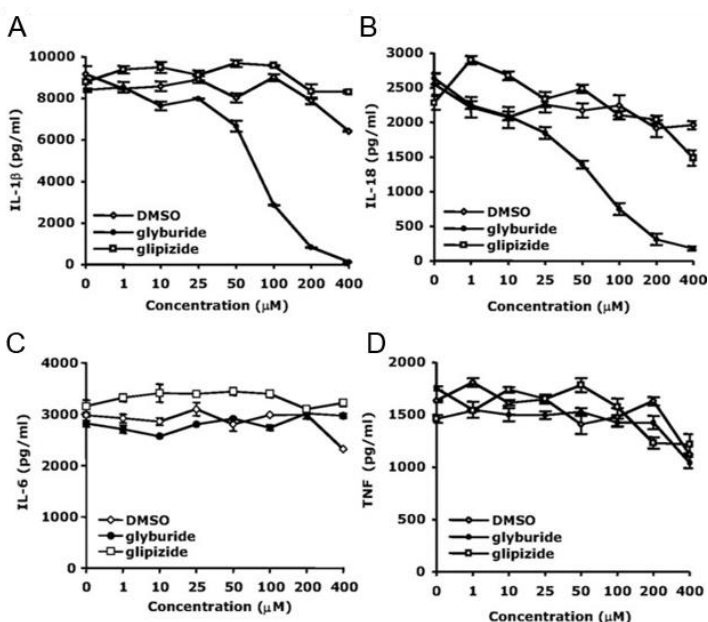


Figure 7. Inhibition of the production of cytokines by glyburide and glipizide. BMDMs were primed with LPS and pre-incubated with drug and stimulated with ATP. A. IL-1 β . B. IL-18. C. IL-6. D. TNF α . Adapted from Lamkanfi et al.¹⁴⁸

antidiabetics which also includes Glipizide **2** (Figure 6). Sulfonylurea antidiabetics treat diabetes by binding to and blocking K⁺ATP channels of the beta cells in the pancreas leading to depolarization of membrane and influx of calcium through Ca²⁺ channels. This triggers the exocytosis of insulin and subsequent lowering of blood sugar.¹⁴⁹ When Glyburide was

tested along-side the sulfonylurea antidiabetic drug, Glipizide, in mouse BMDMs, IL-18

and IL-1 β were dose dependently inhibited, while TNF- α and IL-6 were not suppressed by Glyburide treatments (Figure 7). This clearly indicated the specific inhibition of the NLRP3 inflammasome pathway by Glyburide. Notably, Glipizide did not show any effects on the production of IL-1 β and IL-18 under the same experimental conditions. These results strongly suggested that the observed inhibition on the NLRP3 inflammasome by Glyburide is independent from its anti-diabetic effects. Additionally, Glyburide demonstrated dose dependent inhibition of cleavage of caspase-1, indicating prevention of the NLRP3 inflammasome specific activation of caspase-1 (Figure 8). In addition to presented data, the study also demonstrated that macrophage K_{ATP} channels and the cyclohexylurea moiety on Glyburide is not needed for inhibition of NLRP3, further supporting that the mechanism of action is not through its antidiabetic activity. Also, Glyburide inhibited the NLRP3 inflammasome independently of P2X $_7$ receptor but appeared to act upstream of ASC and caspase-1 given that the activation of caspase-1 with adaptor ASC by other means (Ipaf and NALP1b) was not affected by glyburide. However, the dose of

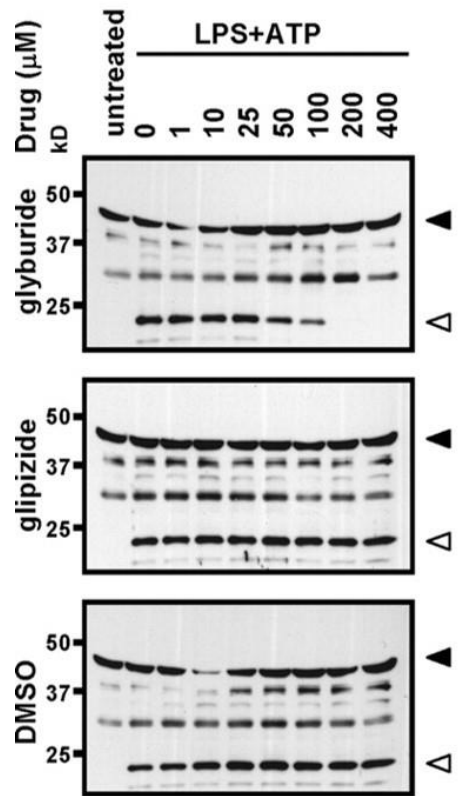


Figure 8. Inhibition of production of caspase-1 cleavage product p20. Black arrows indicate pro-caspase-1 and white arrows indicate cleavage product p20. Adapted from Lamkanfi et al.¹⁴⁸

glyburide needed to inhibit NLRP3 *in vivo* would result in lethal hypoglycemia, thus limiting further development of glyburide as a NLRP3 inflammasome inhibitor.¹⁴⁸

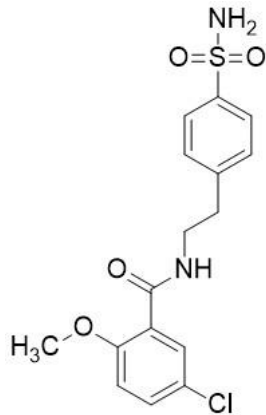


Figure 9.
Structure of
JC-21.¹¹

Based on the structure of glyburide, our group designed a sulfonamide analog, JC-21, and evaluated its inhibitory activity on the NLRP3 inflammasome (Figure 9). For the activity assay of caspase-1, HL-1 cells (immortalized mouse cardiomyocytes) were pretreated with JC-21 followed by priming with LPS and activation of the NLRP3 inflammasome with ATP. The caspase-1 activity was then determined by the cleavage of a fluorogenic substrate and cytotoxicity was determined with the Trypan blue exclusion method.

The results demonstrated that JC-21 retained inhibitory activity on

caspase-1 and rescued HL-1 cells from LPS/ATP treatment induced cell death (Figure 10). Our studies also established that JC-21 is a selective inhibitor to the NLRP3 inflammasome as no activity was observed when NLRC4

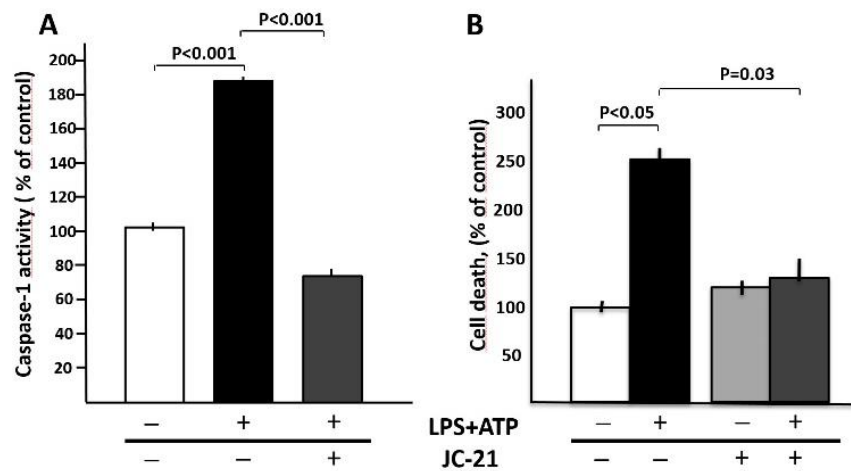


Figure 10. Inhibition of caspase-1 activity and cell death by JC-21 A. Caspase-1 activity measure by CaspASE (Promega, Madison, WI). B. cell death determined by Trypan exclusion method. Adapted from Marchetti et al.¹¹

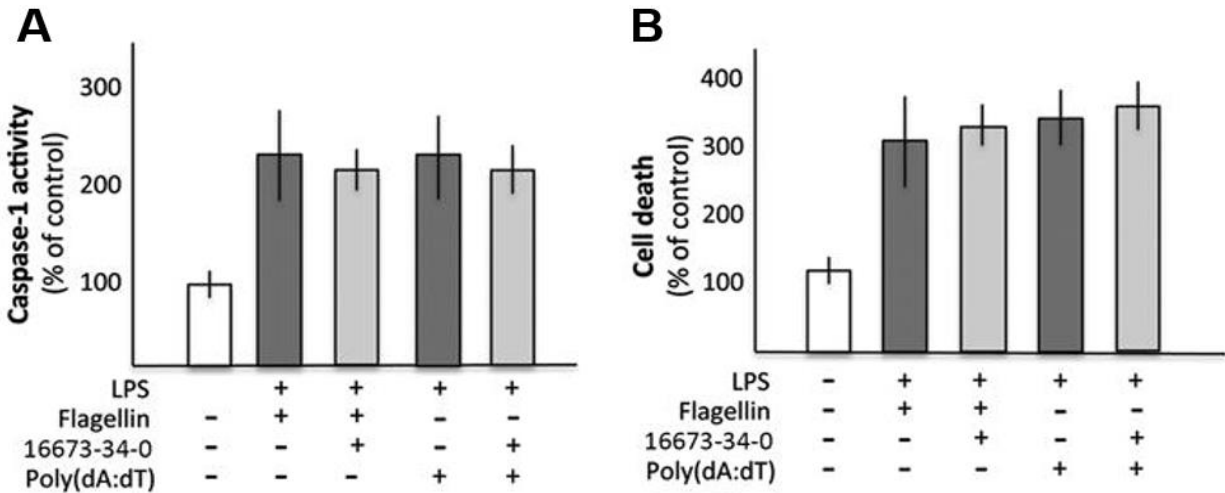


Figure 11. Inhibition of caspase-1 activity and cell death by JC-21 given activators of inflammasome AIM2 and NLRC4. A. Caspase-1 activity measure by CaspASE (Promega). B. cell death determined by Trypan exclusion method. Adapted from Marchetti et al.¹¹

or AIM2 inflammasome was activated with flagellin or poly-deoxyadenylic-deoxythymidylic acid sodium salt (Poly(dA:dT)), respectively (Figure 11). Notably, our studies demonstrated that JC-21 inhibited the production of IL-1 β from BMDM cells from NLRP3^{A350V/CreT} transgenic mice. This specific mutation is heavily associated with Muckle-Wells Syndrome (MWS) and Familial Cold Autoinflammatory Syndrome (FCAS), one of the cryopyrin-associated periodic syndromes (CAPS) characterized by overactivation of the NLRP3 inflammasome due to mutations to NLRP3. This mutant NLRP3 can spontaneously oligomerize into the active NLRP3 inflammasome without the need of activation signals. Collectively, the results from selectivity studies and the BMDMs carrying the mutant NLRP3 suggest that JC-21 may directly target the NLRP3 inflammasome complex.^{10,11}

2.2 JC-21 Analog, JC-171, Inhibits the NLRP3 Inflammasome

Although JC-21 showed promising activity as a novel NLRP3 inflammasome inhibitor, solubility was observed as an issue during the experiments. To improve aqueous solubility and also to evaluate whether structural modifications on the sulfonamide moiety are tolerated, a hydroxy group was introduced by the hydroxamic acid analog JC-171 (Figure 12). The Log P for JC-21 and JC-171 is 0.80 and 0.19, respectively, confirming the increased polarity of JC-171. Our studies in mouse macrophage J774A.1 cells demonstrated a dose-dependent inhibition of IL-1 β by treatment with JC-171 with an IC₅₀ of 8.5 \pm 1.6 μ M but no inhibition of cytokines IL-6 and TNF α (Figure 13).¹²

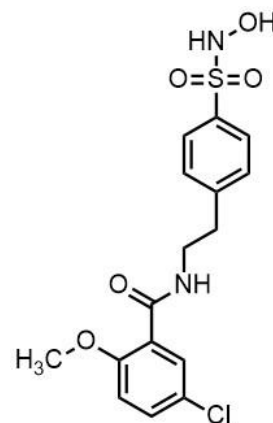


Figure 12. Structure of JC-171.¹²

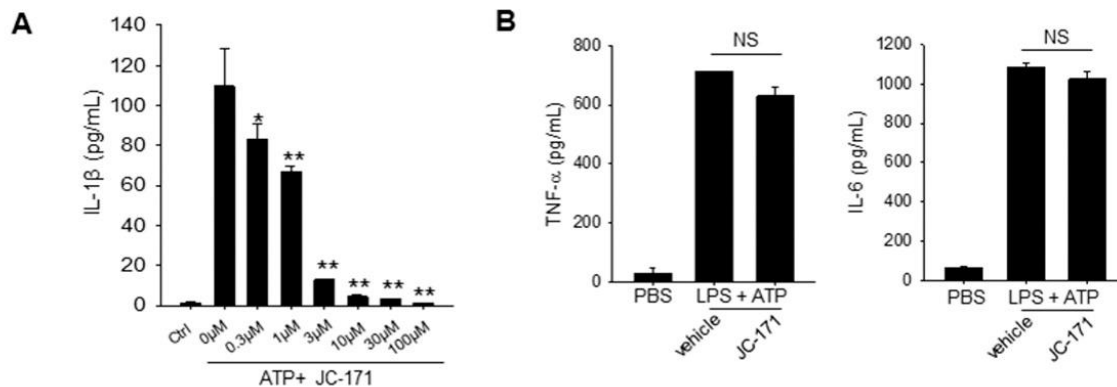


Figure 13. Inhibition of production of cytokines by JC-171. A. Dose-dependent response of inhibition of IL-1 β . B. Inhibition of control cytokines IL-6 and TNF α . Adapted from Guo et al.¹²

Prior studies employing constitutively active NLRP3 suggested that this chemical scaffold might function as an inhibitor by blocking the formation of the NLRP3

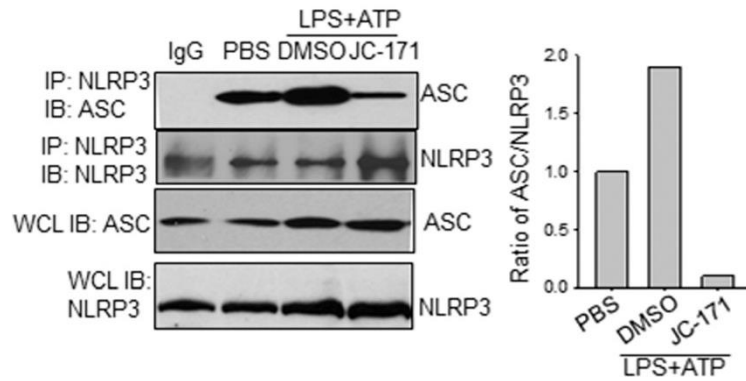


Figure 14. Inhibition of ASC association to NLRP3 by JC-171. NLRP3 and ASC were visualized via immunoblot (left). Ratio of band intensity of ASC to NLRP3 was calculated (right). Adapted from Guo et al.¹²

inflammasome complex. In order to determine this, a co-immunoprecipitation (IP) study was done using primary BMDMs stimulated with LPS and ATP. Shown in Figure 14, treatment of BMDMs with JC-171 blocked the association of ASC to the NLRP3 protein during activation. This provided further evidence to the

hypothesis that this novel chemical scaffold inhibits the NLRP3 inflammasome directly.¹²

Considering neuroinflammation is a critical component of MS pathology and the demonstrated role of the NLRP3 inflammasome in MS,¹⁵⁰⁻¹⁵² JC-171 was tested in experimental autoimmune encephalomyelitis (EAE), a mouse model of MS, for evidence that NLRP3 inhibitors can serve as potential therapeutic agents for MS. The therapeutic potency of JC-171 was tested alongside MCC950 by administration of either compound starting when the clinical scores of individual mice have reached 1 (flaccid tail). Subsequent clinical scores were assigned every other day based on the extent of paralysis of the mouse. Regardless

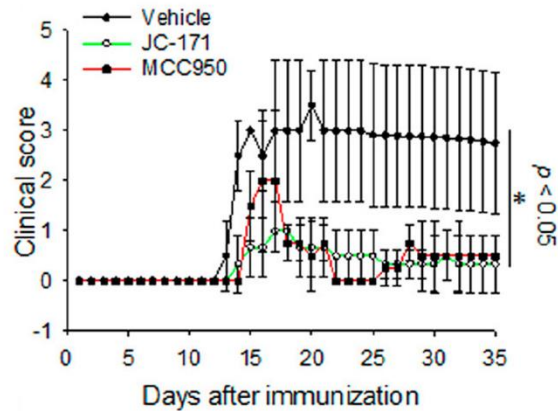


Figure 15. Clinical scores of EAE mice dosed with either 10 mg/kg of JC-171 (green line), 10 mg/kg of MCC950 (red line), or vehicle (black line). Adapted from Guo et al.¹²

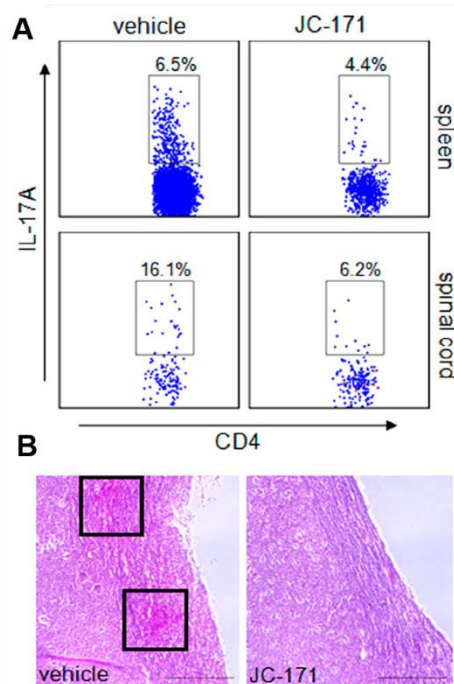


Figure 16. Determination of demyelination of spinal cord and frequency of MOG specific Th17 cells in the spinal cord and spleen. A. The frequency of IL-17A⁺CD4⁺ Th17 cells in the spinal cord and spleen. B. Demyelination (indicated by black squares) in the spinal cord. Adapted from Guo et al.¹²

of the use of a low dose of JC-171 (10 mg/kg) in mice, JC-171 significantly attenuated EAE progression when compared with control (Figure 15). JC-171 exhibited comparable *in vivo* therapeutic activity with MCC950, an NLRP3 inflammasome inhibitor that was recently reported to block EAE development.¹⁵³ Additionally, treatment with JC-171 also led to a substantial decrease in the frequency of MOG₃₅₋₅₅-specific Th17 cells in both the spleen and spinal cords of EAE mice (Figure 16). Consistent with the reduction in clinical score, the histological analysis demonstrated that demyelination was reduced in the white matter of the spinal cords from EAE mice treated with JC-171, as indicated by Luxol fast blue staining (Figure 16). Collectively, the *in vitro* and *in vivo* results of JC-171 and JC-21 suggest that this chemical scaffold is a promising template for the development of small

molecule inhibitors for the NLRP3 inflammasome.^{11,12} Furthermore, this data also encourages the further development of JC-171 and analogues as potential therapeutic agents for MS as well as other inflammatory diseases involving the NLRP3 inflammasome.¹²

Chapter 3: Mechanistic Studies of Sulfonamide-based small molecule NLRP3 inflammasome inhibitors

Our studies suggested that analogs derived from this sulfonamide scaffold may directly interfere with the formation of the NLRP3 inflammasome complex. This was based on the fact that 1) inhibitors block ASC recruitment;¹² 2) they do not directly inhibit caspase-1 activation as NLRC4 and AIM2 pathways are not affected;¹¹ and 3) they block the release of IL-1 β and the activation of caspase-1 in macrophages expressing constitutively active NLRP3 from mutant mice.^{11,12} However, it is not clear how the inhibitors based on this chemical scaffold interfere with the formation of such protein complex. It is therefore our goal in this research project to elucidate the mechanism of action (MOA) for this chemical scaffold as direct NLRP3 inflammasome inhibitors by biophysical, biochemical and computational studies. Specifically, the microscale thermophoresis (MST) assay was utilized to determine the binding affinity of our compounds to various components of the NLRP3 inflammasome. Mechanistic studies involving the ATPase of the protein and molecular modeling were also employed to determine the possible binding site for our compounds. Finally, with liquid chromatography-mass spectrometry, the BBB penetration of our compound was measured.

3.1 MST Assay

3.1.1 Introduction to MST

To measure the affinity of a direct interaction of our compounds with various components of the NLRP3 inflammasome, MST was employed. MCC950, a known

inhibitor that targets the NLRP3 inflammasome pathway was tested alongside our compounds to determine whether there was a shared MOA. As a relatively new technique, MST is used to quantify biomolecular binding interactions. MST uses a laser to create a thermal gradient in each capillary with fluorescently tagged-protein and varying concentrations of the non-labeled ligand or protein. The MST uses any change in thermophoresis caused by a change in the hydration shell around the fluorescent protein, change in size, charge, or conformation of the protein from binding interactions. Such binding interaction will change the movement of the protein in the thermal gradient and then can be detected by the fluorescence from the tagged-protein. Consequently, this enables a quantification of bound versus unbound protein to the ligand and therefore binding affinity (K_D) of the ligand to protein can be calculated.¹⁵⁴

The binding check feature of the MST compares the normalized fluorescence (F_{norm}) of labeled protein to the F_{norm} of the labeled protein with ligand. Additionally, the binding check feature allows determination of any interfering fluorescence from buffer or ligand. The binding check can quickly determine if any binding can be detected without consuming as much protein as the binding affinity test. For the binding affinity test, the protein concentration is kept constant with 12 different concentrations of unlabeled ligand in each capillary. From the ΔF_{norm} calculated in each capillary, a binding dependent sigmoidal curve should appear in the case of a binding event. The fraction bound can then be determined from the ΔF_{norm} curve and a K_D can be determined.^{154,155}

Initial fluorescence in each capillary is measured to ensure each value does not vary more than 10%. If initial fluorescence varies it could indicate either poor pipetting technique or ligand induced fluorescence changes; in either of these cases an accurate

K_D cannot be determined. Additionally, aggregation and adsorption to the capillary wall of the fluorescent protein is also determined to ensure a good quality sample. In addition to these automatic quality control checks, a few rules need to be applied when analyzing data to determine if the results can be reliably distinguished from noise. The amplitude of the noise in the baseline should be at the least 3 times less than the response amplitude between bound and unbound F_{norm} values. Finally, as determined through experimentation with known binding interactions, the cut off response amplitude between bound and unbound should be ≥ 5 for reliable and reproducible results.¹⁵⁵

3.1.2 MST Results and Discussion

3.1.2.1 Binding interaction with the recombinant and full length NLRP3 protein

We first tested the binding interactions of JC-171 and MCC950 with human recombinant full-length NLRP3 protein by MST. The NT-647 labeled full length NLRP3 protein was tested at a final concentration of 50 nM. JC-171 was tested initially at 500 μ M with the binding check feature. The excitation was set to 40% for sufficient fluorescence counts and the power was set to medium for the best signal to noise ratio. The results revealed a response amplitude of 8.1 and a signal to noise ratio of 10. This clearly indicated a binding interaction between JC-171 and the NLRP3 protein. Following the binding check, a binding affinity assay of JC-171 to NLRP3 was then tested in triplicate at a range of 500 μ M -122 nM. The results established a K_D of $2.54 \pm 0.500 \mu$ M, consistent with its IC_{50} for inhibition of the production of IL-1 β . Notably, when MCC950 was tested in MST assays, no binding interaction was observed (Figure 17, 18). The results are in agreement with the published data to show that MCC950 does not interfere with NLRP3-

NLRP3 interactions.¹⁵³ The binding affinity results of JC-171 and MCC950 strongly suggest that they have distinct MOAs to inhibit the NLRP3 inflammasome.

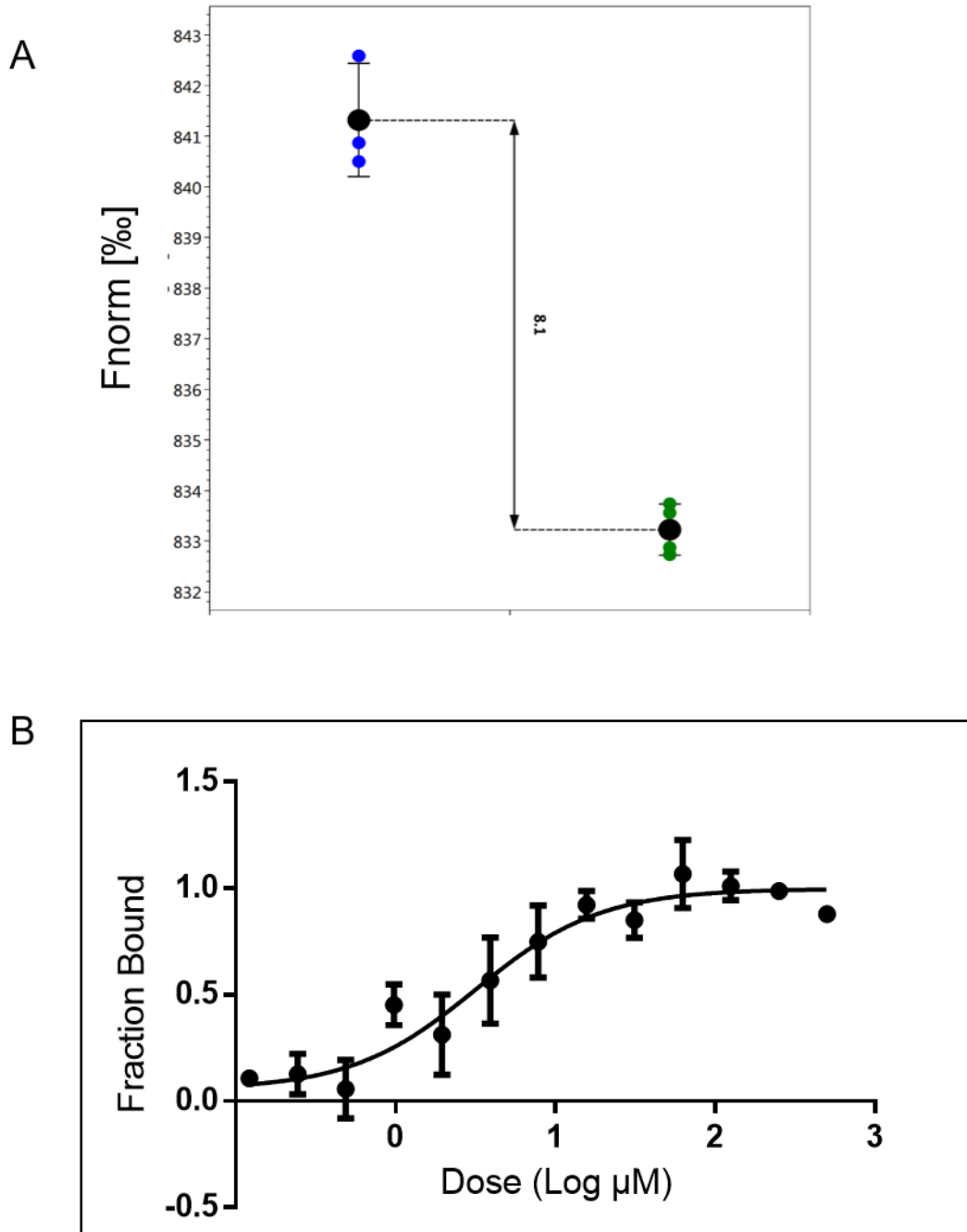


Figure 17. MST assay for affinity of JC-171 for fluorescently tagged (NT-647) full length NLRP3. A. Binding check for JC-171. B. Calculated fraction bound dose-response of binding interaction of JC-171 and full length NLRP3.

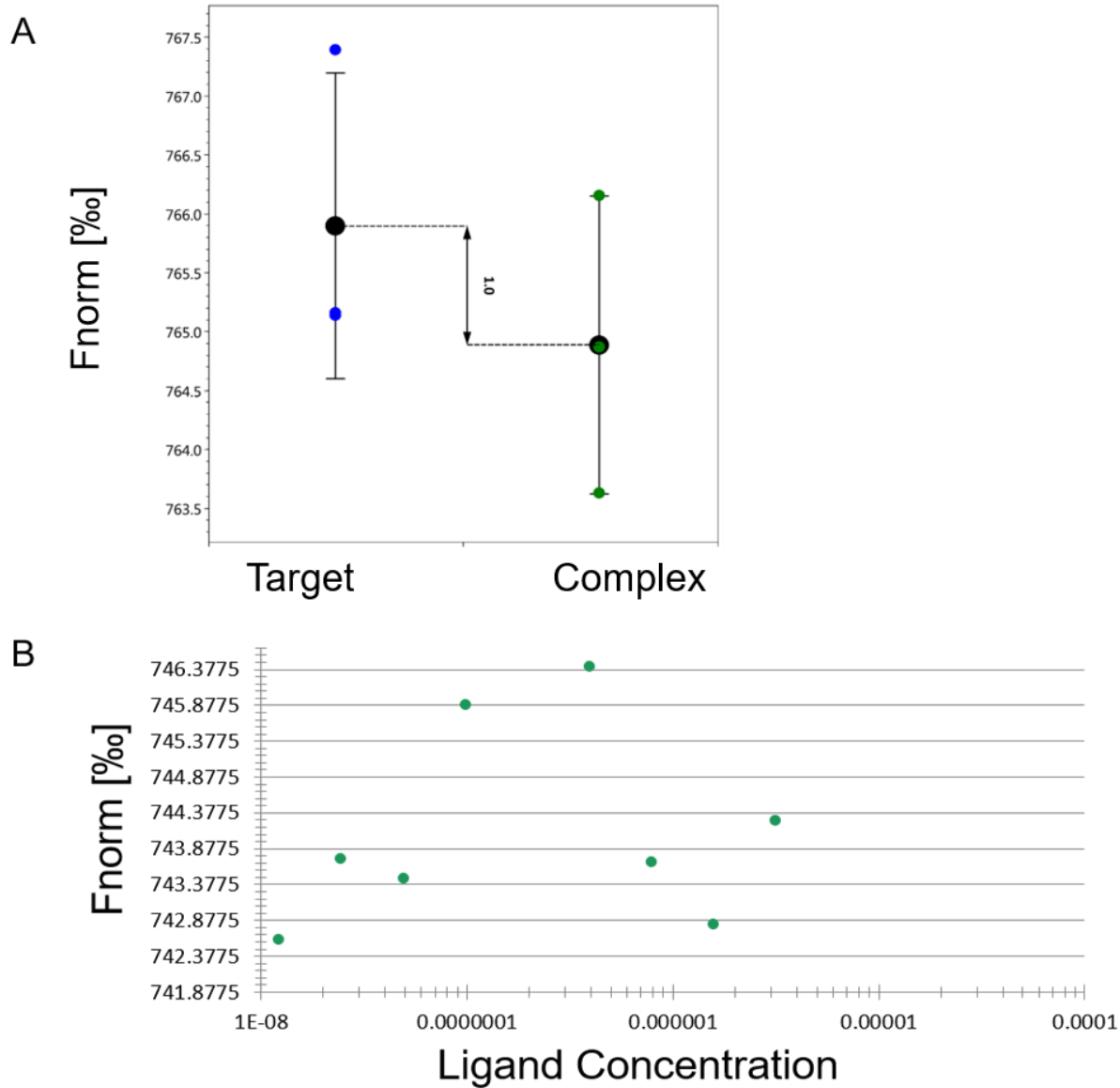


Figure 18. MST assay for affinity of MCC950 for fluorescently tagged (NT-647) full length NLRP3. A. Binding check for MCC950. B. Calculated Fnorm dose-response of MCC950.

3.1.2.2 Binding interaction with the mutant NLRP3 (K232A) Protein

To further identify the binding domain within the NLRP3 protein for our compounds, a fluorescently labeled mutant NLRP3(K232A) was used to explore any change in binding

affinity for JC-171. K232 is one of the amino acids in the walker A motif of the nucleotide-binding domain (NACHT). This amino acid coordinates with the gamma phosphate of ATP and is essential for ATPase activity.¹²⁴ The binding check studies showed a

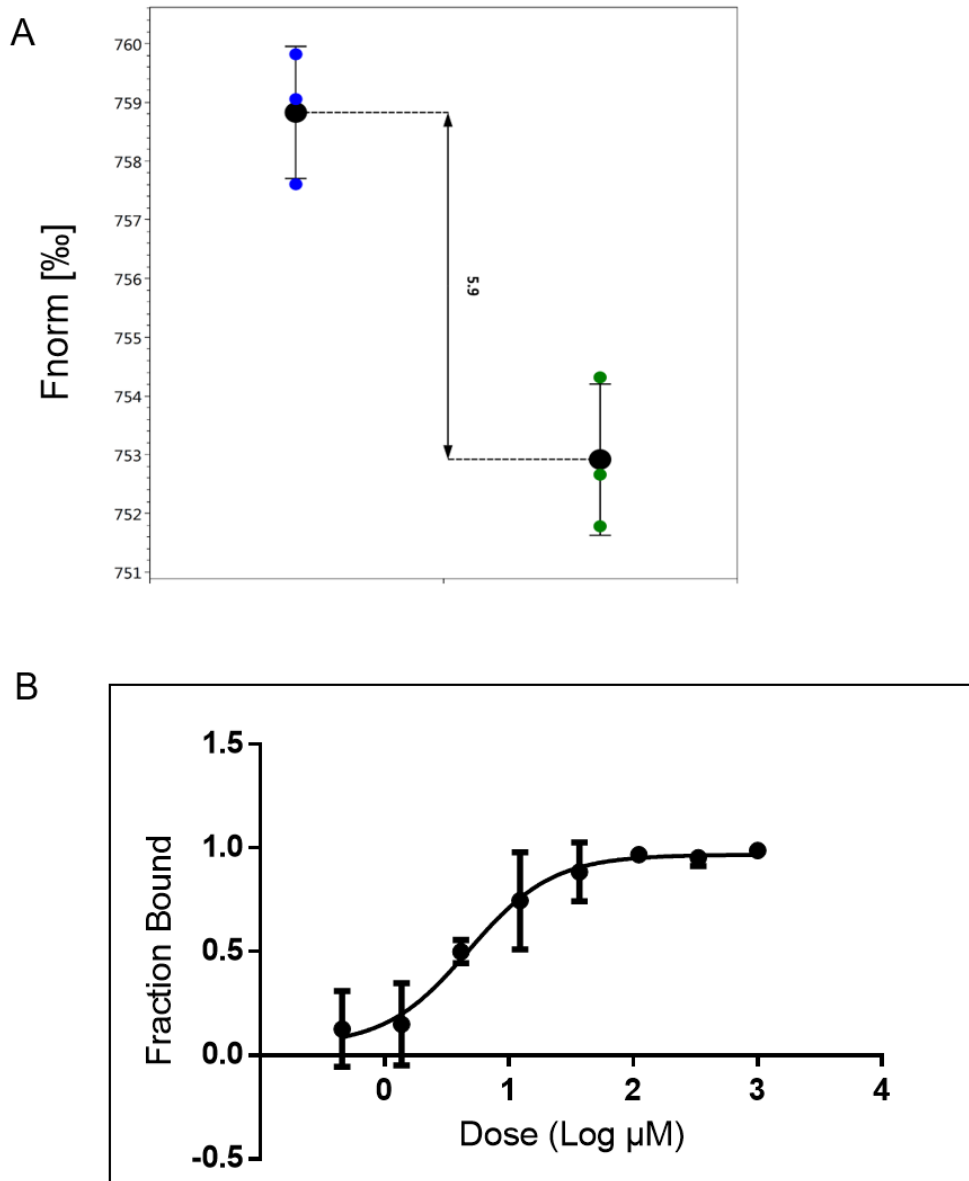


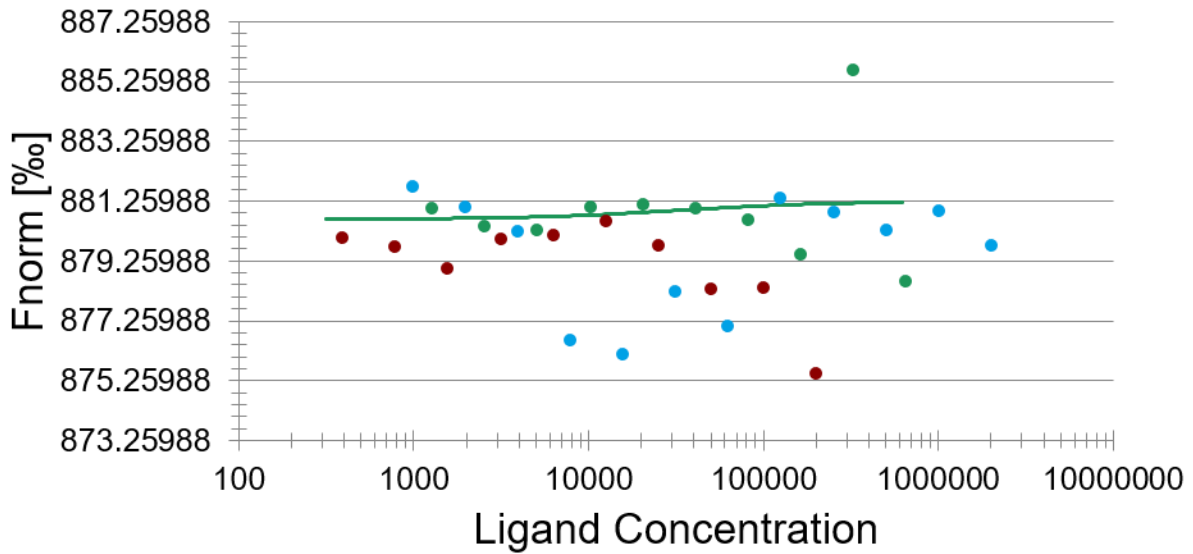
Figure 19. MST assay for affinity of JC-171 for fluorescently tagged (NT-647) full length NLRP3 mutant (K232A). A. Binding check for JC-171. B. Calculated fraction bound dose-response of JC-171.

response amplitude > 5 and a signal to noise ratio of 5, suggesting binding interactions of JC-171 with NLRP3(K232A). Further binding affinity studies established a K_D of $4.58 \pm 2.13 \mu\text{M}$ (Figure 19), comparable to the binding affinity from the full length NLRP3 protein. These results suggest that the binding site for our compound is not overlapping with the ATP binding site.

3.1.2.3 Binding interaction with the LRR Component of the NLRP3 protein

To further investigate which domain of NLRP3 our inhibitors might bind to, MST assays were conducted using the LRR fragment of the NLRP3 protein. In this study, the analogs of JC-171: GA3, HL-12, and HL-16 were tested for binding affinity. In our cellular assays, HL-12 and HL-16 are potent inhibitors on the release of IL-1 β with IC₅₀s of 0.670 μM and 1.30 μM , respectively. Additionally, MCC950 was also tested for binding affinity. The NT-647 labeled LRR component of NLRP3 protein was used at a final concentration of 50 nM. The MST assay conditions were set identical to the ones used in full length NLRP3 protein. GA3 was tested in triplicate with a range of 1 mM to 0.15 μM (Figure 20). MCC950 was tested in triplicate at a range of 200 to 0.07 μM (Figure 20). No binding interactions were observed for both GA3 and MCC950 under the current experimental conditions. This may suggest that our compounds do not bind to the LRR domain within the NLRP3 protein. Similarly, we did not detect binding interactions for analogs HL-12 and HL-16 (Figure 21). Collectively, the results strongly suggest that there are no binding interactions for the tested compounds from our studies to the LRR domain of the NLRP3 protein.

A



B

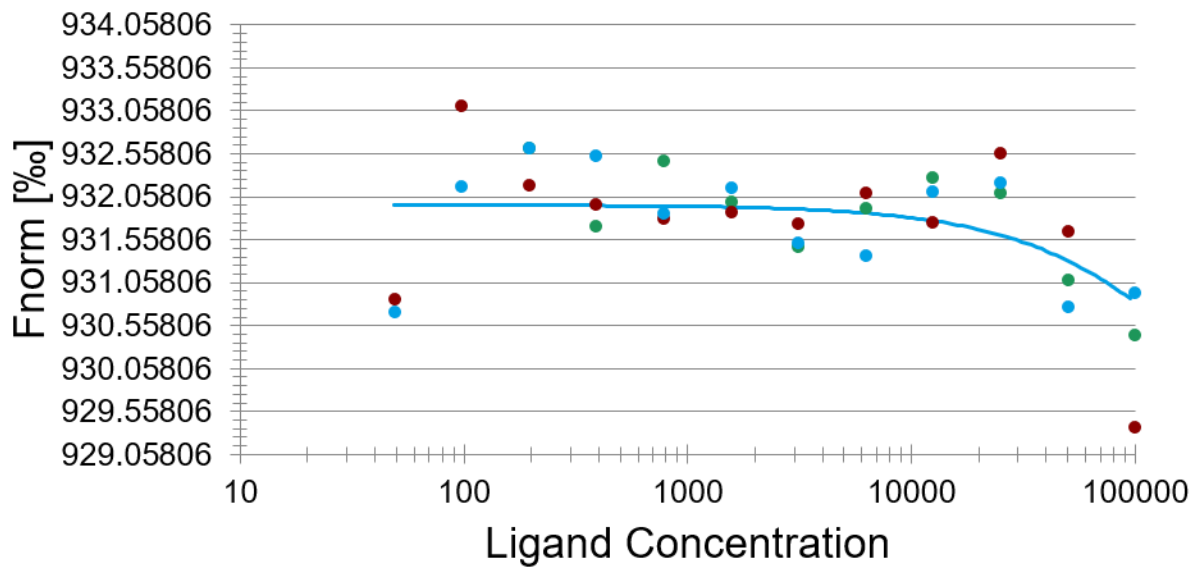


Figure 20. MST assay for affinity of GA3 and MCC950 for fluorescently tagged (NT-647) NLRP3 LRR segment. A. Calculated Fnorm dose-response curves of GA3. B. Calculated Fnorm dose-response curves of MCC950

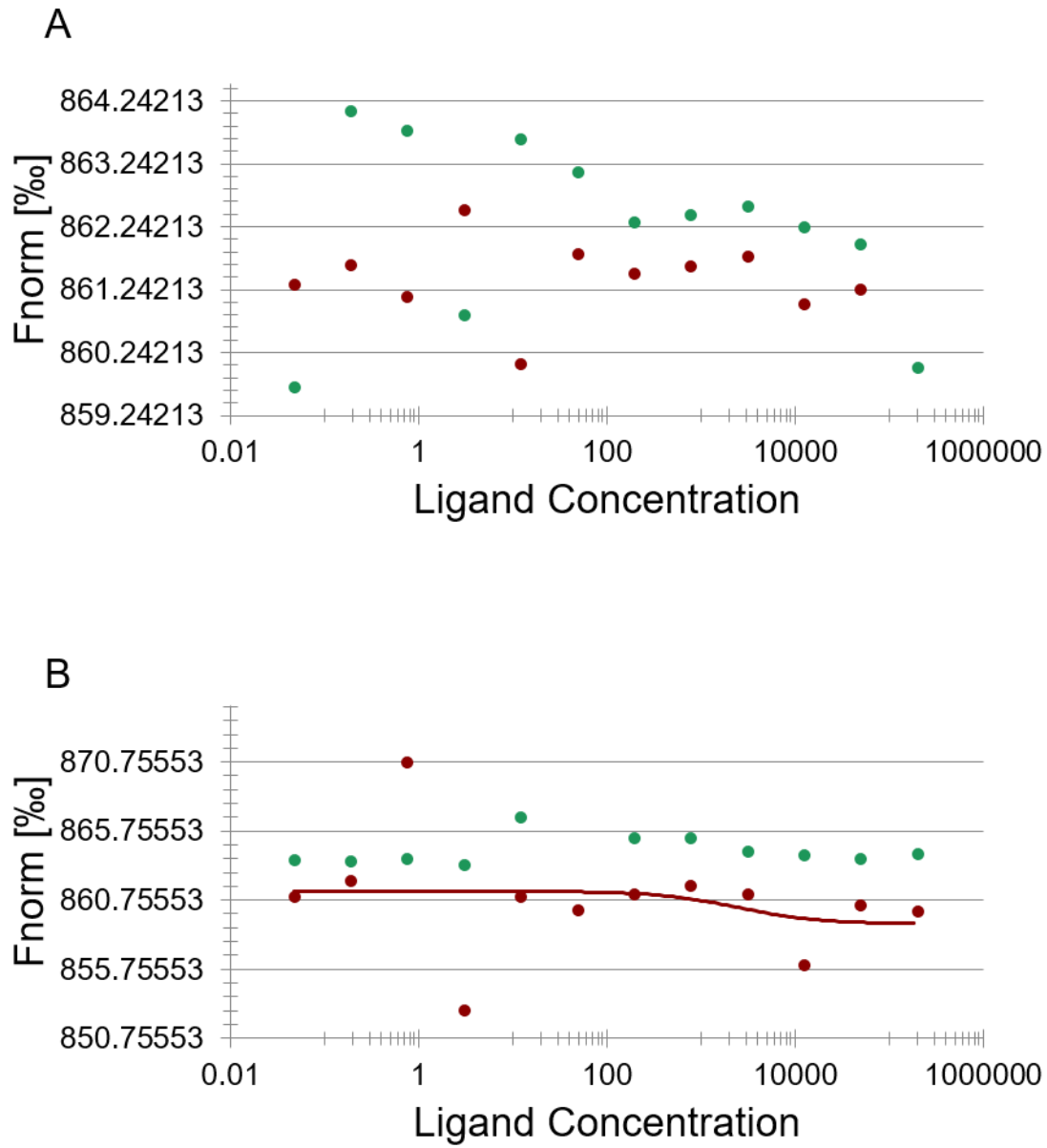


Figure 21. MST assay for affinity of JC-171 analogs for fluorescently tagged (NT-647) NLRP3 LRR segment. A. Calculated Fnorm dose-response curves of HL-12. B. Calculated Fnorm dose-response curves of HL-16.

3.1.2.4 Binding Interactions to the ASC Protein

The NLRP3 inflammasome is a multiprotein complex with at least three proteins: NLRP3, ASC, and caspase-1. Since strong evidence has been presented to disregard

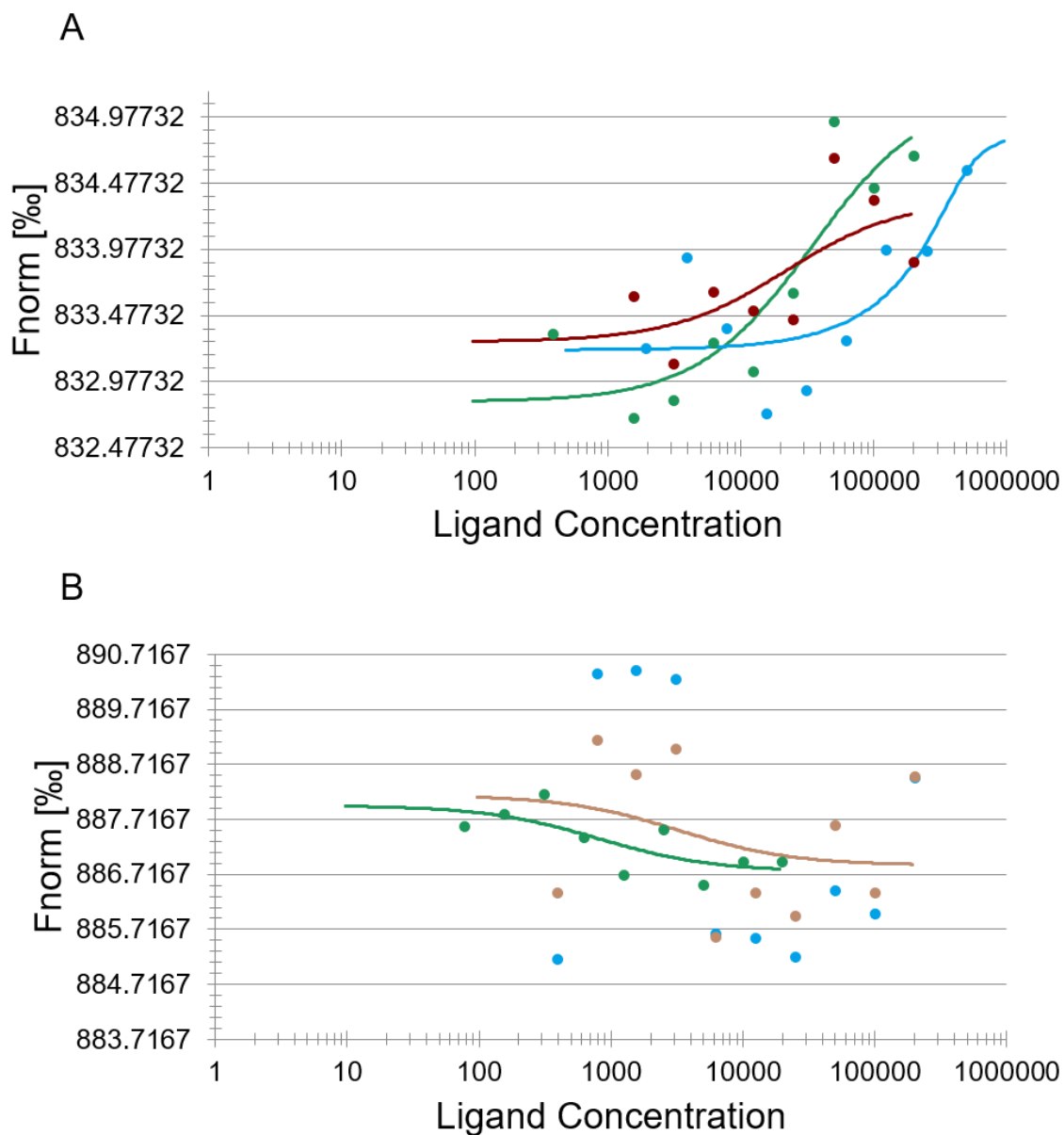


Figure 22. MST assay for affinity of compounds for fluorescently tagged (NT-647) ASC protein. A. Calculated Fnorm dose-response curves of GA3 from MST assay. B. Calculated Fnorm dose-response curves of MCC950 from MST assay.

binding interactions with caspase-1 as the MOA, further investigation into the binding interactions with ASC was investigated to better establish that interaction with ASC was not the MOA of our compounds. To evaluate whether our compounds bind to the adapter protein ASC, MST studies were conducted for GA3 and MCC950. The NT-647 labeled ASC protein was tested at a final concentration of 10 nM. The MST excitation was set to 95% for sufficient fluorescence counts and the MST power was set to medium for the best signal to noise ratio. As shown in Figure 22, a binding curve might be observed for GA3 to ASC protein. However, the response amplitudes remained below 5 and poor signal to noise ratios were observed. This indicated that the signals could not be distinguished from noise. MCC950 was also tested in a range of 200 to 0.07 μ M and no binding interaction was observed as well under the experimental conditions (Figure 22).

3.2 Direct Binding to NLRP3

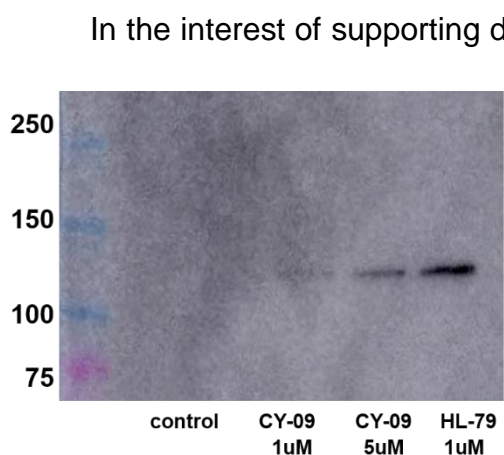


Figure 23. Immunoblot of J774A.1 lysate incubated with biotin probes of CY-09 or JC-171 analog (HL-79) using antibody specific for NLRP3. Positive control is CY-09 probe known to bind to NLRP3 and negative control is cell lysates without probe.

the mechanism of action of the compound, a pull-down assay coupled with immunoblotting was performed by Dr. Liu He. J774A.1 primary mouse macrophage cells were pretreated with LPS to induce production of NLRP3 protein. Cell lysates were incubated with control compound CY-09-probe, a positive control that demonstrated ability to bind to NLRP3 in pull down assay,¹⁴⁶ or a biotin conjugated probe analog of JC-171 compound, HL-79. Lysates

were incubated with beads to capture biotin probes, washed, and then boiled and resultant protein run on SDS-PAGE followed by an immunoblot with primary antibody for NLRP3 and secondary antibody with attached HRP for visualization (Figure 23). HL-79 probe captured NLRP3 better at 1 μ M than positive control CY-09 probe at 5 μ M. This data further supported direct interaction with the NLRP3 protein as being the mechanism of action of these compounds for inhibition of the NLRP3 inflammasome.

3.3 ATPase activity of the NLRP3 protein

3.3.1 Introduction to the NLRP3 ATPase

Due to the conserved nature of the ATP binding pocket among the NACHT domains of inflammasomes, it would be of importance to determine whether our compounds interfere with the ATPase activity of NLRP3, given the fact that our binding studies strongly suggest the interaction of our compounds with the NACHT domain. The ATPase activity study will also support the results of the binding interaction of JC-171 to the mutant NLRP3 (K232A). Furthermore, despite the importance of K232 to ATP binding, other conserved residues are also involved in ATP binding of the walker A motif.¹⁵⁶ Therefore, the investigation of the ATPase interference by our inhibitors will provide valuable information on whether or not there is any interaction with our compounds and the ATP binding pocket. In order to determine the ATPase activity of NLRP3 protein, the ADP-Glo assay (Promega, Madison, WI) was employed.

3.3.2 ADP-Glo Results and Discussion

After incubation of compounds with human recombinant NLRP3 protein following references protocol,¹⁴⁴ ATP was the added for hydrolysis. The positive control contained

only protein and ATP to determine the percent conversion of ATP to ADP. The negative control was a blank with no protein or ATP to determine if there was any background signal. A standard curve of ATP and ADP from 250 μM of ADP (100% conversion) to 0 μM of ADP (0% conversion) and the corresponding concentrations of ATP 0 μM to 250 μM was established (Figure 24). The r^2 of the fit was > 0.991 . The assay was done in triplicate alongside a standard curve for each repeat and the signal from the samples was normalized as a percentage of the positive control to better visualize percent inhibition of the ATPase.

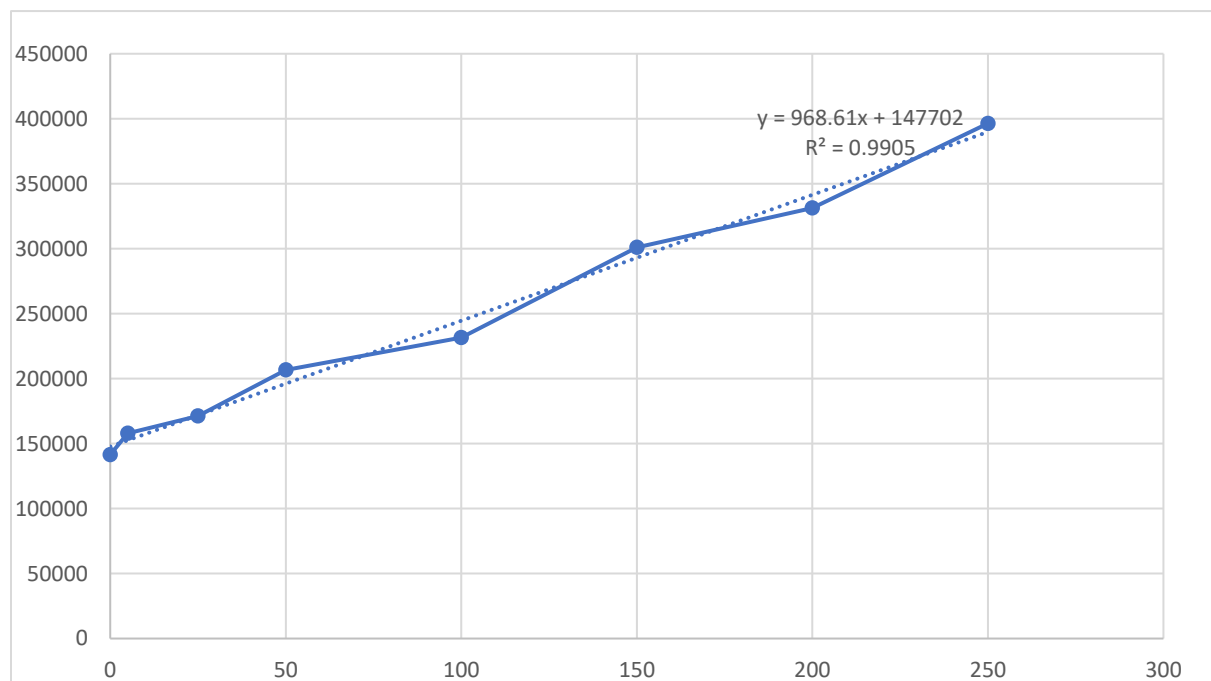


Figure 24. Representative standard curve tested samples from one assay of the triplicate performed. The equation for the fit and r^2 are displayed in the upper right-hand corner of the graph.

As shown in Figure 25, no inhibition on the ATPase activity of NLRP3 was observed for all of the tested compounds. Combining the results of binding interaction with mutant NLRP3 (K232A), the results suggest that our compounds do not bind to the ATP binding

pocket within the NLRP3 protein. However, our results suggested a relatively low conversion rate of ATP ($\leq 5\%$) by the ATPase of NLRP3 under the current experimental conditions. Further testing is warranted with a higher concentration of NLRP3 to decisively conclude none of the compounds interfere with the ATPase activity.

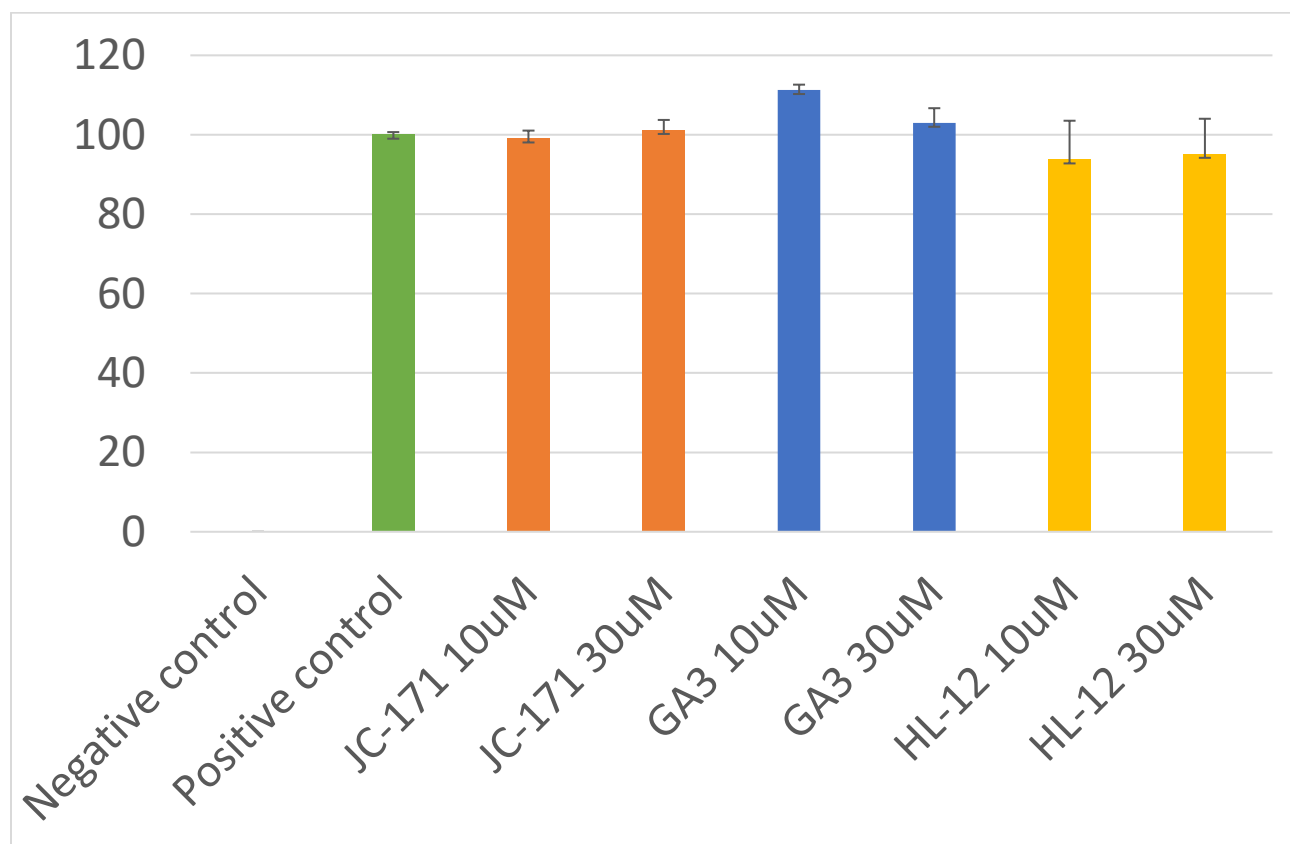


Figure 25. ADP-Glo assay to determine inhibition of ATPase activity of the NLRP3 protein by JC-171 and other analogs. Luminescence signals were normalized as percentage of the positive control.

3.4 Molecular Modeling studies

3.4.1 Introduction to Molecular Modeling of the NLRP3 Protein

The protein binding experiments and ATPase activity studies indicated that JC-171 binds to the NLRP3 protein but not to the adaptor protein ASC of the NLRP3 inflammasome. The results further suggested that our compound may bind to the NACHT

domain of NLRP3 protein, but without interfering with ATP binding. To further support this conclusion and visualize the possible binding sites of our compounds to the NACHT domain of NLRP3, a homology model of the NACHT domain was constructed from the X-ray crystal structure of NLRC4 with MODELLER.^{157,158} NLRC4, Nod-like receptor card domain containing protein, is another member of the NLR family that recruits caspase-1. Unlike NLRP3, NLRC4 contains an N-terminal CARD domain. Additionally, NLRC4 inflammasome is activated by flagellin and type III secretion systems of gram negative bacteria instead of extracellular ATP and other DAMPs that activate NLRP3.¹⁵⁹ The structure of NLRC4 was chosen mainly based on the sequence identity and similarity of its NACHT domain to the NACHT domain of NLRP3 protein. Homology models generated using template structure were filtered by Ramachandran plots. To further validate the model, ADP from the crystal structure was docked back into the nucleotide binding pocket of the model and HINT scores calculated to determine if hydrophobic interactions were favorable.¹⁶⁰ JC-171 was docked with GOLD and HINT score was calculated to gauge if the interaction was favorable.¹⁶¹

3.4.2 Results and Discussion

3.4.2.1 Sequence Alignment

The sequence alignment was conducted using emboss needle pairwise sequence alignment. This sequence alignment program uses the Needleman-Wunsch alignment algorithm to identify the best alignment over entire length of the sequences. The results demonstrated an identity of 24.1% and similarity of 41.2%. Gaps were measured to be 19.4% and the score was 161.¹⁶² The score is the sum of matches minus the penalty for gaps opened (Figure 26). The percentage of identity does not meet the rule of thumb for

homologs, which is $\geq 30\%$.¹⁶³ However, it is well established that these two proteins are related through the NLR family and the NACHT domains of both proteins are share similar functions.¹²⁹ Furthermore, when the sequences of the ATP binding pocket of these proteins compared, the alignment showed a sequence identity of 50% and a similarity of 75%. The alignment was therefore used to generate homology models through MODELLER.¹⁵⁷

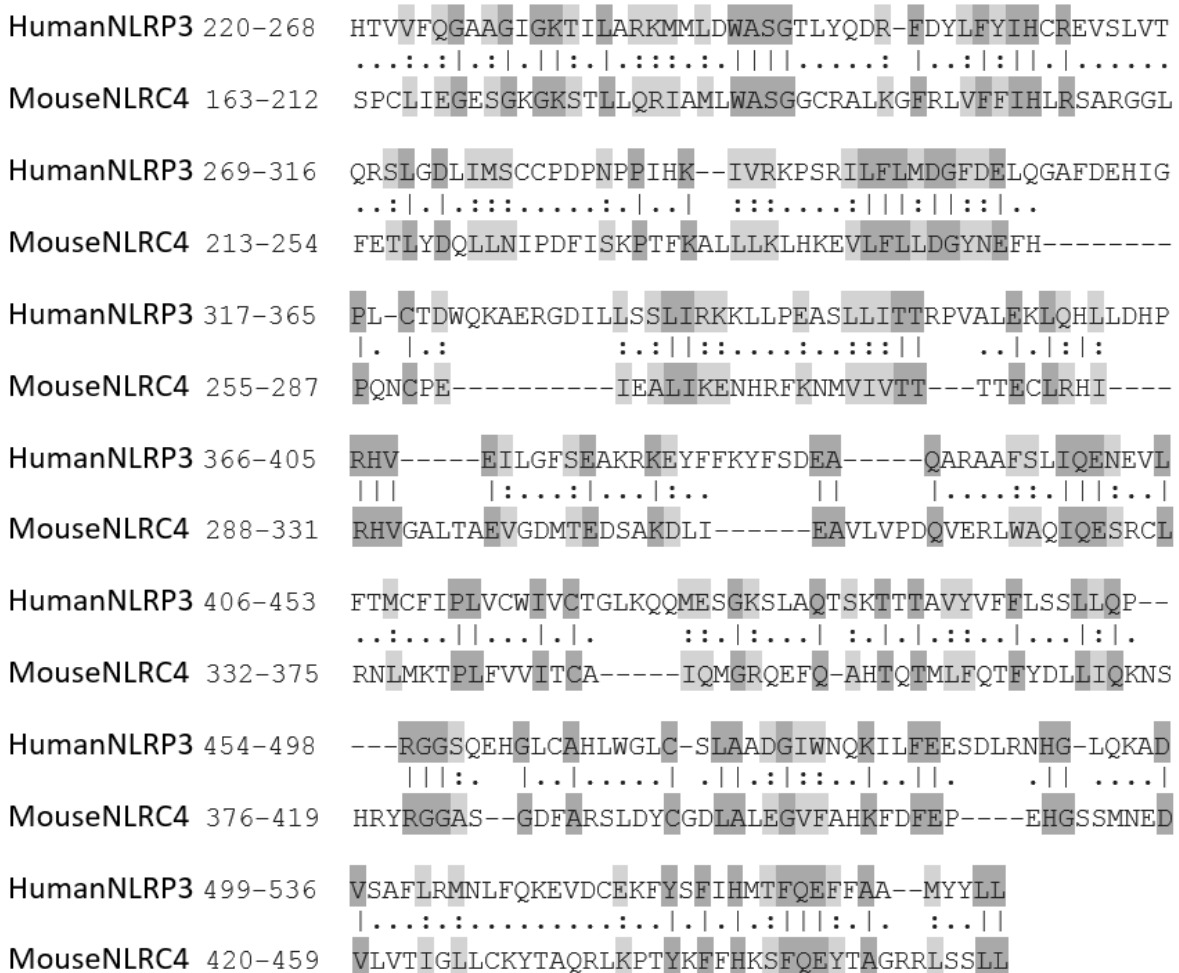


Figure 26. Sequence alignment of mouse NLRC4 NACHT domain with human NLRP3 NACHT domain by emboss needle pairwise sequence alignment. Identical amino acids between the sequences are indicated with a dark grey box. Light grey boxes are used to indicate similar amino acids between the sequence.

3.4.2.2. Structure and Validation

The models were compared by Ramachandran plots. A Ramachandran plot is important for determining the structure and conformation of the protein by comparing the dihedral angles between C α and C (ψ) and between N and C α (ϕ) of the backbone of the protein. Model 70 indicated a beta sheet and right-alpha helix structure and had some

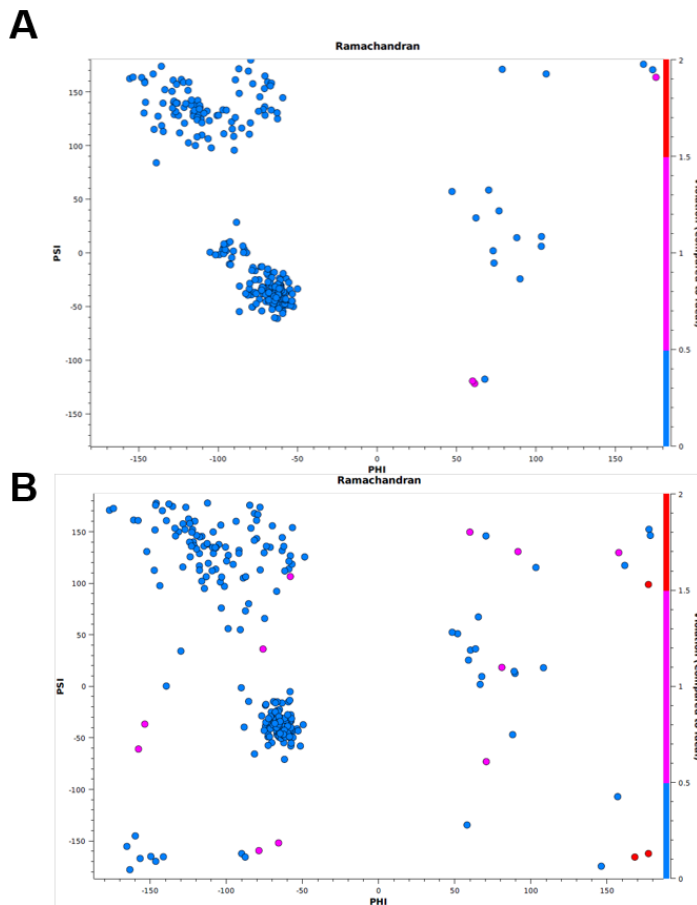


Figure 27. Ramachandran plots of NACHT domain. A. NACHT domain of NLRC4. B. Homology model 70 of NACHT domain of NLRP3. Red dots indicate violations compared to ideal.

indication of left-handed alpha helix structure. The model in general is comparable to the Ramachandran plot of template structure NLRC4 and had few violations (Figure 27). The models with the best Ramachandran plots were next compared by docking the ADP from the crystal structure of NLRC4 back into the nucleotide binding pocket (Figure 28). In model 70, ADP formed H-bond interactions with amino acids Lysine 232, Threonine 233, Glycine 229, Histidine 522, and Arginine 351 (Figure 29). Specifically, the beta phosphate of ADP formed H-bond interactions with Lysine 232, Glycine 229, and

Histidine 522. The alpha phosphate formed H-bond interactions with Lysine 232, Threonine 233, and Arginine 351. Amino acids Lysine 232, Threonine 233, and Glycine 229 correspond with the amino acids Lysine 175, Serine 176, and Glycine 172 of the NLRC4 nucleotide binding pocket where ADP forms interactions within the template crystal structure. Another amino acid that ADP binds to in model 70, Histidine 522, corresponds with the amino acid Histidine 443 in the structure of NLRC4 to which ADP binds.¹⁵⁸ Histidine 522 is a conserved amino acid in the winged helix domain of NACHT

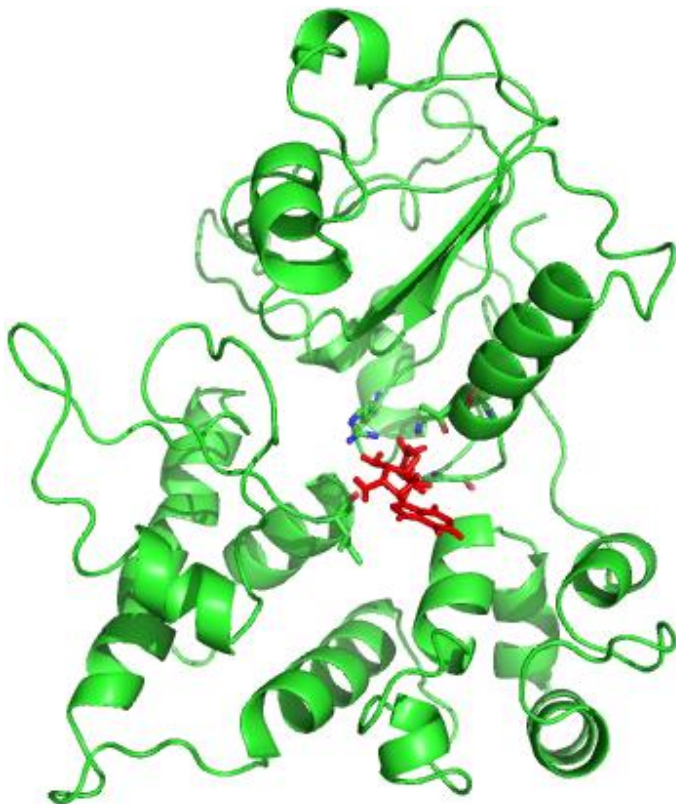


Figure 28. ADP docked in the ATP binding pocket of homology model 70. ADP is indicated in red.

domain and has been suggested to be important for the stabilization of the autoinhibition conformation.¹²⁴ In addition to interactions with the walker A motif and winged helix domain, ADP formed a H-bond interaction with Arginine 351 of the highly conserved sensor 1 motif. This motif is believed to coordinate with the nucleotide binding.¹⁵ In addition to forming hydrogen bonds with important amino acids for nucleotide binding, ADP also demonstrated favorable hydrophobic interactions

with a HINT score of 5,814.¹⁶⁰ Interactions that contributed to this score were: $5.468e^{+03}$ for hydrogen bonds, $6.442e^{+03}$ for acid/base interactions, and $1.257e^{+03}$ for hydrophobic

interactions. Unfavorable interactions that contributed to this score were: $-1.499e^{+03}$ for acid/acid interactions, $-1.766e^{+03}$ for base/base interactions, and $-4.087e^{+03}$ hydrophobic/polar interactions. Based on these observations, Model 70 was chosen for further docking studies.

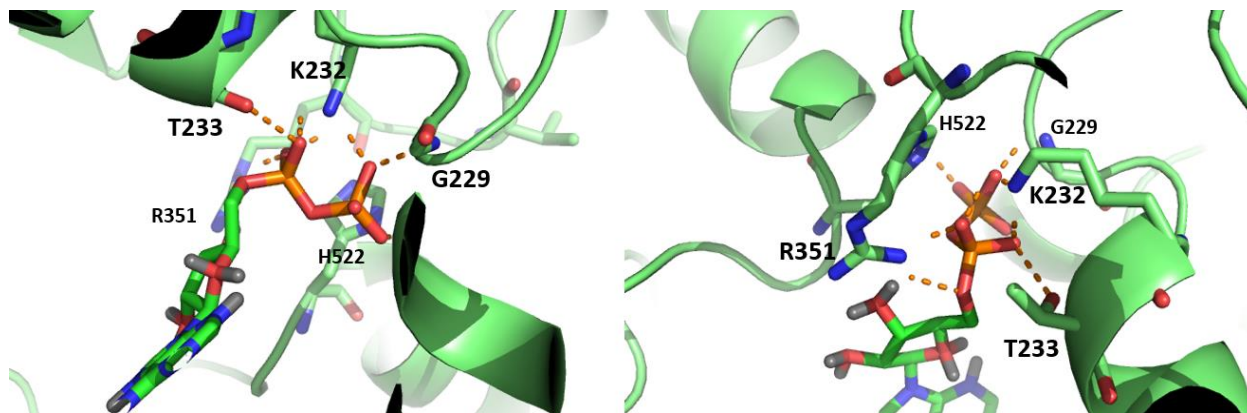


Figure 29. ADP docked into ATP binding pocket. ADP interacted with amino acids of the Walker A motif: Glycine 229, Lysine 232, and Threonine 233. ADP also formed hydrogen bond with conserved amino acid Arginine 351 of the sensor 1 motif, and Histidine 522.

3.4.2.3 Docking studies of JC-171 and other analogs

JC-171 and other analogs were docked into model 70 with GOLD v. 5.4. The binding pocket in which the analogs consistently docked with the highest CHEMPLP scores was located next to the nucleotide binding domain. Although this domain does not overlap entirely with the ADP binding pocket, it does share one amino acid at the edge of the binding pocket, Arginine 351 of the sensor 1 motif (Figure 30). Other amino acids that formed H-bond interactions with JC-171 were Arginine 237, Glutamine 509, and Isoleucine 521 (Figure 31). The CHEMPLP for JC-171 docked in the pocket was 70.53.¹⁶¹ The HINT score was calculated as 880.6.¹⁶⁰ Favorable interactions that contributed to this score include: $2.247e^{+03}$ from acid/base interactions, $9.323e^{+02}$ from hydrogen bond

interactions, and $4.830e^{+02}$ from hydrophobic interactions. Unfavorable interactions that contributed to this score include: $-1.569e^{+03}$ hydrophobic/polar interactions, $-9.325e^{+02}$ base/base interactions, and $-2.808e^{+02}$ acid/acid interactions.

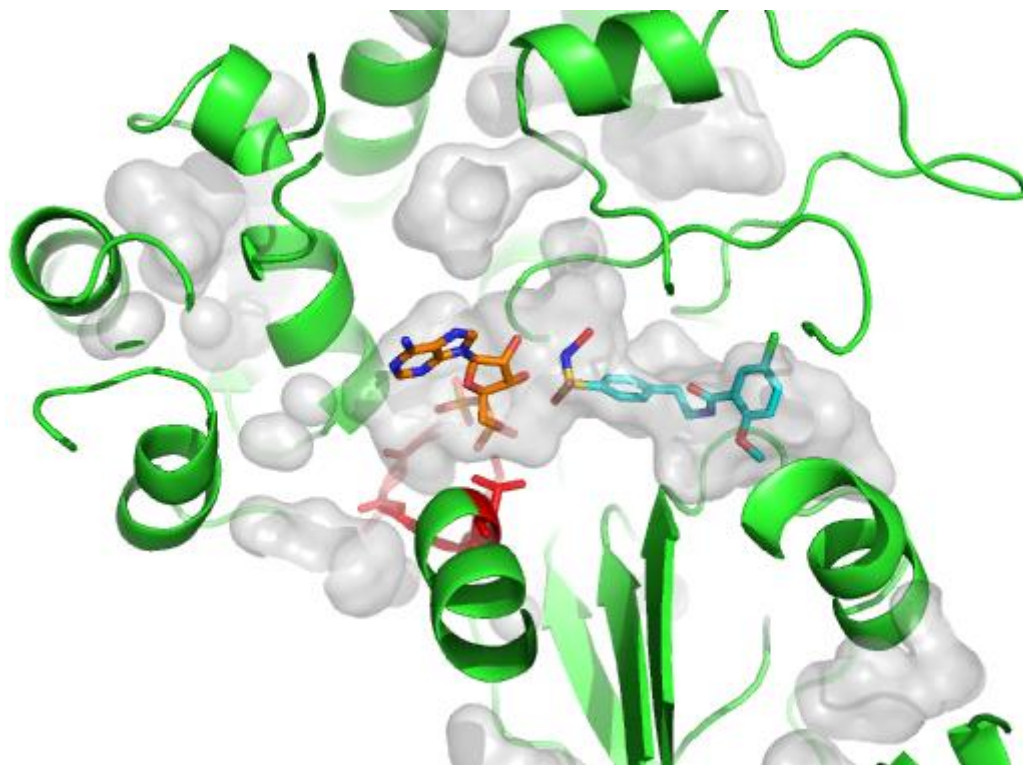


Figure 30. JC-171 docked into the pocket next to nucleotide binding pocket. Walker A motif highlighted in red. ADP is depicted as orange molecule and JC-171 is depicted as cyan molecule.

Although Arginine 351 has been implicated to coordinate with the nucleotide in ATP binding, its role in ATP binding to the NLRP3 protein is not well established.¹²⁴ Due to its close proximity to the ATP binding pocket and interaction with the winged helix domain, the binding pocket where JC-171 and other analogs docked into may represent an allosteric site that supports the autoinhibition conformation and prevents oligomerization of the NACHT domain.¹⁵ Although close to the nucleotide binding pocket, JC-171 does not bind in the binding pocket or to any amino acids in the Walker A motif. This is consistent with the MST binding results of JC-171 with mutant NLRP3 (K232A).

The binding of JC-171 to Arginine 351 does not conclusively assert that JC-171 should inhibit ATPase activity, especially given the unclear role of this residue in ATP binding. But this does raise the question that a higher concentration of NLRP3 protein and/or robust ATPase activity needs to be investigated to rule out the possibility that JC-171 will interfere with the ATPase activity of NLRP3 protein.

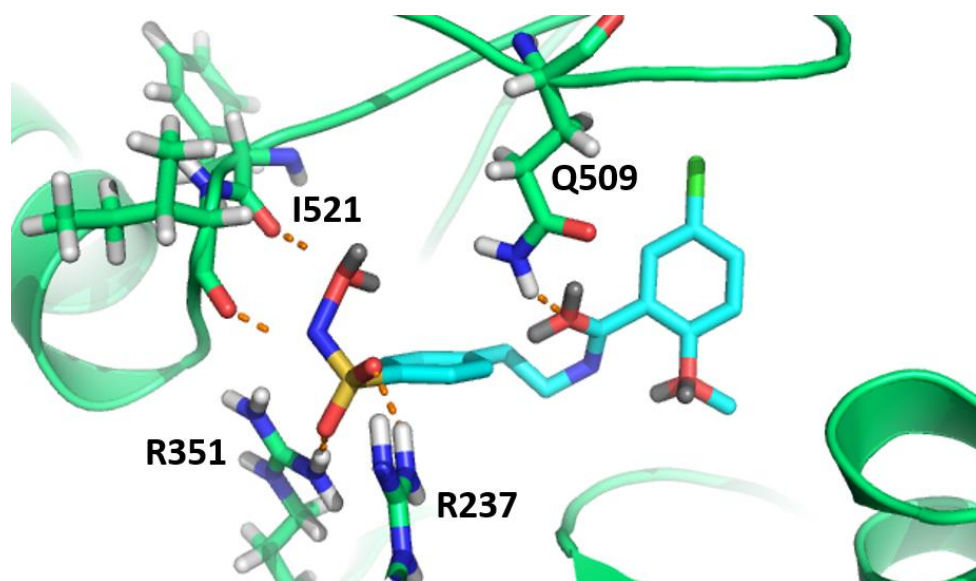


Figure 31. JC-171 binding interactions within binding pocket of the NACHT domain. Hydrogen bonds were formed with amino acids: Arginine 237, Arginine 351, Glutamine 509, and Isoleucine 521.

3.5 Production of NLRP3 protein

3.5.1 Plasmid Preparation

Given the promising results from the binding interaction, modeling, and biochemical studies, and also the need to further characterize the ATPase activity, we decided to engineer human full length NLRP3 proteins, with the expertise of collaborator Dr. Darrell Peterson, to further support our studies and facilitate the discovery of more

potent analogs. To accomplish this, a full length human NLRP3 protein with pEGFP-C2 vector for mammalian expression was obtained (Figure 32).¹³ To facilitate purification process, a His-tag was introduced to the sequence by the polymerase chain reaction (PCR) technique with a forward primer containing a sequence encoding a His-tag.

pEGFP-C2 Vector Information

GenBank Accession #: U57606

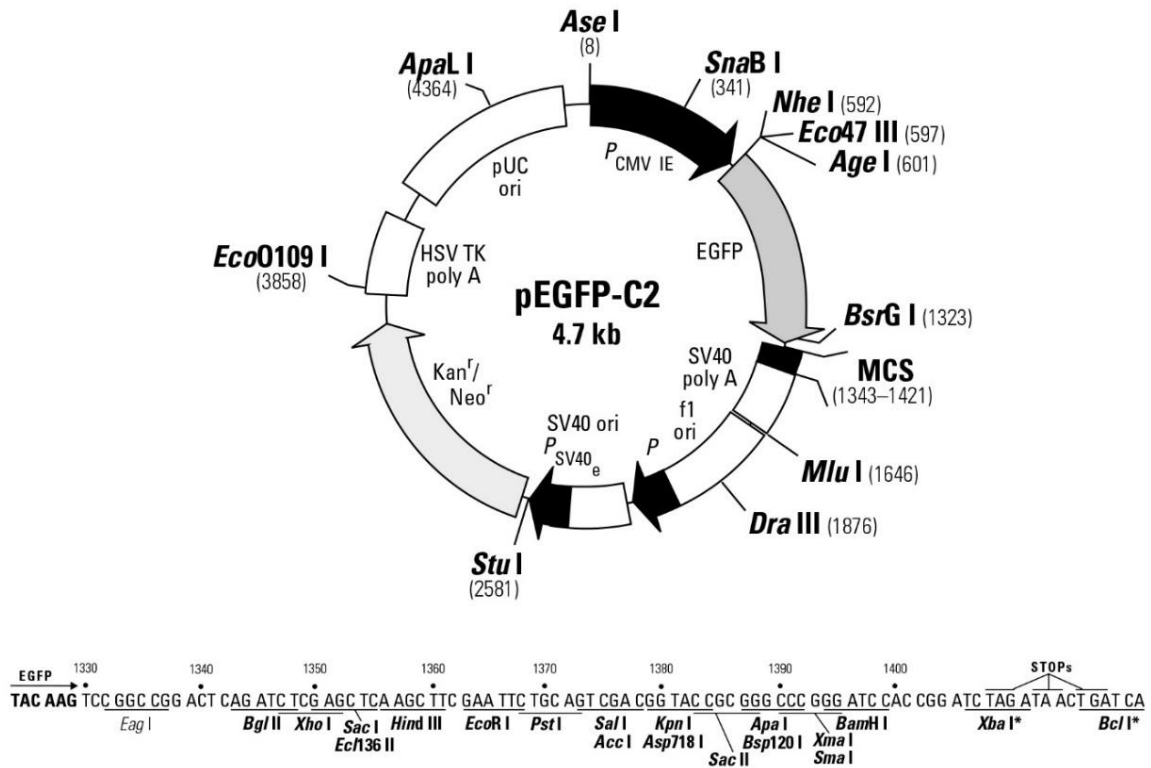


Figure 32. pEGFP-C2 vector with full length human NLRP3 protein insert.

Unfortunately, the attempt with PCR for the full sequence with the primer encoding His-tag did not succeed. The sequence was re-examined for possible restriction sites that could be utilized to synthesize the sequence in parts (Figure 33). Restriction sites are palindromic sequences that specific restriction enzymes can recognize and cleave. Cleavage of the double stranded DNA then leaves an over-hang DNA which can then be

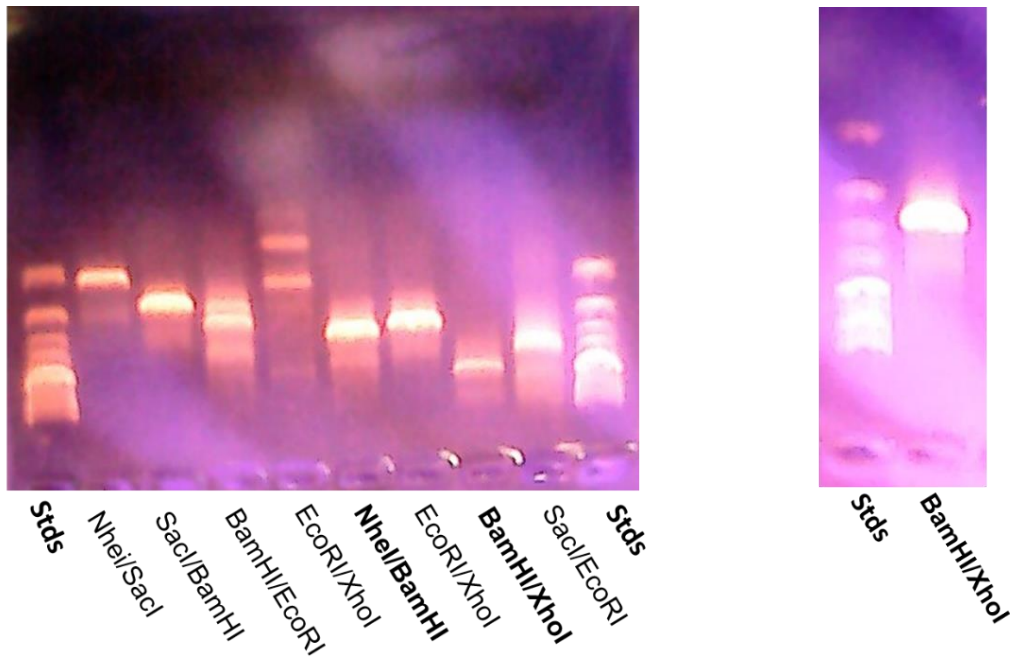


Figure 34. PCR products run on agarose gel. (Left) PCR products for pieces: NheI/SacI, SacI/BamHI, BamHI/EcoRI, EcoRI/XhoI, NheI/BamHI, EcoRI/XhoI, BamHI/XhoI, and SacI/EcoRI. (Right) Second PCR attempt at BamHI/XhoI.

forward primers: NheI/BamHI 5'-ggatgctagcatgcaccatcaccatcaccatgcaagcaccgctgcaagctggccagg-3' and BamHI/XhoI 5'-caggatcccgttgaagcttcccagccgagacgtg-3'. The reverse primers to make these pieces were: BamHI/NheI 5'-gggatcctggaacgttcgtcccttctcttttctc-3' and XhoI/BamHI 5'-gcctcgagctaccaagaaggctc aaagacgacgg-3'. The PCR products for NheI/BamHI and BamHI/XhoI were recovered with Qiaquick gel extraction kit. The expression vector used for NheI/BamHI and BamHI/XhoI was expression vector pcDNA 3.1/Hygro that has all three necessary restriction sites (Figure 35).¹⁶⁵ NheI/BamHI and BamHI/XhoI and their corresponding vectors were ligated together and transformed into BL21 (DE3) competent E. coli cells. The cloned plasmids were collected then digested with appropriate enzymes and visualized on agarose gel.

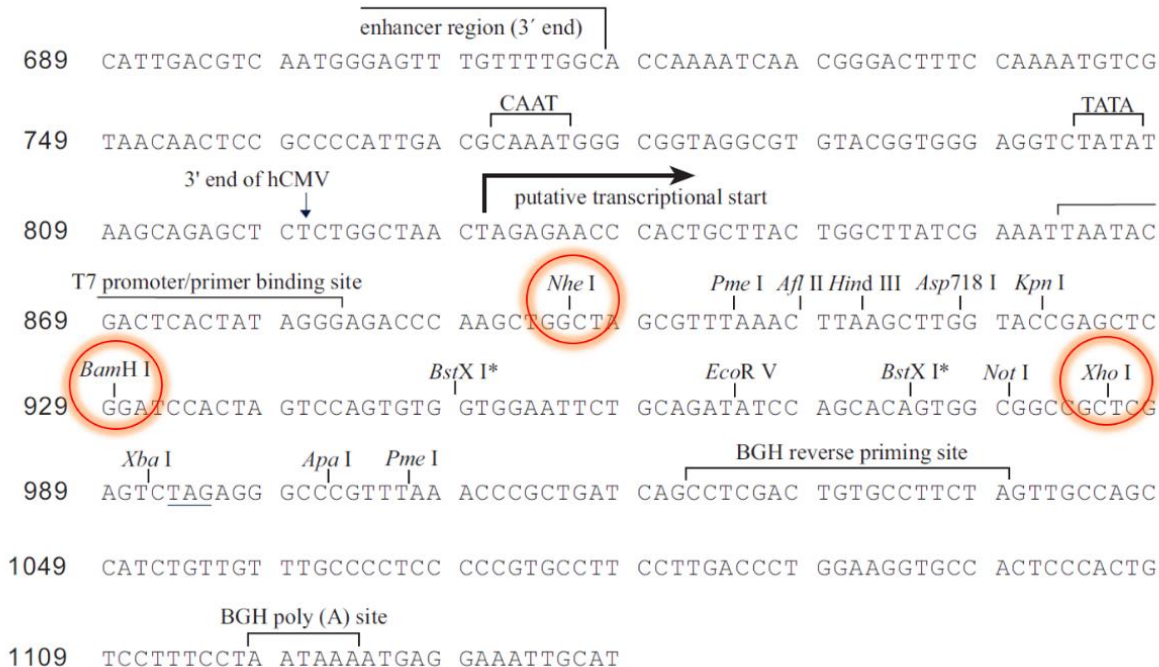


Figure 35. pcDNA 3.1/Hygro mammalian expression vector with necessary restriction sites indicated in red circles.

As shown in Figure 36, the clones showed individual inserts. Inserts were then sequenced (Figure 37).

Purified plasmid with BamHI/XhoI insert was digested with NheI and BamHI restriction enzymes. The insert from the plasmid with NheI/BamHI was then ligated into vector with BamHI/XhoI insert. The newly formed plasmid with entire sequence was then transformed back into competent bacterial cells. Qiagen mini-preps were done for 4 bacterial colonies (Qiagen, Hilden, Germany).

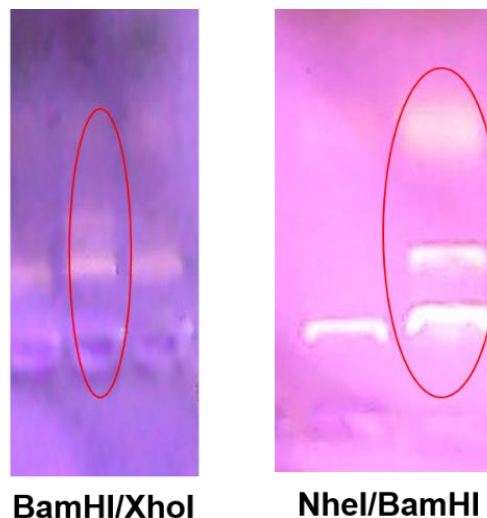


Figure 36. Cloned pcDNA 3.1/Hygro+ inserts digested with appropriate enzymes. (Left) Cloned vector + BamHI/XhoI insert. (Right) Cloned vector + NheI/BamHI insert.

NheI/BamHI full sequence:

H A S T R C K L A R Y L E D L E D V D L K K F K M H L E D Y P P Q K G C I P L P R G Q T E
K A D H V D L A T L M I D F N G E E K A W A M A V W I F A A I N R R D L Y E K A K R D
E P K W G S D N A R V S S P T V I C Q E D S I E E E W M G L L E Y L S R I S I C K M K K D
Y R K K Y R K Y V R S R F Q C I E D R N A R L G V S V S L N K R Y T R L R L I K E H R S Q
Q E R E Q E L L A I G K T K T C E S P V S P I K M H E L L F D P D D E H S E P V H T V V F
Q G A A G I G K T I L A R K M M L D W A S G T L Y Q D R F D Y L F Y I H C R E V S L V T
Q R S L G D L I M S C C P D P N P P I H K I V R K P S R I L F L M D G F D E L Q G A F D E
H I G P L C T D W Q K A E R G D I L L S S L I R K K L L P E A S P L I T T R P V A L E K L Q
H L L D H P R H V E I L G F S E A K R K E Y F F K Y F S D E A Q A R A A F S L I Q E N E V L
F T M C F I P L V C W I V C T G L K Q Q M E S G K S L A Q T S K T T T A V Y V F F L S S L
L Q P R G G S Q E H G L C A H L W G L C S L A A D G V W N Q K I L F E E S D L R N H G
L Q K A D V S A F L R M N L F Q K E V D C E K F Y S F I H M T F Q E F F A A M Y Y L L E
E E K E G R T N V P G S

BamHI/XhoI full sequence:

L G T E L G S R L K L P S R D V T V L L E N Y G K F E K G Y L I F V V R F L F S L V N
Q E R T S Y L E K K L S C K I S Q Q I R L E L L K W I E V K A K A K K L Q I Q P S Q L
E L F Y C L Y E M Q E E D F V Q R A M D Y F P K I E I N L S T R M D H M V S S F C
I E N C H R V E S L S L G F L H N M P K E E E E E K E G R H L D M V Q C V L P S
S S H A A C X H G L V N S H L T S S F C R G L F S V L S T S Q S L T E L D L S D N S
L G D P G M R V L C E T L Q H P G C N I R R L W L G R C G L S H E C C F D I S L V
L S S N Q K L V E L D L S D N A L G D F G I R L P C V G L K H L L C N L K K L W L V
S C C L T S A C C Q G L A S V L S T S H S L T R L Y V G E N A L G D S G V A I L C E
K A K N P Q C N L Q K L G L V N S G L T S V C C S A L S S V L S T N Q N L T H L Y
L R G N T L G D K G I K L L G C E G L L H P D C K L Q V L E L V N C N L T S H C C
W D L S T L L T S S Q S L R K L S L G N N D L G D L G V M M F C E V L K Q Q S C
L L Q N L G L S E M Y F N Y E T K S A L E T L Q E E K P E L T V V F E P S W **Stop**

Figure 37. Cloned pcDNA 3.1/Hygro+ inserts sequenced. (Top sequence) The sequence from insert *NheI/BamHI* insert. (Bottom sequence) The sequence from insert *BamHI/XhoI*.

Plasmids collected from 4 colonies were digested with 2 different sets of restriction enzymes, *NheI/XhoI* or *BamHI/XhoI* enzymes. Colonies 1-3 had the correct inserts for *NheI/XhoI* and *BamHI/XhoI*. However, colony 4 did not have the correct *NheI/XhoI* insert so was discarded (Figure 38). Diluted pooled plasmid was tested for absorption at 280 nm and 260 nm with UV-vis spectrophotometer to estimate the concentration of the

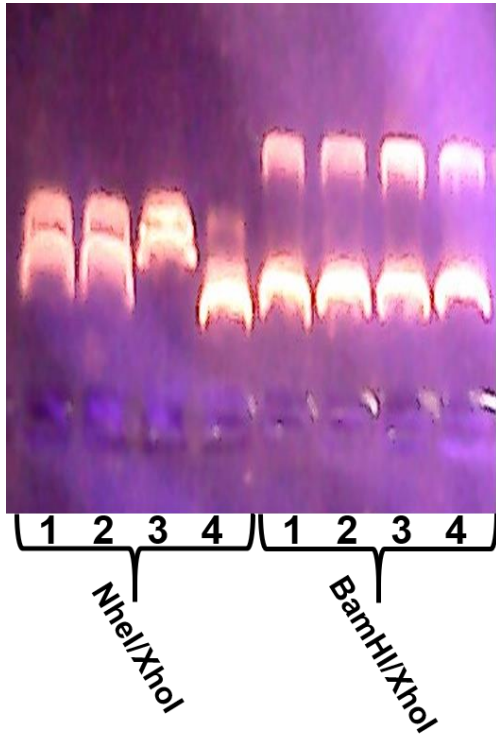


Figure 38. Colonies 1-4 of cloned pcDNA 3.1/Hygro+ full NLRP3 sequence cut with either NheI and XhoI restriction enzymes or BamHI and XhoI restriction enzymes.

plasmid and determine how much bacteria was needed to make enough plasmid for transfection and determine the purity of the sample.

The UV-vis spectrophotometer reading detected 0.517 AU for 280 nm and 0.914 AU for 260 nm. This gave a ratio of 1.77 indicating the nucleic acid content was quite pure. Using the extinction coefficient and Beer-Lambert's law the concentration of plasmid was estimate to be 457 ug/ml. From this it was determined how much more bacteria needed to be used to clone enough plasmid.

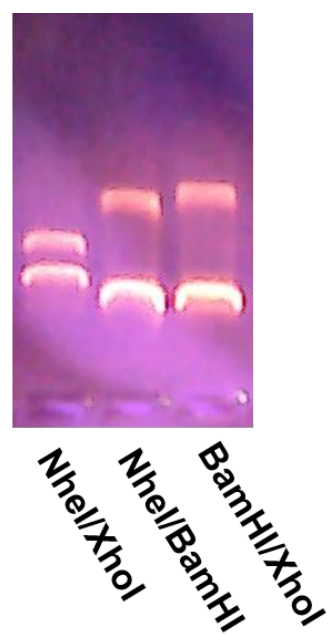


Figure 39. Purified colony of pcDNA 3.1/Hygro+ full NLRP3 sequence. Plasmids were either cut with either NheI and XhoI restriction enzymes, NheI and BamHI, or BamHI and XhoI restriction enzymes.

Plasmids were again collected and purified with and cut with restriction enzyme pairs: NheI/XhoI, NheI/BamHI, and BamHI/XhoI. These digested plasmids were then visualized on agarose gel (Figure 39). When digested with enzymes for the full sequence, NheI/XhoI, or enzymes for either NheI/BamHI and BamHI/XhoI piece, the resulting pieces analyzed by agarose gel were the correct size. The plasmid produced was enough for transfection.

3.5.2 Transfection

Human embryonic kidney 293 cells (HEK-293) were transfected with plasmid using ExpiFectamine™ 293 kit (ThermoFisher Scientific, Waltham, MA). As shown in Figure 40, the optimal time for protein expression were days 1-3, after which the expression of NLRP3 protein decreased due to reduced cell viability. Collectively our results confirmed that we can successfully express full length NLRP3 proteins to support our continuing studies.

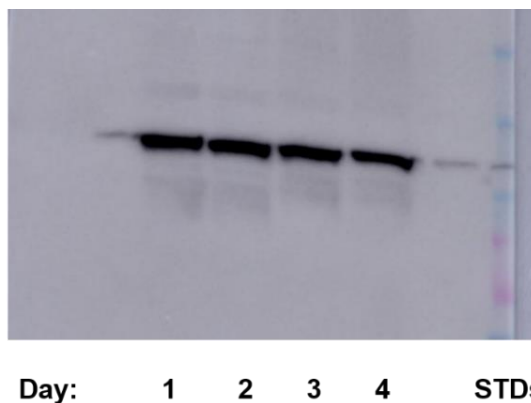


Figure 40. Immunoblot of HEK 293 cells transfected with pcDNA 3.1/Hygro+ full NLRP3 sequence. NLRP3 visualized with anti-NLRP3 and secondary antibody anti-rabbit IgG with conjugated HRP.

3.6 LC-MS

3.6.1 Method development

To evaluate the ability of our compound to penetrate the BBB and compare to the potent NLRP3 inhibitor with comparable therapeutic *in vivo* MS mouse models, MCC950, LC-MS was utilized. In order to quantify the concentration of compounds in the brain samples, first a reliable method had to be established. To help with precision and account for matrix effects, Glipizide, another sulfonamide small-molecule compound, was chosen as the internal standard. Glipizide proved stable and flexible in terms of ionization.

Both positive and negative ion modes of ESI were tested for detection of each compound. However, it was determined that separate ionization modes needed to be

used for each compound for detection. Negative ionization mode of ESI was used for MCC950; the reason for the better signal in this mode was that the compound was purchased as a salt with a negative charge on the nitrogen of the sulfonamide group. JC-171 (GA4), however, gave a better signal in positive ion mode due to its amine. Conveniently, the internal standard Glipizide yielded a significant signal in either positive or negative mode, so the same internal standard could be used for all samples for both method validation and dosed mice brain samples.

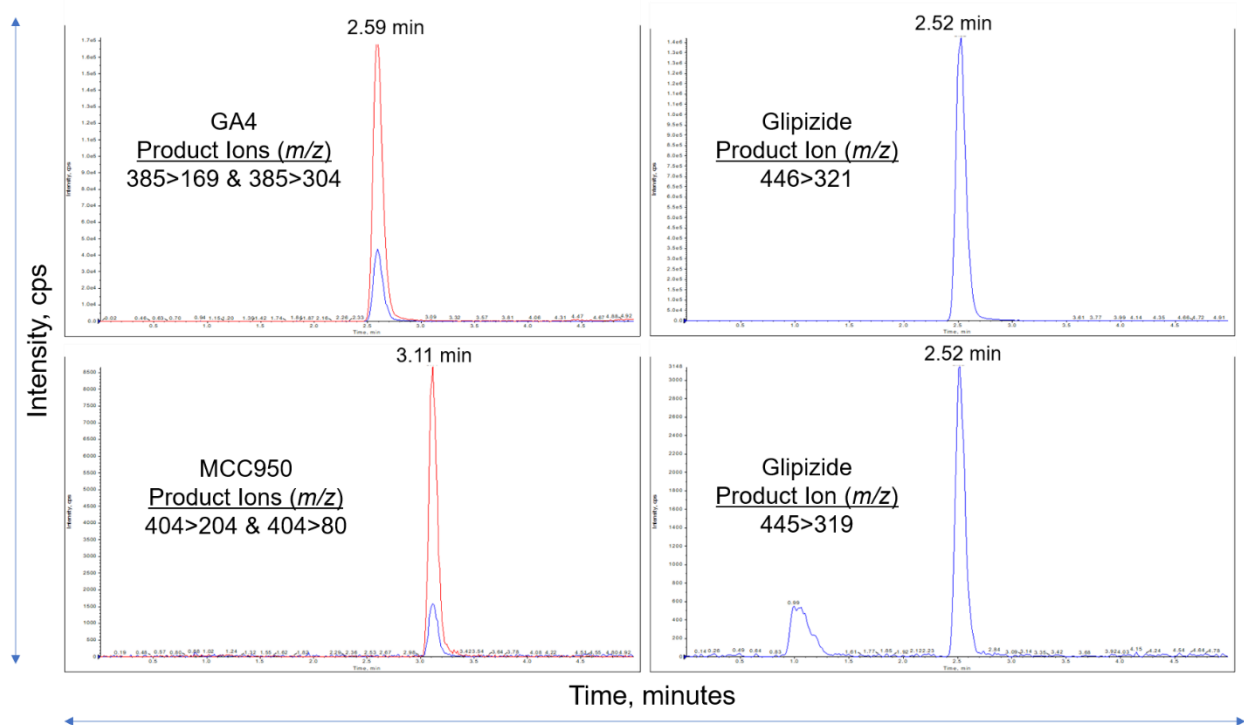


Figure 41. Retention times and extracted ion intensity for product ions of JC-171 (GA4), MCC950, and Glipizide. Product ions for MCC950 and GA4 used for quantification are depicted by red peaks.

In multiple reaction monitoring (MRM) the most significant product ions found for MCC950, with a molecular weight of 404.5 ($C_{20}H_{24}N_2O_5S$), were: 204 ($[M-200]^-$) and 80 ($[M-324]^-$) m/z. The product ion used for quantification was 204 and the retention time for

product ions were 3.110 minutes. The product ions monitored for GA4, with a molecular weight of 385.8 ($C_{16}H_{17}ClN_2O_5S$), were: 304 ($[M + H - 80]^+$) and 169 ($[M + H - 215]^+$) m/z. The product ion used for quantification was 169 and the retention time for product ions were 2.590 minutes. For Glipizide, with a molecular weight of 445.5 ($C_{21}H_{27}N_5O_4S$), either product ion 319 ($[M - H - 126]^-$) for negative ionization ESI mode or 321 ($[M + H - 125]^+$) for positive ionization mode was used. For Glipizide product ion, the retention time was 2.520 minutes (Figure 41). The product ion with the highest signal was monitored for quantification purposes and the other product ion was monitored for quality control. Additionally, to determine if carry over would occur between samples a double blank sample, a sample with neither internal standard or analyte, was used. It was determined that there was minimal carry over between samples (Figure 42).

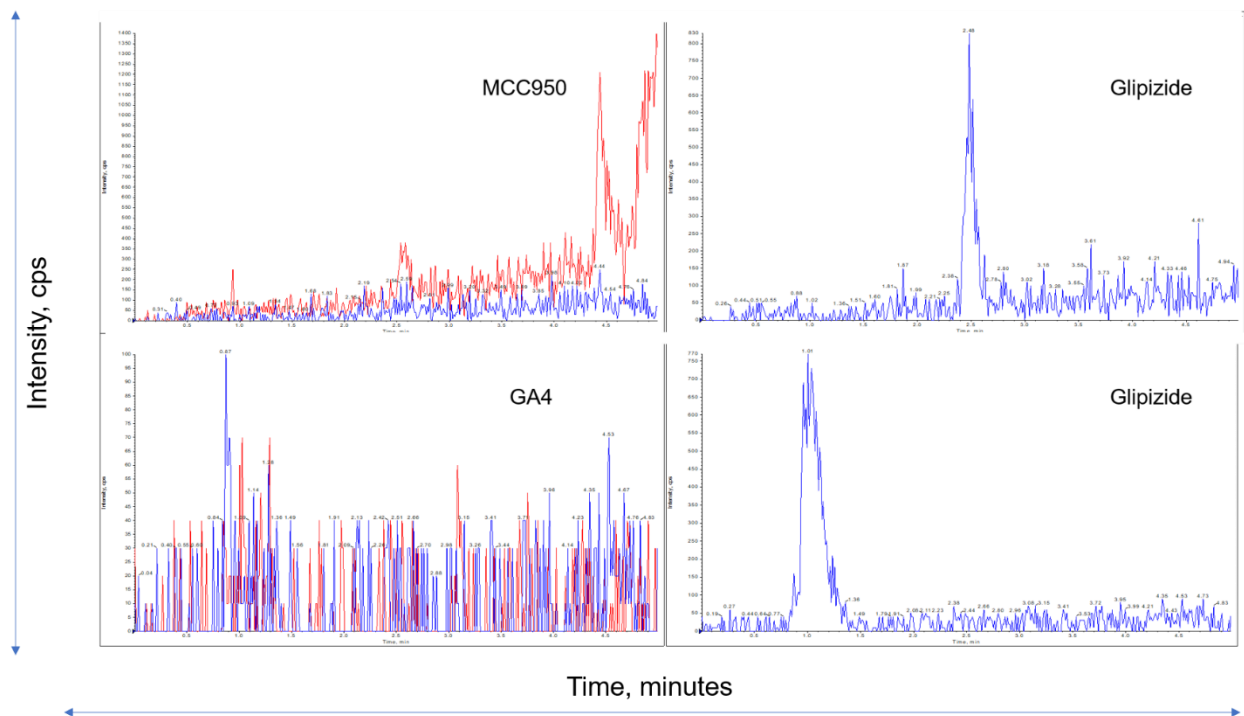


Figure 42. Multiple reaction monitoring for GA4, MCC950, and Glipizide in double blank sample to determine carry over.

3.6.2. Validation

The extraction method had to be adjusted to account for both compounds being run through different ionization ESI modes. When testing different extraction solvents for extracting the analytes from brain tissue, it was determined that 1% FA in ACN was most effective for compound GA4.

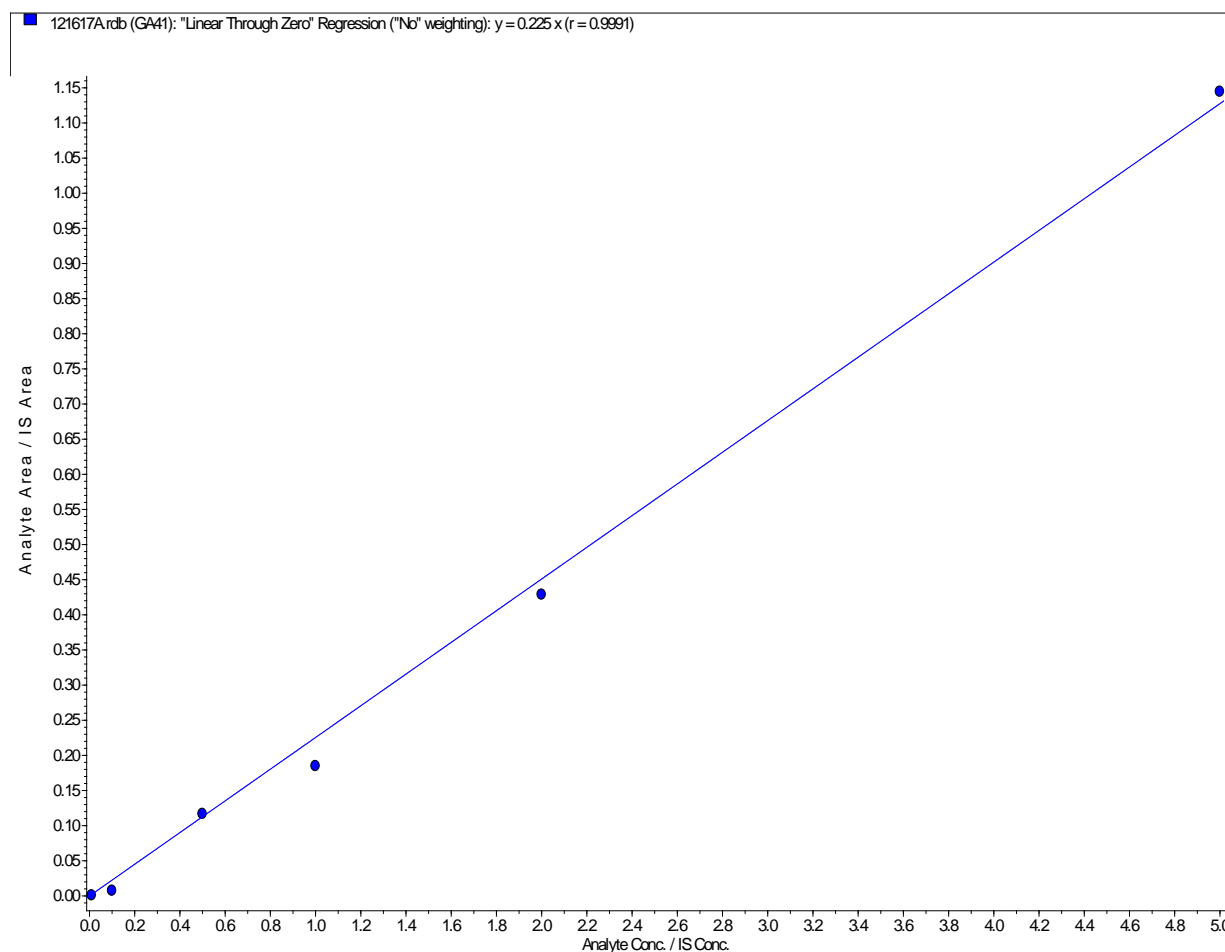


Figure 43. Calibration curve of GA4 from brain tissue at concentrations: 2.5, 25, 125, 250, 500, 1,250 ng/g. Equation ($y = 0.225 x$ ($r=0.9991$))

The extraction solvent 1%FA in ACN could only be used for both if the solvent was completely evaporated after filtering through a phospholipid filter plate (Biotage, Uppsala,

Sweden). Evaporation of solvent removed FA from sample and prevented negative ion suppression of MCC950. The solvent used for reconstitution also required optimization to use for both analytes. MCC950 was more flexible in terms of solvent used for

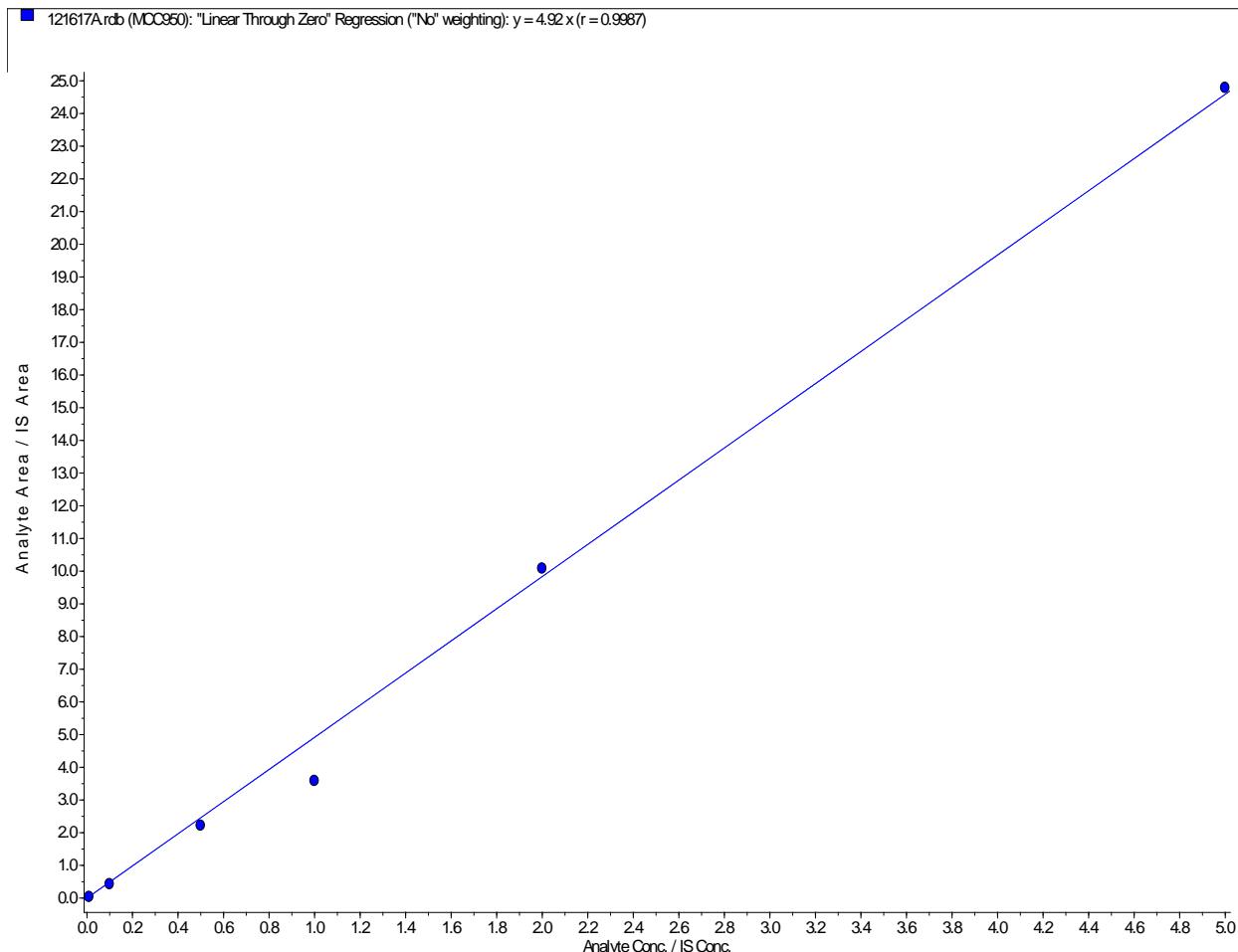


Figure 44. Calibration curve of MCC950 from brain tissue at concentrations: 2.5, 25, 125, 250, 500, 1,250 ng/g. Equation ($y = 4.92x$ ($r=0.9987$))

reconstitution and could be done with ACN or methanol. However, without pure methanol or a 90:10 water/methanol reconstitution solvent, GA4 was retained on the column. For simplicity methanol was the chosen solvent for reconstitution.

To accurately quantify analyte in brain tissue, a six-point calibration curve for both compounds (2.50-1,250 ng/g) were run after extraction from brain tissue (Figure 43, 44).

The calibration curves were reproducible with a coefficient of determination for MCC950 (R^2)= (0.9920-0.9998) and for GA4 (R^2)= (0.9940-0.9982). Neither linear regression equation was weighted. The relative residuals remained below 20% for each point on either calibration curve.

The with-in assay precision and bias were determined for each 3 runs. Each run had a calibration curve and 3 repeats of low (7.5 ng/g), medium (150 ng/g), and high (1,000 ng/g) samples. Both the % CV (precision) and % Bias (accuracy) remained below 20% and within allowable error with 2 exceptions (Table 1-3). The with-in %CV for MCC950 fell in the range of 2.050- 7.100% and the %CV for GA4 fell in the range of 0.5300-6.130%. The % Bias for MCC950 fell in the range of 0-14.90% with the exception of the low (7.5 ng/g) sample in run 3. The %Bias for GA4 fell in the range of 10.20-18.90% with the exception of the high (1,000 ng/g) sample in run 3. The MCC950 low QC samples (7.5 ng/g) ran slightly higher than what was accurate. GA4 high QC samples (1,000 ng/g) were significantly lower than what the values should have read, indicating human error in sample preparation so this data was not included in in-between assay %CV and %Bias calculations.

The in-between precision and accuracy was then calculated from pooled data. The in-between %CV among low, medium, and high samples from MCC950 ranged between 11-15%. The %Bias for MCC950 fell in the range of 1.000-7.000% (Table 4). For GA4, the in-between %CV among low, medium, and high samples ranged from 2.000-5.000%. The %Bias for GA4 fell within 14.00-17.00% (Table 5). All %CV and %Bias fell with-in allowable error $\leq 20\%$, demonstrating that the method was sufficient for use in determining the concentration of these compounds from tissue samples.

| Run 1 | | | Run 1 QC : MCC950 | | | |
|--|---------|---------|----------------------|----------------|-------------------|------------------------|
| Sample Name | MCC950 | GA4 | Repeat | Low (7.5 ng/g) | Mid (150 ng/g) | High (1000 ng/g) |
| Test | 253.5 | 116.5 | 1 | 7.550 | 135.5 | 1035 |
| 2.5 ng/g MCC950 & GA4 | 4.695 | 1.015 | 2 | 6.500 | 136.0 | 1140 |
| 25 ng/g MCC950 & GA4 | 22.45 | 8.300 | 3 | 7.150 | 129.0 | 1125 |
| 125 ng/g MCC950 & GA4 | 119.5 | 132.0 | Mean | 7.067 | 133.5 | 1100 |
| 250 ng/g MCC950 & GA4 | 224.5 | 287.5 | SD | 0.4330 | 3.189 | 46.37 |
| 500 ng/g MCC950 & GA4 | 515.0 | 520.0 | %CV | 6.123 | 2.388 | 4.215 |
| 1250 ng/g MCC950 & GA4 | 1720 | 1235 | %Bias | -5.778 | -11.00 | 10.00 |
| Blank | No Peak | No Peak | | | | |
| Double Blank | No Peak | No Peak | Run 1 QC: GA4 | | | |
| High QC (1000 ng/g MCC950 & GA4) | 1035 | 1145 | Repeat | Low (7.5 ng/g) | Mid (150 ng/g) | High (1000 ng/g) |
| Low QC (7.5 ng/g MCC950 & GA4) | 7.550 | 8.700 | 1 | 8.7 | 155.5 | 1145 |
| High QC (1000 ng/g MCC950 & GA4) | 1140 | 1175 | 2 | 8.7 | 174.5 | 1175 |
| Low QC (7.5 ng/g MCC950 & GA4) | 6.500 | 8.700 | 3 | 8.6 | 166.0 | 1125 |
| High QC (1000 ng/g MCC950 & GA4) | 1125 | 1125 | Mean | 8.667 | 165.3 | 1148 |
| Low QC (7.5 ng/g MCC950 & GA4) | 7.150 | 8.600 | SD | 0.04710 | 7.771 | 20.55 |
| Mid QC (150 ng/g MCC950 & GA4) | 135.5 | 155.5 | %CV | 0.5440 | 4.700 | 1.789 |
| Mid QC (150 ng/g MCC950 & GA4) | 136.0 | 174.5 | %Bias | 15.56 | 10.22 | 14.83 |
| Mid QC (150 ng/g MCC950 & GA4) | 129.0 | | | | | |
| r | 0.9990 | 0.9990 | | | | |
| r2 | 0.9980 | 0.9980 | | | | |

Table 1. Run 1 calibration curve and low, medium, and high QC samples.

| Run 2 | | | Run 2 QC : MCC950 | | | |
|----------------------------------|---------|---------|-------------------|----------------|----------------|------------------|
| Sample Name | MCC950 | GA4 | Repeat | Low (7.5 ng/g) | Mid (150 ng/g) | High (1000 ng/g) |
| 2.5 ng/g MCC950 & GA4 | 1.740 | 0.8700 | 1 | 8.000 | 143.5 | 1100 |
| 25 ng/g MCC950 & GA4 | 21.55 | 8.200 | 2 | 6.900 | 144.0 | 1210 |
| 125 ng/g MCC950 & GA4 | 112.5 | 129.5 | 3 | 7.600 | 137.0 | 1195 |
| 250 ng/g MCC950 & GA4 | 182.0 | 205.0 | Mean | 7.500 | 141.5 | 1168 |
| 500 ng/g MCC950 & GA4 | 510.0 | 475.5 | SD | 0.4550 | 3.189 | 48.70 |
| 1250 ng/g MCC950 & GA4 | 1260 | 1270 | %CV | 6.061 | 2.253 | 4.169 |
| Blank | No Peak | No Peak | %Bias | 0 | -5.667 | 16.83 |
| Double Blank | No Peak | No Peak | | | | |
| High QC (1000 ng/g MCC950 & GA4) | 1100 | 1185 | Run 2 QC: GA4 | | | |
| Low QC (7.5 ng/g MCC950 & GA4) | 8.000 | 8.950 | Repeat | Low (7.5 ng/g) | Mid (150 ng/g) | High (1000 ng/g) |
| High QC (1000 ng/g MCC950 & GA4) | 1210 | 1215 | 1 | 8.950 | 160.5 | 1185 |
| Low QC (7.5 ng/g MCC950 & GA4) | 6.900 | 8.950 | 2 | 8.950 | 180.0 | 1215 |
| High QC (1000 ng/g MCC950 & GA4) | 1195 | 1165 | 3 | 8.850 | 171.0 | 1165 |
| Low QC (7.5 ng/g MCC950 & GA4) | 7.600 | 8.850 | Mean | 8.917 | 170.5 | 1188 |
| Mid QC (150 ng/g MCC950 & GA4) | 143.5 | 160.5 | SD | 0.04710 | 7.969 | 20.55 |
| Mid QC (150 ng/g MCC950 & GA4) | 144.0 | 180.0 | %CV | 0.5290 | 4.674 | 1.729 |
| Mid QC (150 ng/g MCC950 & GA4) | 137.0 | 171.0 | %Bias | 18.89 | 13.67 | 18.83 |
| r | 0.9990 | 0.9990 | | | | |
| r2 | 0.9970 | 0.9980 | | | | |

Table 2. Run 2 calibration curve and low, medium, and high QC samples.

| Run 3 | | | Run 3 QC : MCC950 | | | |
|--|---------|---------|----------------------|-------------------|----------------|---------------------|
| Sample Name | MCC950 | GA4 | Repeat | Low (7.5 ng/g) | Mid (150 ng/g) | High (1000 ng/g) |
| 2.5 ng/g MCC950 & GA4 | 3.500 | 21.20 | 1 | 8.920 | 162.0 | 862.0 |
| 25 ng/g MCC950 & GA4 | 38.40 | 20.80 | 2 | 9.040 | 172.2 | 864.0 |
| 125 ng/g MCC950 & GA4 | 121.8 | 88.20 | 3 | 10.40 | 177.2 | 826.0 |
| 250 ng/g MCC950 & GA4 | 258.0 | 159.6 | Mean | 9.453 | 170.5 | 850.7 |
| 500 ng/g MCC950 & GA4 | 490.0 | 212.0 | SD | 0.6710 | 6.325 | 17.46 |
| 1250 ng/g MCC950 & GA4 | 1252 | 1322 | %CV | 7.100 | 3.711 | 2.053 |
| Blank | No Peak | 4.940 | %Bias | 26.04 | 13.64 | -14.93 |
| Double Blank | No Peak | No Peak | | | | |
| High QC (1000 ng/g MCC950 & GA4) | 862.0 | 218.0 | Run 3 QC: GA4 | | | |
| Low QC (7.5 ng/g MCC950 & GA4) | 8.920 | 7.660 | Repeat | Low (7.5 ng/g) | Mid (150 ng/g) | High (1000 ng/g) |
| High QC (1000 ng/g MCC950 & GA4) | 864.0 | 216.0 | 1 | 7.660 | 178.2 | 218.0 |
| Low QC (7.5 ng/g MCC950 & GA4) | 9.040 | 8.520 | 2 | 8.520 | 179.0 | 216.0 |
| High QC (1000 ng/g MCC950 & GA4) | 826.0 | 212.0 | 3 | 8.880 | 172.0 | 212.0 |
| Low QC (7.5 ng/g MCC950 & GA4) | 10.40 | 8.880 | Mean | 8.353 | 176.4 | 215.3 |
| Mid QC (150 ng/g MCC950 & GA4) | 162.0 | 178.2 | SD | 0.5120 | 3.128 | 2.494 |
| Mid QC (150 ng/g MCC950 & GA4) | 172.2 | 179.0 | %CV | 6.127 | 1.773 | 1.158 |
| Mid QC (150 ng/g MCC950 & GA4) | 177.2 | 172.0 | %Bias | 11.38 | 17.60 | -78.47 |
| r | 0.9999 | 0.9972 | | | | |
| r2 | 0.9998 | 0.9944 | | | | |

Table 3. Run 2 calibration curve and low, medium, and high QC samples.

| MCC950 QC Total | | | | |
|-----------------|------------------|---------------------|----------------|------------------|
| Run | Repeat | Low (7.5 ng/g) | Mid (150 ng/g) | High (1000 ng/g) |
| | 1 | 7.550 | 135.5 | 1035 |
| 1 | 2 | 6.500 | 136.0 | 1140 |
| | 3 | 7.150 | 129.0 | 1125 |
| | 1 | 8.000 | 144.0 | 1100 |
| 2 | 2 | 6.900 | 144.0 | 1210 |
| | 3 | 7.600 | 137.0 | 1195 |
| | 1 | 8.920 | 162.0 | 862.0 |
| 3 | 2 | 9.000 | 172.0 | 864.0 |
| | 3 | 10.40 | 177.2 | 826.0 |
| | Mean | 8.010 | 148.5 | 1040 |
| | SD | 1.170 | 16.50 | 142.3 |
| | %CV | 15.00 | 11.00 | 14.00 |
| | %Bias | 7.000 | -1.000 | 4.000 |
| | Linearity | 2.5ng/g - 1250 ng/g | r2 | 0.9920-0.9998 |

Table 4. In-between precision and bias for low, medium, and high MCC950 samples.

| GA4 QC Total | | | | |
|--------------|------------------|---------------------|----------------|------------------|
| Run | Repeat | Low (7.5 ng/g) | Mid (150 ng/g) | High (1000 ng/g) |
| | 1 | 8.700 | 155.5 | 1145 |
| 1 | 2 | 8.700 | 174.5 | 1175 |
| | 3 | 8.600 | 166.0 | 1125 |
| | 1 | 8.950 | 161.0 | 1185 |
| 2 | 2 | 8.950 | 180.0 | 1215 |
| | 3 | 8.850 | 171.0 | 1165 |
| | 1 | 7.660 | 178.2 | |
| 3 | 2 | 9.000 | 179.0 | |
| | 3 | 8.880 | 172.0 | |
| | Mean | 8.650 | 170.7 | 1168 |
| | SD | 0.3800 | 8.060 | 28.67 |
| | %CV | 4.000 | 5.000 | 2.000 |
| | %Bias | 15.00 | 14.000 | 17.00 |
| | Linearity | 2.5ng/g - 1250 ng/g | r2 | 0.9940-0.9982 |

Table 5. In-between precision and bias for low, medium, and high GA4 samples.

3.6.3. Application and Discussion

To determine the BBB penetration of GA4 and compare to the more potent MCC950, brain samples from mice administered GA4 and MCC950 at 0.1 mg/kg and 0.5 mg/kg via intraperitoneal injection, were collected after 2 h of compound administration. Following the optimized extraction method and established LC-MS method, the samples were weighed, homogenized, and extracted. The estimation of concentrations detected from tissue were calculated based on calibration curves established (Table 6).

On average the concentration of drug extracted from the brain tissue of mice given intraperitoneal injections of 0.1 mg/kg of MCC950 was 0.7530 ng/g. This value fell outside the calibration curve for this compound so this value was from extrapolation and the likelihood of accuracy for this value was lower than interpolated values. However, this does not change the overall conclusion of these results combined. Comparatively, from mice given the same dose of GA4, an average of 9.200 ng/g of drug was detected in the brain tissue.

When mice were injected with 0.5 mg/kg of GA4, the average detected concentration in the brain tissue was 18.12 ng/g. However, the difference between the 2 samples was high. Given the amount of GA4 detected in mice given 0.1 mg/kg, the higher value seemed more reasonable. The reason for this difference did not appear to be an error in extraction or an issue with the method; when the other half of the brain from mouse #7 and #8 was tested the same distinct difference in concentration of drug detected was observed. This indicated that the reason for this difference may have been the sample itself. In mice given the same dose of MCC950, the detected concentration from the brain tissue was only and average of 3.050 ng/g. So, despite this discrepancy in

the brain samples of mice injected with GA4, the amount detected was still higher than the concentration of MCC950 detected from mice given the same dose. GA4 (JC-171), not only demonstrated BBB penetration but was superior to the BBB penetration of the more potent NLRP3 inhibitor MCC950. This may partially explain the reason for comparable therapeutic *in vivo* activity in mouse model of MS.

| Sample # and Drug Dose | MCC905 ng/g | GA4 ng/g |
|-------------------------------|--------------------|-----------------|
| 1-vehicle | ND | ND |
| 2-vehicle | ND | ND |
| 3-MCC950 0.5mg/kg | 3.240 | ND |
| 4-MCC950 0.5mg/kg | 2.860 | ND |
| 5-MCC950 0.1mg/kg | 0.6460 | ND |
| 6-MCC950 0.1mg/kg | 0.8600 | ND |
| 7-GA4 0.5mg/kg | ND | 29.00 |
| 8-GA4 0.5mg/kg | ND | 7.240 |
| 9-GA4 0.1mg/kg | ND | 10.84 |
| 10-GA4 0.1mg/kg | ND | 7.560 |
| ND = None Detected | | |

Table 6. Concentration of drug detected from the brain tissue of mice given the indicated doses of drug by intraperitoneal injection.

Chapter 4: Methods and Materials

4.1 MST

4.1.1 NLRP3 (LRR), NLRP3 (full length), and NLRP3 (K232A)

The proteins used were either recombinant mouse NLRP3 (LRR) with n-terminal His-tag (amino acids: 671-1033) (LS Bio, Seattle, WA), recombinant human NLRP3 with n-terminal His-tag (amino acids: 2-1036) (BPS bioscience, San Diego, CA), or recombinant mutant human NLRP3 (K232A) with n-terminal His-tag (amino acids: 2-1036) (BPS bioscience, San Diego, CA). Protein was labeled with His-tag RED-tris-NTA monolith protein labeling kit according to manufacturer's instructions (Nanotemper, München, Germany). The labeling kit has high efficiency and removal of excess dye or purification is not necessary. Monolith NT. Automated machine was used for MST assay (Nanotemper, München, Germany). 10ul of the NT-647 labeled protein was added to 12 wells of a 384 well plate (Corning, Corning, NY) at a final concentration of 50 nM with the addition of 10 µl of 12 different concentrations ligand and a final concentration of 5% DMSO in each well. MST premium-coated capillary chip was inserted into the 12 wells and then placed into the MST machine. The MST excitation was set to 40% for sufficient fluorescence counts and the MST power was set to medium for the best signal to noise ratio. All binding data used passed MST quality checks such as: no aggregation, consistent initial fluorescence, and no photo-bleaching.

4.1.2 ASC

The protein used was recombinant human ASC/TMS1 with GST tag (Novus, Littleton, CO). Protein was labeled with cysteine reactive monolith protein labeling kit red-

maleimide and purified according to manufacturer's instructions (Nanotemper, München, Germany). The fractions were run through UV-1800 Shimadzu spectrophotometer the absorption at wavelengths at 280 and 680nm were compared by using the molar absorbance of the dye ($250,000 \text{ M}^{-1}\text{cm}^{-1}$) to calculate degree of labeling and the molar extinction coefficient of the protein (67123) to calculate the protein concentration in each fraction (Shimadzu, Kyoto, Japan).

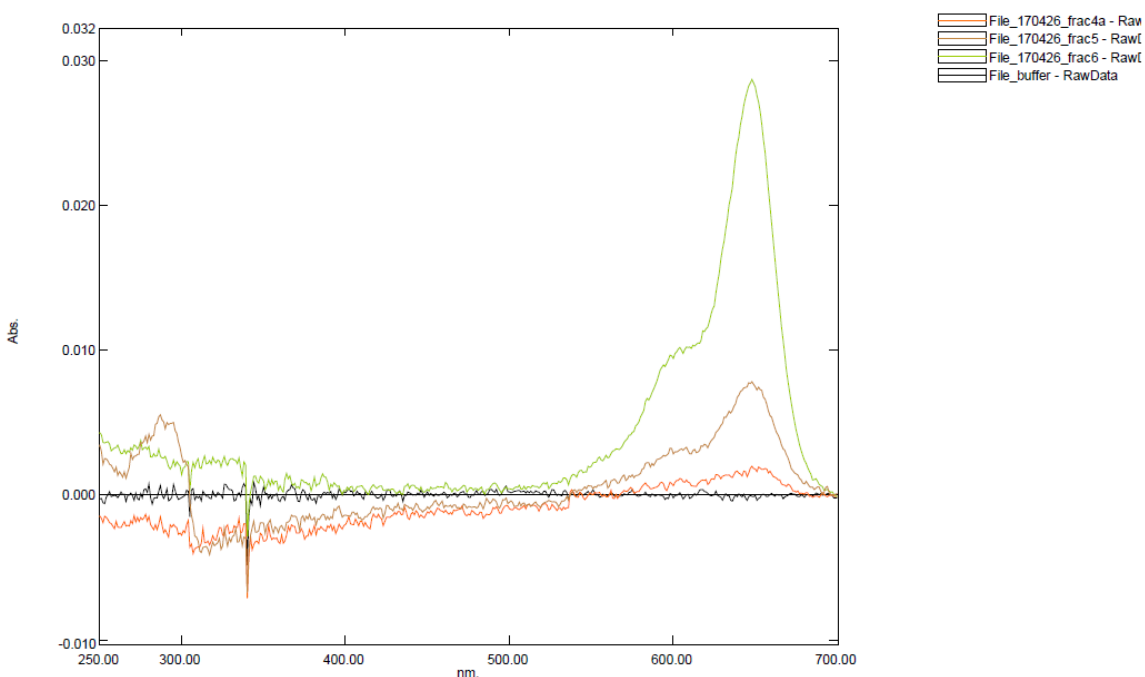


Figure 45. Purified fractions from fluorescently tagged (NT-647) ASC protein.

The best fraction with nearly equal signal from protein and fluorescent tag, fraction 5, was used in MST experiments (Figure 45). Monolith NT. Automated machine was used for MST assay (Nanotemper, München, Germany). 10ul of the NT-647 labeled ASC protein was added to 12 wells of a 384 well plate (Corning, Corning, NY) at a final concentration of 10nM with the addition of 10 μl of 12 different concentrations ligand and a final

concentration of 5% DMSO in each well. MST premium-coated capillary chip was inserted into the 12 wells and then placed into the Monolith NT.Automated MST machine (Nanotemper, München, Germany). The MST excitation was set to 95% for sufficient fluorescence counts and the MST power was set to medium for the best signal to noise ratio.

4.2 ADP-Glo

3 µl of recombinant human NLRP3 aa 2-1036 80117 (BPS Bioscience, San Diego, CA) was incubated in a 384 well white plate (Greiner Bio-one, Kremsmünster, Austria) at a concentration of 7ng/ul with 1 µl of the given concentration of compounds mentioned for 15 min at 37 °C in reaction buffer 20 mM Tris-HCl (pH 7.8), 20 mM MgCl₂, 133 mM NaCl, 3 mM KCl, 0.56 mM EDTA, and 2% DMSO, following the reference protocol.¹⁴⁴ 250 µM of ultra-pure ATP, provided by ADP-Glo kit (Promega, Madison, WI), was added to each well and further incubated at 37 °C for 40 minutes. Due to the small quantities added in each step, protein, compound, and ATP were all added via acoustic liquid handling technology, Echo 555 (Labcyte, San Jose, CA). Luminescent ADP-Glo Kinase Assay kit was used to detect and quantify ADP produced by ATP hydrolysis of the ATPase of NLRP3 per manufacturer's protocol (Promega, Madison, WI). Clariostar multi-mode microplate reader was used to quantify luminescence produced from each reaction (BMG Labtech, Ortenburg, Germany).

4.3 Molecular Modeling

With no crystal structure of NBD domain of NLRP3, homology models were generated from template crystal structure of NLRC4 (PDB code 4KXF)¹⁵⁸. Template 4KXF

was chosen based on sequence similarity in BLAST search of FASTA sequence of NBD (aa 220-536) of human NLRP3 (Uniprot code Q96P20). Sequence alignment was done via EMBOSS needle pairwise sequence alignment (EMBL-EBI, Hinxton, UK).¹⁶² 100 models were generated using MODELLER v 9.17.¹⁵⁷ Models were compared via Ramachandran plots. The model 70 was chosen based on acceptable Ramachandran plot and further validation by docking ADP from the crystal structure of NLRC4 back into the nucleotide binding pocket. Model 70 was minimized using SYBL-X 2.1.1 (Tripos Associates, St. Louis, MO) using Tripos force field and Gasteiger-Hückel charges. Compounds were docked into a chosen model using GOLD 5.4 (The Cambridge Crystallographic Data Centre, Cambridge, England). Pictures of protein and docked ligands were generated using PyMol (Schrödinger, LLC, New York, NY). HINT scores were calculated to determine if hydrophobic interactions were favorable.¹⁶⁰

4.4 NLRP3 production

4.4.1 Plasmid and General Procedure

Plasmid pEGFP-C2-NLRP3 (catalog # 73955) was purchased from nonprofit plasmid repository addgene.¹³ Purification of plasmid from bacteria was done with Qiagen mini-prep per manufacturer's protocol (Qiagen, Hilden, Germany). When PCR was attempted using forward primer with added histidine tag on amino terminus (5' ggatgctagcatgcacatcaccatcaccatgcaagcaccgctgcaagctggccagg 3') and reverse primer (5' cgggatccctaccaagaaggctcaaagacgacggctcag 3') the correct sequence could not be produced from PCR. To get correct sequence extra restriction sites had to be used to divide the sequence to be cloned into 2 parts. Restriction sites used included: NheI at amino terminus, BamHI in the middle of the sequence, and XhoI at the carboxy terminus.

Primers to introduce sequences and clone protein sequence in 2 parts were purchased from Invitrogen: NheF (5' ggatgctagcatgcaccatcaccatcaccatgcaagcaccgctgcaagctggc cagg 3'), BamR(5' ggggatcctggaacgttcgtccttccttcctttcctc 3'), BamF (5' caggatcccgttgaa gcttcccagccgagacgtg 3'), and XhoR (5' gcctcgagctaccaagaaggctcaaagacgacgg 3') (Invitrogen, Carlsbad, CA) .

4.4.2 PCR

DreamTaq Green PCR Master mix (2x) (ThermoFisher Scientific, Waltham, MA) was thawed, vortexed and quickly centrifuged. A PCR tube was cooled down on ice and to it was added: 25 µl of DreamTaq Green PCR Master mix, 0.5µM of each forward primer, 0.5 µM of each reverse primers and 0.5 µg of the template DNA, and enough nuclease-free DI water to bring the total volume up to 50 µl. Sample was vortexed and spun down. A thermocycler was then used for 2 minutes at 95°C for initial denaturing of DNA. After initial denaturing, 30 cycles of denaturation at 95°C for 30 seconds, annealing at 72°C for 30 seconds, then extension at 72°C for 1 minute. For the final extension, 1 cycle was done at 72°C for 10 minutes (ThermoFisher Scientific, Waltham, MA). 10 µL of PCR mixture was directly added to gel to analyze via agarose gel electrophoresis according to protocol (Agarose Gel Electrophoresis protocol, Addgene, Cambridge, MA). PCR products were recovered using Qiaquick gel extraction kit following the manufacturer's protocol (Qiagen, Hilden, Germany). PCR products were sent to Eurofins Scientific were utilized to determine the sequence (Eurofins Scientific, Brussels, Belgium).

4.4.3 Transformation

Purified PCR products and vector pcDNA 3.1/Hygro were then digested with the appropriate enzymes and each piece separately ligated into vector with DNA ligase according to manufacturer's protocol (DNA ligation kit, ThermoFisher Scientific, Waltham, MA). BL21 (DE3) competent E. coli cells were thawed on ice for 10 minutes. 5 μ L of 5 ng of plasmid was added to thawed bacteria cells and mixed by gently tapping. Vials were left to incubate on ice for 30 minutes. Vials of bacteria and plasmid were heat shocked by placing vial into a 42°C water bath for 30 seconds. Vial was then placed on ice. 250 μ L of pre-warmed SOC medium was then added to vial. Vial was set to incubate at 37°C on cell shaker for 1 hour at 225 rpm (ThermoFisher Scientific, Waltham, MA). 50 μ L was plated on pre-warmed plate at 37°C, LB agar selection plates containing 100 μ g/ml of ampicillin, and the rest in the other plate. Plates were inverted and incubated at 37°C overnight. Qiagen mini-prep was used to collect plasmid from the bacteria (Qiagen, Hilden, Germany).

4.4.4 Transfection

6 x 10⁷ HEK293 cells were seeded into 30mL of Expi293™ expression medium and incubated at 37 °C in a humidified environment with 8% CO₂ with cell shaker set to 125 rpm (ThermoFisher Scientific, Waltham, MA). A 100 μ L aliquot of the cell solution was added to 0.4% solution of trypan blue dye in PBS at a 1:1 ratio. This trypan blue/cell solution was then loaded onto a hemocytometer to determine cell density and viability. Once the cells reached a density between 3-5 x 10⁶ /mL cell density and were still above 95% viability the cells were ready for transfection. 7.5 x 10⁷ cell were then diluted with 25.5 mL of Expi293™ expression medium in a 125 mL flask. 30 μ g of purified plasmid was then suspended in 1.5 mL of Opti-MEM reduced serum medium and gently mixed.

81 μ l of ExpiFectamine™ 293 reagent was then diluted in Opti-MEM I medium to final volume of 1.5 mL, this was then mixed gently and incubated at room temperature for 5 minutes. The plasmid and ExpiFectamine™ reagent were then mixed together and left to incubate at room temperature for 20 minutes. The plasmid/ ExpiFectamine™ mix was then carefully added to the flask of cells in a dropwise manner. The cells were then left to incubate for 20 hours at 37 °C in a humidified environment with 8% CO₂ with cell shaker set to 125 rpm. After 20 hours, 150 μ l of ExpiFectamine™ transfection enhancer 1 and 1.5 mL of enhancer 2 were added to the flask of cell solution (Transfecting Expi293F™ Cells protocol, ThermoFisher Scientific, Waltham, MA). Since the best time for protein expression depends of the protein, 2 1 mL fractions of the cell solution were collected every day for 4 days. 1 of the 1mL fractions from each day was spun down at 10,000 g for 10 minutes and supernatant removed. Pellets were frozen at -20 °C for 20 minutes. Cells were lysed with NP-40 RIPA lysis buffer and protease inhibitor. Protein concentration was calculated via the Bradford assay.

4.4.5 SDS-PAGE

HEK 293 cells were lysed with buffer cooled down to 0 °C containing: 150 mM NaCl, 1% NP-40, 50 mM Tris (pH 8) and SIGMAFAST™ protease inhibitor cocktail (Sigma-Aldrich, St. Louis, MO). 350 μ l of lysis buffer was added to each aliquot of ~5 million cells for each of the 4 days cells were collected. Mixture was left on ice for 15 minutes. Mixture was then sonicated for 5 seconds and left on ice for 15 minutes. Cell lysates were then centrifuged at 15,000 rpm at 4°C for 20 minutes. The Bradford assay was then employed to estimate protein concentration of cell lysates. Sample buffer was made with 50 μ l of 2-Mercaptoethanol and 950 μ l of 2x Laemmli Sample buffer (BIO-

RAD, Hercules, CA). 15 µl of cell lysates were then diluted with 15 µl of sample buffer and boiled at 90°C for 10 minutes in a water bath and then placed on ice. Cell lysates were spun down at 4°C at 2,350 rpm for 3 minutes. Diluted sample was injected into Criterion™ 4-15% Tris-HCl 18 well Precast gel (BIO-RAD, Hercules, CA). Gel was run with BIO-RAD Criterion™ Cell electrophoresis set to 100 V for 2 hours (BIO-RAD, Hercules, CA).

4.4.6 Immunoblot

Immun-Blot PVDF membrane was soaked in methanol (BIO-RAD, Hercules, CA). Criterion™ blotter pads were then soaked in Tris/Glycine transfer buffer. Protein was transferred to membrane with Criterion™ blotter set to 0.4 A for 2 hours. Blot was then submerged in blocking solution (5% nonfat dry milk, and 50 mL TBST solution) for 1 hour. Anti-NLRP3 antibody was thawed to room temperature. 1 mg/mL of antibody was diluted 1:800 in 5% nonfat dry milk TBST solution. Blot was washed with TBST solution (Tris buffered saline with 0.1% Tween-20 (Sigma-Aldrich, St. Louis, MO)) 3 times. Secondary antibody, anti-rabbit IgG HRP-linked antibody, was thawed and diluted 1:1000 in 5% nonfat dry milk TBST solution and applied to membrane and incubated at 4°C overnight. Blot was washed with TBST solution 3 times and chemiluminescent substrate solution was added to the blot and labeled protein visualized with GE gel imager (Amersham, Little Chalfont, UK).

4.5 LC-MS

4.5.1 Materials

The plasma purchased for method validation was C57BL/6 mouse K₂EDTA plasma (BioreclamationIVT, Westbury, NY). Brains from C57BL/6 mice dosed with known concentrations of compound by intraperitoneal injection were obtained from collaborators (Dr. Xiang-Yang Wang Lab). The brain tissue used for controls and calibration curve. To remove protein and phospholipids after extraction ISOLUTE PPT+ 96 well filter plate was used (Biotage, Uppsala, Sweden). LC-MS samples were run using a Shimadzu LC-30AD pump, Shimadzu SIL-30AC autosampler (Shimadzu, Kyoto, Japan), with an AB SCIEX linear ion trap quadrupole 6500+ (SCIEX, Framingham, MA). The column used to achieve separation was a Xterra MS C18 3.5 um 2.1x100mm (Waters, Manchester, UK).

4.5.2 Brain extraction

½ of brain from mice dosed with drug or control mice was homogenized in PBS at a ratio of 1.5mL of PBS per 0.5g of brain. 500uL of brain homogenate from each sample was spiked with 150ul of 50ng/ml of Glipizide in methanol. Samples were then extracted with 500ul of ACN with 1% FA and vortexed then left to sit on ice for 15 min. Samples were then centrifuged at highest rpm for 10 min at 4°C. Supernatant was collected and then samples were extracted a second time with 500ul of ACN with 1% FA and the same protocol. Supernatant was combined and then filtered through phospholipid/protein filter plate, solvent evaporated and then reconstituted with 150ul of methanol and injected onto LC-MS.

4.5.3 LC-MS Calibration and QC

Standard concentrations and QC samples of each compound were prepared in PBS and then added to blank mouse plasma or blank mouse brain tissue for the correct

concentration of ng of drug to g of brain or plasma. The samples were homogenized and then spiked with 150ul of 50ng/ml Glipizide internal standard and extracted with 1000uL of ACN with 1% FA and left to sit on ice for 15 min. Samples were centrifuged at highest rpm for 10min at 4°C, and then supernatant was filtered through phospholipid/protein filter. Filtrate was evaporated and then reconstituted with 150ul of methanol and then ran through LC-MS. The final calibration standard concentrations were: 1,250, 500, 250, 125, 25, 2.5 ng/g. The final QC drug concentrations were 7.5, 150 and 1000 ng/g.

4.5.4 LC-MS Parameters

JC-171 samples were run in positive ion mode and MCC950 was run in negative. Mobile phase A consisted of water with 10mM ammonium acetate and mobile phase B was methanol. Injection volume was 2uL with a flow rate of 300 uL/min. The optimized LC-MS parameters for GA4 and internal standard Glipizide were set to: ionspray voltage (IS) +4500 V, temperature 500 °C, nebulizer gas (GS1) 60, TurbolonSpray gas (GS2) 50, collision-activated dissociation (CAD) gas medium, declustering potential (DP) +60 V, and entrance potential (EP) +10 V. Collision cell exit potential (CXP) settings for GA4 was 10.5 eV. The MRM (Multiple Reaction Monitoring) transitions for GA4 were m/z 385 → 304 with CE of 21 eV and 385 → 169 with collision energy (CE) of 32 eV. For Glipizide, the MRM was m/z 446 → 321 with CE of 20 eV. Dwell times for both GA4 and Glipizide were 100 milliseconds.

The optimized LC-MS parameters for MCC950 and internal standard Glipizide were set to: ionspray voltage (IS) -4500 V, temperature 500 °C, nebulizer gas (GS1) 60, TurbolonSpray gas (GS2) 50, collision-activated dissociation (CAD) gas medium, declustering potential (DP) -60 V, and entrance potential (EP) -10 V. Collision

cell exit potential (CXP) settings for MCC950 was -18.5 eV. The MRM (Multiple Reaction Monitoring) transitions for MCC950 were m/z 403.5 \rightarrow 80 with CE of -45 eV and 403.5 \rightarrow 204 with collision energy (CE) of -30 eV. For Glipizide, the MRM was m/z 445 \rightarrow 319 with CE of -20 eV. Dwell times for both MCC950 and Glipizide were 100 milliseconds.

4.5.5 LC-MS Analysis

MRM data acquisition, chromatographic peak integration, data regression using peak area ratios of the analyte to internal standard, and chromatographic review were performed using Sciex Analyst, version 1.6.3 software. Linear regression of calibration curve for MCC950 had an r^2 of 0.992-0.9998 and 0.994-0.9982 for GA4. The unweighted linear regression equation calculated from the calibration curve of each compound was used to predict the concentration of analyte in each brain sample. The CV was calculated in excel by dividing the SD by the mean.

Conclusion

To conclude, our studies demonstrated direct binding of JC-171 to the NLRP3 protein. The binding affinity of JC-171 to the NLRP3 protein was not significantly altered in mutant NLRP3 (K232A). Additionally, ATPase studies indicated that JC-171 and its analogs did not interfere with the ATPase activity of NLRP3. This data supports the notion that JC-171 may bind to the NACHT domain of NLRP3 in a site that is distinct from the ATP binding site. Molecular modeling studies of JC-171 to the homology model of the NACHT domain of the NLRP3 protein indicated a possible binding site for JC-171 and analogs next to the ATP binding pocket, further supporting the assertion that JC-171 binds to the NACHT domain. LC-MS analysis of brain tissue in mice dosed with MCC950 and JC-171 confirmed that JC-171 not only penetrates the BBB but demonstrated better BBB penetration when compared to MCC950. This data, as well as the binding data suggesting an alternative MOA, might aid in the explanation of JC-171's comparable efficacy in ameliorating the progression of disease pathology in EAE, mouse model of MS, with MCC950, a compound with significantly higher inhibitory potency *in vitro*. Together, these results strongly support that our compounds inhibit the NLRP3 inflammasome by directly interacting with the NLRP3 protein, a novel MOA when compared to other known inhibitors of the NLRP3 inflammasome. These results strongly encourage further development of such inhibitors as potential therapeutics for neurodegenerative diseases.

Literature Cited

1. Bertram, L.; Tanzi, R. E. The genetic epidemiology of neurodegenerative disease. *J. Clin. Invest.* **2005**, *115* (6), 1449–1457.
2. Chen, W. W.; Zhang, X.; Huang, W. J. Role of neuroinflammation in neurodegenerative diseases (review). *Mol. Med. Rep.* **2016**, *13* (4), 3391–3396.
3. Morales, I.; Guzmán-Martínez, L.; Cerda-Troncoso, C.; Farías, G. A.; Maccioni, R. B. Neuroinflammation in the pathogenesis of Alzheimer’s disease. A rational framework for the search of novel therapeutic approaches. *Front. Cell. Neurosci.* [Online] **2014**, *8*, Article 112.
<https://www.frontiersin.org/articles/10.3389/fncel.2014.00112/full> (accessed Mar 27, 2018).
4. Høglund, R. A.; Maghazachi, A. A. Multiple sclerosis and the role of immune cells. *World J. Exp. Med.* **2014**, *4* (3), 27–37.
5. Heneka, M. T.; Golenbock, D. T.; Latz, E. Innate Immunity in Alzheimer’s Disease. *Nat. Publ. Gr.* **2015**, *16* (3), 229–236.
6. Hemmer, B.; Archelos, J. J.; Hartung, H. P. New concepts in the immunopathogenesis of multiple sclerosis. *Nat. Rev. Neurosci.* **2002**, *3* (4), 291–301.
7. Gris, D.; Ye, Z.; Iocca, H. A.; Wen, H.; Craven, R. R.; Gris, P.; Huang, M.; Schneider, M.; Miller, S. D.; Ting, J. P.-Y. NLRP3 plays a critical role in the

- development of experimental autoimmune encephalomyelitis by mediating Th1 and Th17 responses. *J. Immunol.* **2010**, *185* (2), 974–981.
8. Shao, B.-Z.; Xu, Z.-Q.; Han, B.-Z.; Su, D.-F.; Liu, C. NLRP3 inflammasome and its inhibitors: a review. *Front. Pharmacol.* [Online] **2015**, *6*, Article 262.
<https://www.frontiersin.org/articles/10.3389/fphar.2015.00262/full> (accessed Mar 30, 2018).
 9. Lawlor, K. E.; Vince, J. E. Ambiguities in NLRP3 inflammasome regulation: Is there a role for mitochondria? *Biochim. Biophys. Acta, Gen. Subj.* **2014**, *1840* (4), 1433–1440.
 10. Marchetti, C.; Toldo, S.; Chojnacki, J.; Mezzaroma, E.; Liu, K.; Salloum, F. N.; Nordio, A.; Carbone, S.; Mauro, A. G.; Das, A.; et al. Pharmacologic inhibition of the NLRP3 inflammasome preserves cardiac function after ischemic and nonischemic injury in the mouse. *J. Cardiovasc. Pharmacol.* **2015**, *66* (1), 1–8.
 11. Marchetti, C.; Chojnacki, J.; Toldo, S.; Mezzaroma, E.; Tranchida, N.; Rose, S. W.; Federici, M.; Van Tassell, B. W.; Zhang, S.; Abbate, A. A novel pharmacologic inhibitor of the NLRP3 inflammasome limits myocardial injury after ischemia-reperfusion in the mouse. *J. Cardiovasc. Pharmacol.* **2014**, *63* (4), 316–322.
 12. Guo, C.; Fulp, J. W.; Jiang, Y.; Li, X.; Chojnacki, J.; Wu, J.; Wang, X.; Zhang, S. Development and characterization of a hydroxyl-sulfonamide analogue, 5-chloro-*N*-[2-(4-hydroxysulfamoyl-phenyl)-ethyl]-2-methoxy-benzamide, as a novel NLRP3 inflammasome inhibitor for potential treatment of multiple sclerosis. *ACS Chem. Neurosci.* **2017**, *8*, 2194–2201.

13. Khare, S.; Dorfleutner, A.; Bryan, N. B.; Yun, C.; Radian, A. D.; de Almeida, L.; Rojanasakul, Y.; Stehlik, C. An NLRP7-Containing Inflammasome Mediates Recognition of Microbial Lipopeptides in Human Macrophages. *Immunity* **2012**, *36* (3), 464–476.
14. Yacoubian, T. A. Neurodegenerative disorders: why do we need new therapies? .In drug discovery approaches for the treatment of neurodegenerative disorders. [Online]; Elsevier Academic Press: Amsterdam, Netherlands, **2017**; pp 1–16. <https://www.sciencedirect.com/science/article/pii/B9780128028100000015> (Accessed Feb 25, 2018)
15. Winner, B.; Kohl, Z.; Gage, F. H. Neurodegenerative disease and adult neurogenesis. *Eur. J. Neurosci.* **2011**, *33* (6), 1139–1151.
16. Costa, N.; Deruemaux-Burel, H.; Molinier, L. What are indirect costs in neurodegenerative diseases? A methodological review. *Value Heal.* **2014**, *17* (3), A186.
17. Alzheimer’s Association. 2017 Alzheimer’s disease facts and figures. *Alzheimer’s Dement.* **2017**, *13* (4), 325–373.
18. Alzheimer’s Association. 2018 Alzheimer’s disease facts and figures. *Alzheimer’s Dement.* **2018**, *14* (3), 367–429.
19. Kowal, S. L.; Dall, T. M.; Chakrabarti, R.; Storm, M. V.; Jain, A. The current and projected economic burden of parkinson’s disease in the United States. *Mov. Disord.* **2013**, *28* (3), 311–318.

20. Files, D.; Jausurawong, T.; Katrajian, R.; Danoff, R. Multiple sclerosis. *Prim. Care* **2015**, *42* (2), 159–175.
21. Zhu, Y.; Fotinos, A.; Mao, L. L. J.; Atassi, N.; Zhou, E. W.; Ahmad, S.; Guan, Y.; Berry, J. D.; Cudkowicz, M. E.; Wang, X. Neuroprotective agents target molecular mechanisms of disease in ALS. *Drug Discov. Today* **2015**, *20* (1), 65–75.
22. Vishal, S.; Sourabh, A.; Harkirat, S. Alois Alzheimer (1864-1915) and the Alzheimer syndrome. *J. Med. Biogr.* **2011**, *19* (1), 32-33.
23. National Institute on Aging. What are the signs of Alzheimer’s disease? <https://www.nia.nih.gov/health/what-are-signs-alzheimers-disease> (accessed Mar 29, 2018).
24. Cacace, R.; Sleegers, K.; Van Broeckhoven, C. Molecular genetics of early-onset Alzheimer’s disease revisited. *Alzheimer’s Dement.* **2016**, *12* (6), 733–748.
25. Bloom, G. S. Amyloid- β and tau the trigger and bullet in Alzheimer disease pathogenesis. *JAMA Neurol.* **2014**, *71* (4), 505-508.
26. Calderón-Garcidueñas, L.; Reed, W.; Maronpot, R. R.; Henriquez-Roldán, C.; Delgado-Chavez, R.; Calderón-Garcidueñas, A.; Dragustinovis, I.; Franco-Lira, M.; Aragón-Flores, M.; Solt, A. C.; et al. Brain inflammation and Alzheimer’s-like pathology in individuals exposed to severe air pollution. *Toxicol. Pathol.* **2004**, *32* (6), 650–658.
27. Richardson, J. R.; Roy, A.; Shalat, S. L.; von Stein, R. T.; Hossain, M. M.; Buckley, B.; Gearing, M.; Levey, A. I.; German, D. C. Elevated serum pesticide

- levels and risk for Alzheimer disease. *JAMA Neurol.* **2014**, *71* (3), 284-290.
28. Guo, Z.; Cupples, L. A.; Kurz, A.; Auerbach, S. H.; Volicer, L.; Chui, H.; Green, R. C.; Sadovnick, A. D.; Duara, R.; DeCarli, C.; et al. Head injury and the risk of AD in the MIRAGE study. *Neurology* **2000**, *54* (6), 1316–1323.
29. Veld, B. A.; Ruitenber, A.; Hofman, A.; Launer, L. J.; van Duijn, C. M.; Stijnen, T.; Breteler, M. M. B.; Stricker, B. H. C. Nonsteroidal antiinflammatory drugs and the risk of Alzheimer's disease. *N. Engl. J. Med.* **2001**, *345* (21), 1515–1521.
30. Akter, K.; Lanza, E. A.; Martin, S. A.; Myronyuk, N.; Rua, M.; Raffa, R. B. Diabetes mellitus and Alzheimer's disease: shared pathology and treatment? *Br. J. Clin. Pharmacol.* **2011**, *71* (3), 365–376.
31. Isik, A. T. Late onset Alzheimer's disease in older people. *Clin. Interv. Aging* **2010**, *5*, 307–311.
32. Nagele, R. G.; Wegiel, J.; Venkataraman, V.; Imaki, H.; Wang, K. C.; Wegiel, J. Contribution of glial cells to the development of Amyloid plaques in Alzheimer's disease. *Neurobiol. Aging* **2004**, *25* (5), 663–674.
33. Mufson, E. J.; Counts, S. E.; Perez, S. E.; Ginsberg, S. D. Cholinergic system during the progression of Alzheimer's disease: therapeutic implications. *Expert Rev. Neurother.* **2008**, *8* (11), 1703–1718.
34. Jin, J. Alzheimer disease. *JAMA* **2015**, *313* (14), 1488.
35. Jakob-Roetne, R.; Jacobsen, H. Alzheimer's disease: from pathology to therapeutic approaches. *Angew. Chemie Int. Ed. Engl.* **2009**, *48* (17), 3030–3059.

36. Reitz, C. Alzheimer's disease and the amyloid cascade hypothesis: a critical review. *Int. J. Alzheimers. Dis.* [Online] **2012**, 2012, Article 369808. <https://www.hindawi.com/journals/ijad/2012/369808/> (accessed Mar 02, 2018).
37. Kaether, C.; Haass, C. A lipid boundary separates APP and secretases and limits amyloid beta-peptide generation. *J. Cell Biol.* **2004**, 167 (5), 809–812.
38. Edelstein-keshet, L.; Spiros, A. Exploring the formation of Alzheimer's disease senile plaques in silico. *J. Theor. Biol.* **2002**, 216 (3), 301–326.
39. Van Der Kant, R.; Goldstein, L. S. Cellular functions of the amyloid precursor protein from development to dementia. *Dev. Cell* **2015**, 32 (4), 502–515.
40. Salminen, A.; Ojala, J.; Kauppinen, A.; Kaarniranta, K.; Suuronen, T. Inflammation in Alzheimer's disease: amyloid- β oligomers trigger innate immunity defence via pattern recognition receptors. *Prog. Neurobiol.* **2009**, 87 (3), 181–194.
41. Giovannini, M. G.; Scali, C.; Prosperi, C.; Bellucci, A.; Vannucchi, M. G.; Rosi, S.; Pepeu, G.; Casamenti, F. Beta-amyloid-induced inflammation and cholinergic hypofunction in the rat brain in vivo: involvement of the p38MAPK pathway. *Neurobiol. Dis.* **2002**, 11 (2), 257–274.
42. Hurtado, D. E.; Molina-Porcel, L.; Iba, M.; Aboagye, A. K.; Paul, S. M.; Trojanowski, J. Q.; Lee, V. M.-Y. A β accelerates the spatiotemporal progression of tau pathology and augments tau amyloidosis in an Alzheimer mouse model. *Am. J. Pathol.* **2010**, 177 (4), 1977–1988.
43. Götz, J.; Chen, F.; van Dorpe, J.; Nitsch, R. M. Formation of neurofibrillary tangles

- in P301I tau transgenic mice induced by abeta 42 fibrils. *Science* **2001**, 293 (5534), 1491–1495.
44. Lewis, J.; Dickson, D. W.; Lin, W. L.; Chisholm, L.; Corral, A.; Jones, G.; Yen, S. H.; Sahara, N.; Skipper, L.; Yager, D.; et al. Enhanced neurofibrillary degeneration in transgenic mice expressing mutant tau and APP. *Science* **2001**, 293 (5534), 1487–1491.
45. Gentleman, S. M.; Nash, M. J.; Sweeting, C. J.; Graham, D. I.; Roberts, G. W. Beta-amyloid precursor protein (beta APP) as a marker for axonal injury after head injury. *Neurosci. Lett.* **1993**, 160 (2), 139–144.
46. Johnson, V. E.; Stewart, W.; Smith, D. H. Traumatic brain injury and amyloid- β pathology: a link to alzheimer's disease? *Nat. Rev. Neurosci.* **2010**, 11 (5), 361–370.
47. Wallace, W. C.; Bragin, V.; Robakis, N. K.; Sambamurti, K.; VanderPutten, D.; Merrill, C. R.; Davis, K. L.; Santucci, A. C.; Haroutunian, V. Increased biosynthesis of Alzheimer amyloid precursor protein in the cerebral cortex of rats with lesions of the nucleus basalis of Meynert. *Brain Res. Mol. Brain Res.* **1991**, 10 (2), 173–178.
48. Kametani, F.; Hasegawa, M. Reconsideration of amyloid hypothesis and tau hypothesis in Alzheimer's disease. *Front. Neurosci.* [Online] **2018**, 12, Article 25. <https://www.frontiersin.org/articles/10.3389/fnins.2018.00025/full> (accessed Mar 13, 2018).
49. Bejanin, A.; Schonhaut, D. R.; La Joie, R.; Kramer, J. H.; Baker, S. L.; Sosa, N.;

- Ayakta, N.; Cantwell, A.; Janabi, M.; Lauriola, M.; et al. Tau pathology and neurodegeneration contribute to cognitive impairment in Alzheimer's disease. *Brain* **2017**, *140* (12), 3286–3300.
50. Johnson, K. A.; Schultz, A.; Betensky, R. A.; Becker, J. A.; Sepulcre, J.; Rentz, D.; Mormino, E.; Chhatwal, J.; Amariglio, R.; Papp, K.; et al. Tau positron emission tomographic imaging in aging and early Alzheimer disease. *Ann. Neurol.* **2016**, *79* (1), 110–119.
51. Braak, H.; Del Tredici, K. Are cases with tau pathology occurring in the absence of A β deposits part of the AD-related pathological process? *Acta Neuropathol.* **2014**, *128* (6), 767–772.
52. Rodríguez-Martín, T.; Cuchillo-Ibáñez, I.; Noble, W.; Nyenya, F.; Anderton, B. H.; Hanger, D. P. Tau phosphorylation affects its axonal transport and degradation. *Neurobiol. Aging* **2013**, *34* (9), 2146–2157.
53. Ballatore, C.; Lee, V. M.-Y.; Trojanowski, J. Q. Tau-mediated neurodegeneration in Alzheimer's disease and related disorders. *Nat. Rev. Neurosci.* **2007**, *8* (9), 663–672.
54. Kimura, T.; Ishiguro, K.; Hisanaga, S.-I. Physiological and pathological phosphorylation of tau by cdk5. *Front. Mol. Neurosci.* [Online] **2014**, *7*, Article 65. <https://www.frontiersin.org/articles/10.3389/fnmol.2014.00065/full> (accessed Feb, 25, 2018).

55. Quintanilla, R. A.; Orellana, D. I.; González-Billault, C.; Maccioni, R. B. Interleukin-6 induces Alzheimer-type phosphorylation of tau protein by deregulating the cdk5/p35 pathway. *Exp. Cell Res.* **2004**, *295* (1), 245–257.
56. Liu, X.; Ma, W.; Surprenant, A.; Jiang, L.H. Identification of the amino acid residues in the extracellular domain of rat P2X(7) receptor involved in functional inhibition by acidic pH. *Br. J. Pharmacol.* **2009**, *156* (1), 135–142.
57. Ries, M.; Sastre, M. Mechanisms of A β clearance and degradation by glial cells. *Front. Aging Neurosci.* [Online] **2016**, *8*, Article 160.
<https://www.frontiersin.org/articles/10.3389/fnagi.2016.00160/full> (accessed Feb, 21, 2018).
58. Compston, A. The 150th anniversary of the first depiction of the lesions of multiple sclerosis. *J. Neurol. Neurosurg. Psychiatry* **1988**, *51* (10), 1249–1252.
59. Kumar, D. R.; Aslinia, F.; Yale, S. H.; Mazza, J. J. Jean-Martin Charcot: the father of neurology. *Clin. Med. Res.* **2011**, *9* (1), 46–49.
60. Clanet, M. Jean-Martin Charcot. 1825 to 1893. *Int. MS J.* **2008**, *15* (2), 59–61.
61. Compston, A.; Coles, A. Multiple sclerosis. *Lancet* **2008**, *372* (9648), 1502–1517.
62. Gold, R.; Wolinsky, J. S.; Amato, M. P.; Comi, G. Evolving expectations around early management of multiple sclerosis. *Ther. Adv. Neurol. Disord.* **2010**, *3* (6), 351–367.
63. Multiple Sclerosis Association of America. Types of multiple sclerosis
<https://mymsaa.org/ms-information/overview/types/> (accessed Apr 3, 2018).

64. Link, J.; Kockum, I.; Lorentzen, A. R.; Lie, B. A.; Celius, E. G.; Westerlind, H.; Schaffer, M.; Alfredsson, L.; Olsson, T.; Brynedal, B.; et al. Importance of human leukocyte antigen (HLA) class I and II alleles on the risk of multiple sclerosis. *PLoS One* [Online] **2012**, 7 (5), Article e36779.
<https://doi.org/10.1371/journal.pone.0036779> (accessed Mar, 22, 2018).
65. Vandebroek, K.; Alvarez, J.; Swaminathan, B.; Alloza, I.; Matesanz, F.; Urcelay, E.; Comabella, M.; Alcina, A.; Fedetz, M.; Ortiz, M. A.; et al. A cytokine gene screen uncovers SOCS1 as genetic risk factor for multiple sclerosis. *Genes Immun.* **2012**, 13 (1), 21–28.
66. Ascherio, A.; Munger, K. L.; Lennette, E. T.; Spiegelman, D.; Hernán, M. A.; Olek, M. J.; Hankinson, S. E.; Hunter, D. J. Epstein-barr virus antibodies and risk of multiple sclerosis. *JAMA* **2001**, 286 (24), 3083–3088.
67. Franklin, R. J. M.; Ffrench-Constant, C. Remyelination in the CNS: from biology to therapy. *Nat. Rev. Neurosci.* **2008**, 9 (11), 839–855.
68. Podbielska, M.; Banik, N. L.; Kurowska, E.; Hogan, E. L. Myelin recovery in multiple sclerosis: the challenge of remyelination. *Brain Sci.* **2013**, 3 (3), 1282–1324.
69. Popescu, B. F. G.; Pirko, I.; Lucchinetti, C. F. Pathology of multiple sclerosis: where do we stand? *Continuum (Minneap. Minn.)* **2013**, 19 (4), 901–921.
70. Venigalla, M.; Sonogo, S.; Gyengesi, E.; Sharman, M. J.; Münch, G. Novel

- promising therapeutics against chronic neuroinflammation and neurodegeneration in Alzheimer's disease. *Neurochem. Int.* **2016**, *95*, 63–74.
71. Suresh, R.; Mosser, D. M. Pattern recognition receptors in innate immunity, host defense, and immunopathology. *Adv. Physiol. Educ.* **2013**, *37* (4), 284–291.
 72. Dranoff, G. Cytokines in cancer pathogenesis and cancer therapy. *Nat. Rev. Cancer* **2004**, *4* (1), 11–22.
 73. Breedveld, A.; Groot Kormelink, T.; van Egmond, M.; de Jong, E. C. Granulocytes as modulators of dendritic cell function. *J. Leukoc. Biol.* **2017**, *102* (4), 1003–1016.
 74. Xiong, Z.-Q.; Qian, W.; Suzuki, K.; McNamara, J. O. Formation of complement membrane attack complex in mammalian cerebral cortex evokes seizures and neurodegeneration. *J. Neurosci.* **2003**, *23* (3), 955–960.
 75. Markiewski, M. M.; Lambris, J. D. The role of complement in inflammatory diseases from behind the scenes into the spotlight. *Am. J. Pathol.* **2007**, *171* (3), 715–727.
 76. Mosser, D. M.; Edwards, J. P. Exploring the full spectrum of macrophage activation. *Nat. Rev. Immunol.* **2008**, *8* (12), 958–969.
 77. Clark, G. J.; Angel, N.; Kato, M.; López, J. A.; MacDonald, K.; Vuckovic, S.; Hart, D. N. The role of dendritic cells in the innate immune system. *Microbes Infect.* **2000**, *2* (3), 257–272.
 78. Lanier, L. L.; Sun, J. C. Do the terms innate and adaptive immunity create

- conceptual barriers? *Nat. Rev. Immunol.* **2009**, 9 (5), 302–303.
79. Iwasaki, A.; Medzhitov, R. Regulation of adaptive immunity by the innate immune system. *Science* **2010**, 327 (5963), 291–295.
 80. Akira, S.; Uematsu, S.; Takeuchi, O. Pathogen recognition and innate immunity. *Cell* **2006**, 124 (4), 783–801.
 81. Ransohoff, R. M.; Brown, M. A. Innate immunity in the central nervous system. *J. Clin. Invest.* **2012**, 122 (4), 1164–1171.
 82. Cooper, M. D.; Alder, M. N. The evolution of adaptive immune systems. *Cell* **2006**, 124 (4), 815–822.
 83. Wang, P.; Zheng, S. G. Regulatory T cells and B cells: implication on autoimmune diseases. *Int. J. Clin. Exp. Pathol.* **2013**, 6 (12), 2668–2674.
 84. Kurosaki, T.; Kometani, K.; Ise, W. Memory B cells. *Nat. Rev. Immunol.* **2015**, 15 (3), 149–159.
 85. Sallusto, F.; Lenig, D.; Förster, R.; Lipp, M.; Lanzavecchia, A. Two subsets of memory T lymphocytes with distinct homing potentials and effector functions. *Nature* **1999**, 401 (6754), 708–712.
 86. Desai, B. S.; Monahan, A. J.; Carvey, P. M.; Hendey, B. Blood–brain barrier pathology in Alzheimer’s and Parkinson’s disease: implications for drug therapy. *Cell Transplant.* **2007**, 16 (3), 285–299.
 87. Engelhardt, B. Development of the blood-brain barrier. *Cell Tissue Res.* **2003**, 314 (1), 119–129.

88. Barker, R. A.; Widner, H. Immune problems in central nervous system cell therapy. *NeuroRx* **2004**, *1* (4), 472–481.
89. Gage, F. H.; Brundin, P.; Isacson, O.; Björklund, A. Rat fetal brain tissue grafts survive and innervate host brain following five day pregraft tissue storage. *Neurosci. Lett.* **1985**, *60* (2), 133–137.
90. Daneman, R.; Prat, A. The blood–brain barrier. *Cold Spring Harb. Perspect. Biol.* [Online] **2015**, *7* (1), Article a020412.
<http://cshperspectives.cshlp.org/content/7/1/a020412> (accessed Mar 01, 2018).
91. Lohrberg, M.; Wilting, J. The lymphatic vascular system of the mouse head. *Cell Tissue Res.* **2016**, *366* (3), 667–677.
92. Brierley, J. B.; Field, E. J. The connexions of the spinal sub-arachnoid space with the lymphatic system. *J. Anat.* **1948**, *82*, 153–166.
93. Földi, M.; Csanda, E.; Simon, M.; Obál, F.; Schneider, I.; Dobranovics, I.; Zoltán, Ö. T.; Kozma, M.; Poberai, M. Lymphogenic haemangiopathy. "prelymphatic" pathways in the wall of cerebral and cervical blood vessels *Angiologica* **1968**, *5* (4), 250–262.
94. Louveau, A.; Da Mesquita, S.; Kipnis, J. Lymphatics in neurological disorders: a neuro-lympho-vascular component of multiple sclerosis and Alzheimer's disease? *Neuron* **2016**, *91* (5), 957–973.
95. Absinta, M.; Ha, S.-K.; Nair, G.; Sati, P.; Luciano, N. J.; Palisoc, M.; Louveau, A.; Zaghoul, K. A.; Pittaluga, S.; Kipnis, J.; et al. Human and nonhuman primate

- meninges harbor lymphatic vessels that can be visualized noninvasively by MRI. *Elife* [Online] **2017**, 6, Article e29738. <https://elifesciences.org/articles/29738> (accessed Mar 11, 2018).
96. Jäkel, S.; Dimou, L. Glial cells and their function in the adult brain: a journey through the history of their ablation. *Front. Cell. Neurosci.* [Online] **2017**, 11, Article 24. <https://www.frontiersin.org/articles/10.3389/fncel.2017.00024/full> (accessed Mar 11, 2018).
 97. Jessen, K. R. Glial cells. *Int. J. Biochem. Cell Biol.* **2004**, 36 (10), 1861–1867.
 98. Waisman, A.; Ginhoux, F.; Greter, M.; Bruttger, J. Homeostasis of microglia in the adult brain: review of novel microglia depletion systems. *Trends Immunol.* **2015**, 36 (10), 625–636.
 99. Perry, V. H.; Teeling, J. Microglia and macrophages of the central nervous system: the contribution of microglia priming and systemic inflammation to chronic neurodegeneration. *Semin. Immunopathol.* **2013**, 35 (5), 601–612.
 100. Waisman, A.; Ginhoux, F.; Greter, M.; Bruttger, J. Homeostasis of microglia in the adult brain: review of novel microglia depletion systems. *Trends Immunol.* **2015**, 36 (10), 625–636.
 101. Haga, S.; Akai, K.; Ishii, T. Demonstration of microglial cells in and around senile (neuritic) plaques in the Alzheimer brain. *Acta Neuropathol.* **1989**, 77 (6), 569–575.
 102. Lee, C. Y. D.; Landreth, G. E. The role of microglia in amyloid clearance from the

- AD brain. *J. Neural Transm.* **2010**, 117 (8), 949–960.
103. Mayo, L.; Quintana, F. J.; Weiner, H. L. The innate immune system in demyelinating disease. *Immunol. Rev.* **2012**, 248 (1), 170–187.
104. Nagele, R. G.; Wegiel, J.; Venkataraman, V.; Imaki, H.; Wang, K.-C.; Wegiel, J. Contribution of glial cells to the development of amyloid plaques in Alzheimer's disease. *Neurobiol. Aging* **2004**, 25 (5), 663–674.
105. Nagele, R. G.; D'Andrea, M. R.; Lee, H.; Venkataraman, V.; Wang, H.-Y. Astrocytes accumulate A beta 42 and give rise to astrocytic amyloid plaques in Alzheimer disease brains. *Brain Res.* **2003**, 971 (2), 197–209.
106. Rodríguez-Arellano, J. J.; Parpura, V.; Zorec, R.; Verkhratsky, A. Astrocytes in physiological aging and Alzheimer's disease. *Neuroscience* **2016**, 323, 170–182.
107. Sofroniew, M. V. Astrogliosis. *Cold Spring Harb. Perspect. Biol.* [Online] **2014**, 7 (2), Article a020420. <http://cshperspectives.cshlp.org/content/7/2/a020420> (accessed Mar 15, 2018).
108. Son, S. M.; Cha, M.-Y.; Choi, H.; Kang, S.; Choi, H.; Lee, M.-S.; Park, S. A.; Mook-Jung, I. Insulin-degrading enzyme secretion from astrocytes is mediated by an autophagy-based unconventional secretory pathway in Alzheimer disease. *Autophagy* **2016**, 12 (5), 784-800.
109. Correale, J.; Farez, M. F. The role of astrocytes in multiple sclerosis progression. *Front. Neurol.* [Online] **2015**, 6, Article 180. <https://www.frontiersin.org/articles/10.3389/fneur.2015.00180/full> (accessed Mar

- 25, 2018).
110. Wyss-Coray, T.; Mucke, L. Inflammation in neurodegenerative disease—a double-edged sword. *Neuron* **2002**, *35* (3), 419–432.
 111. Akiyama, H.; Barger, S.; Barnum, S.; Bradt, B.; Bauer, J.; Cole, G. M.; Cooper, N. R.; Eikelenboom, P.; Emmerling, M.; Fiebich, B. L.; et al. Inflammation and Alzheimer's disease. *Neurobiol Aging* **2000**, *21* (3), 383–421.
 112. Kigerl, K. A.; de Rivero Vaccari, J. P.; Dietrich, W. D.; Popovich, P. G.; Keane, R. W. Pattern recognition receptors and central nervous system repair. *Exp. Neurol.* **2014**, *258*, 5–16.
 113. Land, W. G. The role of damage-associated molecular patterns (DAMPs) in human diseases: part II: DAMPs as diagnostics, prognostics and therapeutics in clinical medicine. *Sultan Qaboos Univ. Med. J.* **2015**, *15* (2), 157-170.
 114. Lee, M. S.; Kim, Y.-J. Signaling pathways downstream of pattern-recognition receptors and their cross talk. *Annu. Rev. Biochem.* **2007**, *76* (1), 447–480.
 115. Kawai, T.; Akira, S. Signaling to NF- κ B by toll-like receptors. *Trends Mol. Med.* **2007**, *13* (11), 460–469.
 116. Salminen, A.; Ojala, J.; Kauppinen, A.; Kaarniranta, K.; Suuronen, T. Inflammation in Alzheimer's disease: amyloid-beta oligomers trigger innate immunity defence via pattern recognition receptors. *Prog. Neurobiol.* **2009**, *87* (3), 181–194.
 117. Domingues, C.; da Cruz E Silva, O. A. B.; Henriques, A. G. Impact of cytokines and chemokines on Alzheimer's disease neuropathological hallmarks. *Curr.*

- Alzheimer Res.* **2017**, *14* (8), 870–882.
118. Mosley, R. L.; Benner, E. J.; Kadiu, I.; Thomas, M.; Boska, M. D.; Hasan, K.; Laurie, C.; Gendelman, H. E. Neuroinflammation, oxidative stress and the pathogenesis of Parkinson's disease. *Clin. Neurosci. Res.* **2006**, *6* (5), 261–281.
119. Yang, J.; Liu, Z.; Xiao, T. S. Post-translational regulation of inflammasomes. *Cell. Mol. Immunol.* **2017**, *14* (1), 65–79.
120. Wilson, S. P.; Cassel, S. L. Inflammasome-mediated autoinflammatory disorders. *Postgrad. Med.* **2010**, *122* (5), 125–133.
121. Jin, T.; Perry, A.; Jiang, J.; Smith, P.; Curry, J. A.; Unterholzner, L.; Jiang, Z.; Horvath, G.; Rathinam, V. A.; Johnstone, R. W.; et al. Structures of the HIN domain:DNA complexes reveal ligand binding and activation mechanisms of the AIM2 inflammasome and IFI16 receptor. *Immunity* **2012**, *36* (4), 561–571.
122. Yin, J.; Zhao, F.; Chojnacki, J. E.; Fulp, J.; Klein, W. L.; Zhang, S.; Zhu, X. NLRP3 inflammasome inhibitor ameliorates amyloid pathology in a mouse model of Alzheimer's disease. *Mol. Neurobiol.* **2018**, *55* (3), 1977–1987.
123. Inoue, M.; Shinohara, M. L. NLRP3 inflammasome and MS/EAE. *Autoimmune Dis.* [Online] **2013**, *2013*, Article 859145.
<https://www.hindawi.com/journals/ad/2013/859145/> (accessed Apr 13, 2018).
124. MacDonald, J. A.; Wijekoon, C. P.; Liao, K.-C.; Muruve, D. A. Biochemical and structural aspects of the ATP-binding domain in inflammasome-forming human NLRP proteins. *IUBMB Life* **2013**, *65* (10), 851–862.

125. Man, S. M.; Kanneganti, T.-D. Regulation of inflammasome activation. *Immunol. Rev.* **2015**, *265* (1), 6–21.
126. Pellegrini, C.; Antonioli, L.; Lopez-Castejon, G.; Blandizzi, C.; Fornai, M. Canonical and non-canonical activation of NLRP3 inflammasome at the crossroad between immune tolerance and intestinal inflammation. *Front. Immunol.* [Online] **2017**, *8*, Article 36.
<https://www.frontiersin.org/articles/10.3389/fimmu.2017.00036/full> (accessed Apr 14, 2018).
127. Hornung, V.; Latz, E. Critical functions of priming and lysosomal damage for NLRP3 activation. *Eur. J. Immunol.* **2010**, *40* (3), 620–623.
128. Shao, B.-Z.; Xu, Z.-Q.; Han, B.-Z.; Su, D.-F.; Liu, C. NLRP3 inflammasome and its inhibitors: a review. *Front. Pharmacol.* [Online] **2015**, *6*, Article 262.
<https://www.frontiersin.org/articles/10.3389/fphar.2015.00262/full> (accessed Apr 14, 2018).
129. Franchi, L.; Warner, N.; Viani, K.; Nuñez, G. Function of nod-like receptors in microbial recognition and host defense. *Immunol. Rev.* **2009**, *227* (1), 106–128.
130. Tsai, Y.-L.; Hua, K.-F.; Chen, A.; Wei, C.-W.; Chen, W.-S.; Wu, C.-Y.; Chu, C.-L.; Yu, Y.-L.; Lo, C.-W.; Ka, S.-M. NLRP3 inflammasome: pathogenic role and potential therapeutic target for IgA nephropathy. *Sci. Rep.* [Online] **2017**, *7*, Article 41123. <https://www.nature.com/articles/srep41123> (accessed Apr 14, 2018).
131. Teng, X.; Zhang, H.; Snead, C.; Catravas, J. D. Molecular mechanisms of iNOS induction by IL-1 β and IFN- γ in rat aortic smooth muscle cells. *Am. J. Physiol.*

- Physiol.* **2002**, 282 (1), 144–152.
132. Rossi, F.; Bianchini, E. Synergistic induction of nitric oxide by beta-amyloid and cytokines in astrocytes. *Biochem. Biophys. Res. Commun.* **1996**, 225 (2), 474–478.
133. Lukens, J. R.; Barr, M. J.; Chaplin, D. D.; Chi, H.; Kanneganti, T.-D. Inflammasome-derived IL-1 β regulates the production of GM-CSF by CD4(+) T Cells and $\gamma\delta$ T Cells. *J. Immunol.* **2012**, 188 (7), 3107–3115.
134. Fitzgerald, S. M.; Chi, D. S.; Hall, H. K.; Reynolds, S. A.; Aramide, O.; Lee, S. A.; Krishnaswamy, G. GM-CSF induction in human lung fibroblasts by IL-1beta, TNF-alpha, and macrophage contact. *J. Interf. Cytokine Res.* **2003**, 23 (2), 57–65.
135. Rubio-Perez, J. M.; Morillas-Ruiz, J. M. A review: inflammatory process in Alzheimer's disease, role of cytokines. *Sci. World J.* [Online] **2012**, 2012, Article 756357. <https://www.hindawi.com/journals/tswj/2012/756357/> (accessed Apr 15, 2018).
136. Sutinen, E. M.; Korolainen, M. A.; Häyrynen, J.; Alafuzoff, I.; Petratos, S.; Salminen, A.; Soininen, H.; Pirttilä, T.; Ojala, J. O. Interleukin-18 alters protein expressions of neurodegenerative diseases-linked proteins in human SH-SY5Y neuron-like cells. *Front. Cell Neurosci.* [Online] **2014**, 8, Article 214. <https://www.frontiersin.org/articles/10.3389/fncel.2014.00214/full> (accessed Apr 15, 2018).
137. Alboni, S.; Cervia, D.; Sugama, S.; Conti, B. Interleukin 18 in the CNS. *J. Neuroinflammation* [Online] **2010**, 7, Article 9.

<https://jneuroinflammation.biomedcentral.com/articles/10.1186/1742-2094-7-9>
(accessed Apr 15, 2018).

138. Salim, T.; Sershen, C. L.; May, E. E. Investigating the role of TNF- α and IFN- γ activation on the dynamics of iNOS gene expression in LPS stimulated macrophages. *PLoS One* [Online] **2016**, *11* (6), Article e0153289.
<http://journals.plos.org/plosone/article?id=10.1371/journal.pone.0153289>
(accessed Apr 15, 2018).
139. Saco, T.; Parthasarathy, P. T.; Cho, Y.; Lockey, R. F.; Kolliputi, N. Inflammasome: a new trigger of Alzheimer's disease. *Front. Aging Neurosci.* [Online] **2014**, *6*, Article 80. <https://www.frontiersin.org/articles/10.3389/fnagi.2014.00080/full>
(accessed Apr 15, 2018).
140. Heneka, M. T.; Kummer, M. P.; Stutz, A.; Delekate, A.; Schwartz, S.; Vieira-Saecker, A.; Griep, A.; Axt, D.; Remus, A.; Tzeng, T.-C.; et al. NLRP3 Is activated in Alzheimer's disease and contributes to pathology in APP/PS1 mice. *Nature* **2013**, *493* (7434), 674–678.
141. Koudriavtseva, T.; Mainero, C. Neuroinflammation, neurodegeneration and regeneration in multiple sclerosis: intercorrelated manifestations of the immune response. *Neural Regen. Res.* **2016**, *11* (11), 1727–1730.
142. Furlan, R.; Filippi, M.; Bergami, A.; Rocca, M. A.; Martinelli, V.; Poliani, P. L.; Grimaldi, L. M.; Desina, G.; Comi, G.; Martino, G. Peripheral levels of caspase-1 mRNA correlate with disease activity in patients with multiple sclerosis; a preliminary study. *J. Neurol. Neurosurg. Psychiatry* **1999**, *67* (6), 785–788.

143. Ming, X.; Li, W.; Maeda, Y.; Blumberg, B.; Raval, S.; Cook, S. D.; Dowling, P. C. Caspase-1 expression in multiple sclerosis plaques and cultured glial cells. *J. Neurol. Sci.* **2002**, *197* (1–2), 9–18.
144. Cocco, M.; Pellegrini, C.; Martínez-Banaclocha, H.; Giorgis, M.; Marini, E.; Costale, A.; Miglio, G.; Fornai, M.; Antonioli, L.; López-Castejón, G.; et al. Development of an acrylate derivative targeting the NLRP3 inflammasome for the treatment of inflammatory bowel disease. *J. Med. Chem.* **2017**, *60* (9), 3656–3671.
145. Youm, Y.-H.; Nguyen, K. Y.; Grant, R. W.; Goldberg, E. L.; Bodogai, M.; Kim, D.; D'Agostino, D.; Planavsky, N.; Lupfer, C.; Kanneganti, T. D.; et al. The ketone metabolite β -hydroxybutyrate blocks NLRP3 inflammasome-mediated inflammatory disease. *Nat. Med.* **2015**, *21* (3), 263–269.
146. Jiang, H.; He, H.; Chen, Y.; Huang, W.; Cheng, J.; Ye, J.; Wang, A.; Tao, J.; Wang, C.; Liu, Q.; et al. Identification of a selective and direct NLRP3 inhibitor to treat inflammatory disorders. *J. Exp. Med.* **2017**, *214* (11), 3219–3238.
147. Perregaux, D. G.; McNiff, P.; Laliberte, R.; Hawryluk, N.; Peurano, H.; Stam, E.; Egger, J.; Griffiths, R.; Dombroski, M. A.; Gabel, C. A. Identification and characterization of a novel class of interleukin-1 post-translational processing inhibitors. *J. Pharmacol. Exp. Ther.* **2001**, *299* (1), 187–197.
148. Lamkanfi, M.; Mueller, J. L.; Vitari, A. C.; Misaghi, S.; Fedorova, A.; Deshayes, K.; Lee, W. P.; Hoffman, H. M.; Dixit, V. M. Glyburide inhibits the cryopyrin/nalp3 inflammasome. *J. Cell Biol.* **2009**, *187* (1), 61–70.

149. Serrano-Martín, X.; Payares, G.; Mendoza-León, A. Glibenclamide, a blocker of K⁺(ATP) channels, shows antileishmanial activity in experimental murine cutaneous leishmaniasis. *Antimicrob. Agents Chemother.* **2006**, *50* (12), 4214–4216.
150. Sutton, C.; Brereton, C.; Keogh, B.; Mills, K. H. G.; Lavelle, E. C. A crucial role for interleukin (IL)-1 in the induction of IL-17-producing T cells that mediate autoimmune encephalomyelitis. *J. Exp. Med.* **2006**, *203* (7), 1685–1691.
151. Sutton, C. E.; Lalor, S. J.; Sweeney, C. M.; Brereton, C. F.; Lavelle, E. C.; Mills, K. H. G. Interleukin-1 and IL-23 induce innate IL-17 production from gammadelta T cells, amplifying Th17 responses and autoimmunity. *Immunity* **2009**, *31* (2), 331–341.
152. Inoue, M.; Williams, K. L.; Gunn, M. D.; Shinohara, M. L. NLRP3 inflammasome induces chemotactic immune cell migration to the CNS in experimental autoimmune encephalomyelitis. *Proc. Natl. Acad. Sci. U. S. A.* **2012**, *109* (26), 10480–10485.
153. Coll, R. C.; Robertson, A. A. B.; Chae, J. J.; Higgins, S. C.; Muñoz-Planillo, R.; Inserra, M. C.; Vetter, I.; Dungan, L. S.; Monks, B. G.; Stutz, A.; et al. A small-molecule inhibitor of the NLRP3 inflammasome for the treatment of inflammatory diseases. *Nat. Med.* **2015**, *21* (3), 248–255.
154. Jerabek-Willemsen, M.; André, T.; Wanner, R.; Roth, H. M.; Duhr, S.; Baaske, P.; Breitsprecher, D. Microscale thermophoresis: interaction analysis and beyond. *J. Mol. Struct.* **2014**, *1077*, 101–113.

155. Nanotemper Technologies. User Starting Guide Monolith ® NT.115.
156. MacDonald, J. A.; Wijekoon, C. P.; Liao, K.-C.; Muruve, D. A. Biochemical and structural aspects of the ATP-binding domain in inflammasome-forming human NLRP proteins. *IUBMB Life* **2013**, *65* (10), 851–862.
157. Šali, A.; Blundell, T. L. Comparative protein modelling by satisfaction of spatial restraints. *J. Mol. Biol.* **1993**, *234* (3), 779–815.
158. Hu, Z.; Yan, C.; Liu, P.; Huang, Z.; Ma, R.; Zhang, C.; Wang, R.; Zhang, Y.; Martinon, F.; Miao, D.; et al. Crystal structure of NLRC4 reveals its autoinhibition mechanism. *Science* **2013**, *341* (6142), 172–175.
159. Romberg, N.; Al Moussawi, K.; Nelson-Williams, C.; Stiegler, A. L.; Loring, E.; Choi, M.; Overton, J.; Meffre, E.; Khokha, M. K.; Huttner, A. J.; et al. Mutation of NLRC4 causes a syndrome of enterocolitis and autoinflammation. *Nat. Genet.* **2014**, *46* (10), 1135–1139.
160. Kellogg, G. E.; Scarsdale, J. N.; Fornari, F. A.; Jr. Identification and hydrophobic characterization of structural features affecting sequence specificity for doxorubicin intercalation into DNA double-stranded polynucleotides. *Nucleic Acids Res.* **1998**, *26* (20), 4721–4732.
161. Jones, G.; Willett, P.; Glen, R. C.; Leach, A. R.; Taylor, R. Development and validation of a genetic algorithm for flexible docking. *J. Mol. Biol.* **1997**, *267* (3), 727–748.
162. Rice, P.; Longden, I.; Bleasby, A. EMBOSS: the european molecular biology open

- software suite. *Trends Genet.* **2000**, 16 (6), 276–277.
163. Pearson, W. R. An introduction to sequence similarity ("homology") searching. *Curr. Protoc. Bioinforma.* **2013**, 41 (1), 3.1.1-3.1.8.
164. Heffron, F.; So, M.; Mccarthy, B. J. In vitro mutagenesis of a circular DNA molecule by using synthetic restriction sites. *Biochemistry* **1978**, 75 (12), 6012–6016.
165. Invitrogen. pcDNA™ 3.1/Hygro (+) pcDNA™ 3.1/Hygro (-) protocol.

Vita

Ashley Grace Boice was born May 1, 1990 in Orlando, Florida to parents, William and Tamara Boice. She graduated from Virginia Commonwealth University with Bachelor of Science in Health Preparation/Professional Sciences with a minor in biology in 2014. She joined the Department of Medicinal Chemistry at Virginia Commonwealth University in the fall of 2014 to pursue her Ph.D.